

*Ordered
2/25/80*

John H. Murray

LEVEL II

*(D)
B.S.*

AD A090110

R-947

**INSTRUMENTED FULL-SCALE TESTS
OF A DRIFTING BUOY AND DROGUE**

by
William A. Vachon

December 1975

**DTIC
ELECTE
S OCT 6 1980 D
A**



The Charles Stark Draper Laboratory, Inc.
Cambridge, Massachusetts 02139

DDC FILE COPY

Approved for public release; distribution unlimited.

80 9 3 083

REPORT DOCUMENTATION PAGE		READ INSTRUCTIONS BEFORE COMPLETING FORM
1. REPORT NUMBER R-947	2. GOVT ACCESSION NO. AD-A090110	3. RECIPIENT'S CATALOG NUMBER
4. TITLE (and Subtitle) Instrumented Full Scale Tests of a Drifting Buoy and Drogue		5. TYPE OF REPORT & PERIOD COVERED Final Report, Dec 1973 - Jun 1975
7. AUTHOR(s) William A. Vachon		8. CONTRACT OR GRANT NUMBER(s) NAS8-30318
9. PERFORMING ORGANIZATION NAME AND ADDRESS Charles Stark Draper Laboratory, Inc. 555 Technology Square Cambridge, Mass. 02139		10. PROGRAM ELEMENT, PROJECT, TASK AREA & WORK UNIT NUMBERS
11. CONTROLLING OFFICE NAME AND ADDRESS NOAA Data Buoy Office National Space Technology Laboratories Bay St. Louis, MS 39520		12. REPORT DATE December 1975
14. MONITORING AGENCY NAME & ADDRESS (if different from Controlling Office) SAME		13. NUMBER OF PAGES 180
		15. SECURITY CLASS (of this report) Unclassified
		15a. DECLASSIFICATION/DOWNGRADING SCHEDULE
16. DISTRIBUTION STATEMENT (of this Report) Approved for public release; distribution unlimited.		
17. DISTRIBUTION STATEMENT (of the abstract entered in Block 20, if different from Report)		
18. SUPPLEMENTARY NOTES		
19. KEY WORDS (Continue on reverse side if necessary and identify by block number) drifting oceanographic buoys, drogued buoys, buoys, drogues, current measurement, drogue testing, Lagrangian oceanographic buoys		
20. ABSTRACT (Continue on reverse side if necessary and identify by block number) The design of a full scale window shade drogue is described and illustrated. The results from a test program for measuring the drag coefficient, slippage, and dynamic response of a full scale window shade drogue are given along with a description of a dynamic motion sensing instrument, called a Force Vector Recorder (FVR), which is employed during the tests. Full scale, instrumented drogue towing tests were performed in a water-filled quarry in an effort to measure the drogue drag coefficient under ideal,		

408386

DM

(R-947)

non-dynamic conditions. The results are interpreted and compared with the results of previously reported scale model drogue tests in a tow tank. A maximum full scale drag coefficient of 2.6 was derived for a vertically aligned drogue. In addition, the tilt angle of the top of the drogue was measured by the FVR and related to the slip velocity and towing force through a simple mathematical model of drogue drag force as a function of the tilt angle. Measured drag data agreed within 20% of the math model.

The vertical drag coefficient of a full scale window shade drogue was measured in ocean tests by the use of the FVR. An average value of approximately $(C_D)_{D//} = 0.03$ (based on full drogue lateral area) for the drogue and spreader bar combination was measured. Estimates were made of the effect of the vertical drag coefficient on buoy-drogue dynamics.

Additional ocean tests measured the dynamics of a window shade drogue supported at a mean depth of 24 meters beneath a Nova minibuoy in a drifting configuration. The data were measured and internally recorded in digital form on the FVR attached to the top spreader bar of the drogue. It was found that the FVR recorded the vertical excursions and drogue dynamics in a manner which would be useful for the verification of dynamic math models of a drogue response. It was also found, however, that estimates of drogue horizontal drag force from a measure of drogue tilt angle were approximately a factor of 2 larger than those estimated from the sum of wind and surface current forces. Lastly, the FVR data showed that the plane of a window shade drogue did not weathervane normal to the estimated net relative velocity at the drogue, caused by error-inducing forces. The error between the measured drogue normal and the estimated slip direction varied between 33 and 84 degrees during four different FVR measurement bursts.

The trajectories of two different buoys, with window shade drogues at 24 meters, are shown to track each other rather well over nearly two tidal periods in spite of the presence of a wind-induced surface current flowing nearly opposite to the current at the drogue depth. Mathematical estimates of Nova buoy drogue slippage were derived from both the FVR data and by "correcting" the trajectories of independent drogued buoys. A computerized analysis iterated on the corrected trajectory of the Nova minibuoy in order to make it agree with that of the corrected trajectory of a non-surface-following drogued float which is postulated to be less subject to slippage errors caused by buoy-drogue dynamics, wind, waves, and surface currents. Estimates of the accuracy of correcting trajectory data by the application of constant drag coefficient, square-law drag equations for wind and surface current forces are given along with estimates of the sensitivity of these corrections to values of assumed constants. For the tests described, it was estimated that wind forces on the buoy give rise to approximately 70 percent of the drogue slippage forces averaged over nearly two tidal periods (23 hours).

Accession For	
NTS CRUI	<input checked="" type="checkbox"/>
DOC REP	<input type="checkbox"/>
Unprocessed	<input type="checkbox"/>
Justification	
Distribution/	
Availability Codes	
Avail and/or	
Special	
A	

R-947

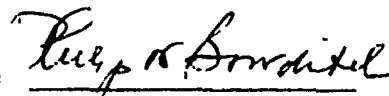
INSTRUMENTED FULL-SCALE TESTS
OF A DRIFTING BUOY AND DROGUE

by

William A. Vachon

December 1975

Approved:



Philip N. Bowditch
Head, Scientific Research Dept.

The Charles Stark Draper Laboratory, Inc.
555 Technology Square
Cambridge, Massachusetts 02139

Approved for public release; distribution unlimited.

ACKNOWLEDGMENT

This report was prepared by The Charles Stark Draper Laboratory, Inc. under Contract NAS 8-30318 with the NOAA Data Buoy Office and administered by the National Aeronautics and Space Administration.

The author wishes to thank all those who contributed to the work described. Special thanks are due to Lt. Lee Gillis, Mr. Ed Kerut, and Cmdr. C. Niederman of the NOAA Data Buoy Office for their support and encouragement. Special thanks are also due to the following personnel at CSDL who assisted in this work: Mr. P. Bowditch and Mr. J. Dahlen for constructive comments and guidance; to Mssrs. T. Anderson, W. DeRusso, C. Martorella, E. Scioli, and M. Soikkeli for assistance with equipment and tests, to Mr. J. Scholten for assistance with computer programming, and to Ms. K. Ahearn, Ms. K. Hall, and the technical publications department for their patience in typing the manuscript.

The publication of this report does not constitute approval by the NOAA Data Buoy Office of the findings or conclusions contained herein. It is published only for the exchange and stimulation of ideas.

TABLE OF CONTENTS

<u>Section</u>		<u>Page</u>
	Abstract.....	xi
1.0	INTRODUCTION.....	1
2.0	WINDOW SHADE DROGUE DESIGN.....	3
	2.1 Analysis.....	3
	2.2 Model Testing.....	7
	2.3 Full Scale Drogue Description.....	8
	2.4 Drogue Material.....	11
3.0	FORCE VECTOR RECORDER (FVR) DESIGN.....	14
	3.1 FVR Description.....	14
	3.2 FVR Capabilities.....	16
	3.3 FVR Design Considerations.....	21
4.0	CONTROLLED FULL SCALE DROGUE TESTS.....	22
	4.1 Test Description.....	22
	4.2 Walden Pond Test.....	26
	4.3 Quarry Test No. 1.....	28
	4.4 Quarry Test No. 2.....	34
	4.5 Check on Quality of FVR Data.....	42
	4.6 Interpretation of Quarry Test Data.....	45
	4.7 Recommended Window Shade Drogue Drag Coefficient.....	50
5.0	DROGUE OCEAN TESTS.....	51
	5.1 Measurement of Drogue Vertical Drag Coefficient.....	51

TABLE OF CONTENTS (cont.)

<u>Section</u>	<u>Page</u>
5.2	Drogued Ocean Test..... 54
5.2.1	Details of Slippage Test..... 64
5.2.2	Analysis of Slippage Data..... 68
6.0	FORCE VECTOR RECORDER (FVR) RESULTS DURING OCEAN SLIPPAGE TEST..... 102
6.1	Measured Orientation of Window Shade Droque..... 102
6.2	Droque Dynamics..... 103
6.3	Estimated Droque Horizontal Drag Force from FVR Tilt Angle..... 113
7.0	CONCLUSIONS AND RECOMMENDATIONS FROM OCEAN SLIPPAGE AND FVR TESTS..... 117
	REFERENCES..... 121
Appendix A	Ocean Test Data Derived During Droque Slippage Test - Including Computer-Derived Velocity Vectors..... 122
Appendix B	Trajectories of Drogued Buoys Employing Differential Ship LORAN C for Buoy Position-Fixing..... 131
Appendix C	Force Vector Recorder (FVR) Timing and Calibration Data..... 135
Appendix D	Force Vector Recorder (FVR) Euler Angle Determination..... 140
Appendix E	Estimated Window Shade Droque Dynamic Loads Induced by an Inelastic Tether Line to a Surface-Following Buoy..... 148

TABLE OF CONTENTS (cont.)

<u>Section</u>	<u>Page</u>
Appendix F Listing of Computer Program Employed to Correct Drogued Buoy Trajectories Based on Wind and Surface Current Forces (Containing Section Which Iterates on Nova Buoy Drag Areas in Order to Produce a Corrected Trajectory Coincident with that of a Drogued Float).....	155

LIST OF FIGURES

<u>Figure</u>		<u>Page</u>
1	Window Shade Drogue Spreader Bar Bending Stresses.....	4
2	Draper Lab Window Shade Drogue Design.....	9
3	Detail - Window Shade Drogue Spreader Bar Section.....	10
4	CSDL Neutrally Buoyant Force Vector Recorder (FVR).....	15
5	Shallow Water Tests of Window Shade Drogue.....	23
6	Window Shade Drogue, Test Results from Full Scale Quarry Test No. 1.....	32
7	Effect of Unbalanced Weight on Window Shade Drogue.....	33
8	Full Scale Window Shade Drogue, Quarry Test Results.....	37
9	Drogue Under Heavy Tow.....	38
10	Window Shade Drogue Stationary in Water.....	38
11	FVR Data-Computerized Plot from Quarry Test No. 2.....	44
12	Forces on an Unstable or Gliding Parachute.....	49
13	Nova Minibuoy Outline, Including Major Dimensions.....	56
14	Drogued Float Configuration.....	57
15	Surface-Drogued Float Configuration.....	58
16	Estimated Wind Forces on Test Buoys.....	60
17	Estimated Surface Current Forces on Test Buoys.....	61
18	Description of Ocean Drift Test Site and Location of Radar Navigation Transponders.....	62
19	Drogue Slippage Test Velocity Definitions.....	65
20	Paths of Drogued Buoys During Sea Test.....	74
21	Tracks of Surface-Drogued Float During Sea Test.....	75

LIST OF FIGURES (cont.)

<u>Figure</u>		<u>Page</u>
22	Virtual Trajectory of Surface-Drogued Buoy and Estimated Surface Current Trajectory.....	84
23	Corrected and Uncorrected (measured) Trajectories of Drogued Buoys Showing Estimated Slippage.....	85
24	Plot of Estimated Error-Inducing Forces on Buoy-2 as Function of Time.....	87
25	Estimated Components of Buoy-2 Drogue Slip Velocity.....	88
26	Estimated History of Error-Inducing Forces on Buoy-1 <u>Before</u> Trajectory Iterations.....	89
27	Estimated Components of Buoy-1 Drogue Slip Velocity <u>Before</u> Trajectory Iterations.....	90
28	Estimated History of Error-Inducing Forces on Buoy-1 <u>After</u> Trajectory Iterations.....	91
29	Estimated Components of Buoy-1 Drogue Slip Velocity <u>After</u> Trajectory Iterations.....	92
30	FVR Attachment to Drogue Top Spreader Bar.....	103
31	Estimated Forces, Velocities, and Measured Drogue Azimuth for Nova Minibuoy.....	107
32	Drogue Depth History During Portion of Second FVR Burst.....	109
33	Drogue Tilt Angle History (θ) During Portion of Second FVR Burst.....	110
34	History of Drogue ϕ Euler Angle (Roll) During Portion of Second FVR Burst.....	111
35	History of Drogue ψ Euler Angle (Yaw) During Portion of Second FVR Burst.....	112

LIST OF FIGURES (cont.)

<u>Figure</u>		<u>Page</u>
36	History of Drogue True Azimuth Angle During Portion of Second FVR Burst.....	113
A-1	Computer Program for Conversion of Radar Range Data to Drifting Buoy Velocities.....	130
B-1	Buoy Trajectories Determined by Decca Radar Positioning and Differential LORAN C.....	132
C-1	FVR Burst Mode Timing Sequence.....	135
C-2	FVR Time Profile During Initial Portion of Drogued Ocean Test.....	136
D-1	FVR Axis Definitions.....	141
D-2	FVR Euler Angle Definitions.....	142
E-1	Estimated Maximum Dynamic Force from Window Shade Drogue on Surface-Following Buoy.....	150
E-2	Estimated Window Shade Drogue Dynamic Shock Load Conditions.....	153

LIST OF TABLES

<u>Table</u>		<u>Page</u>
1	Herculite Fabric Test Summary.....	12
2	FVR Drag Force Sensitivity Study.....	19
3	Test Results - Shallow Water Test of Window Shade Drogue.....	27
4	Shallow Water Window Shade Drogue Tow Test Results - Phase 2.....	31
5	Shallow Water Window Shade Drogue Tow Test Results - Test No. 3.....	36
6	Quarry Test No. 2, FVR Results Using Full Drogue Weight.....	40
7	Quarry Test No. 2, FVR Results Using One-Half of Drogue Weight.....	41
8	Quarry Test Accelerometer Data.....	43
9	Summary of Drogue Drop Tests.....	53
10	Assumed Drag Areas on Test Buoys and Tether Lines.....	59
11	Summary of Drogue Dimensions and Drag Areas.....	64
12	Drogued Buoy Velocity Vectors During Sea Test.....	67
13	Velocity Vectors of Surface-Drogued Buoy and Wind During Sea Test.....	70
14	Weather Conditions Recorded at Eastern Point, Gloucester During Sea Test.....	71
15	Weather Conditions Recorded at Boston Lightship During Sea Test.....	72
16	Effective Wind Forces on Test Buoys During Sea Test...	76

LIST OF TABLES (cont.)

<u>Table</u>		<u>Page</u>
17	Slip Velocity Relative to Surface Buoy and Corrected True Surface Current During Sea Test.....	77
18	Drogued Buoy Slip Velocities Relative to True Surface Current.....	78
19	Surface Current Forces on Drogued Buoys.....	79
20	Drogue Slippage Forces on Nova Buoy and Float.....	80
21	Drogued Buoy Slip Velocities.....	81
22	Estimate of True Current at Drogue Depth.....	82
23	Summary of Computerized Drogued Buoy Trajectory Iterations and Drogue Drag Coefficient Sensitivity Study.....	95
24	List of Measured and Inferred Average and Maximum Velocities During Drogued Ocean Test.....	97
25	List of Inferred Velocity Ratios From Measurements Made During Drogued Ocean Test.....	97
26	Summary of Surface and Deep Currents as Well as Slip Velocity Averaged Over Buoy Trajectories.....	98
27	Ratios of Total Slip, Water Parcel, and Wind Velocities for Surface and Deep Currents.....	100
28	One-Hundred Second Average Values of FVR Data for First Four Bursts.....	104
29	Summary of Measured Euler and Azimuth Angles of Drogue Top Spreader Bar... ..	105
30	Summary of One-Minute Average Values of FVR Euler Angles and Estimate of Drogue Horizontal Drag Force	107
A-1	Drogued Nova Buoy Position Data.....	123-124
A-2	Drogued Float Position Data.....	125-126
A-3	Surface Drogued Float Position Data.....	127-129

SECTION 1

INTRODUCTION

During the year 1974-1975, a number of tests have been conducted, all aimed at measuring the performance of a window shade drogue. The goals of the tests have been the following:

- 1) Measure the drag coefficient of a full-scale window-shade drogue under ideal conditions and compare with values derived in scale-model tests.
- 2) Measure the slippage velocity of a window-shade drogue at sea while coupled to a Nova buoy.
- 3) Measure the vertical drag coefficient of a window-shade drogue.
- 4) Attempt to correlate the slippage velocity and associated drogue forces to the environmental forcing parameters (wind, waves, currents, etc.) in an attempt to get a first-order corrective scheme of general applicability to the oceanographic community.

In the process of working towards the above goals, a useful tool for measuring the forces and dynamic motion of a window-shade drogue has been developed. This instrument is called a Force Vector Recorder (FVR). The major source of money for the development of the FVR has been supplied by the Office of Naval Research in support of the Draper Laboratory program studying mooring dynamics. This instrument is described.

Based on tests and analysis carried out on scale-model drogues in the previous year's contract, a number of general guidelines had been developed to be used in the ocean. These guidelines were applied to the design of a full-scale drogue. The analysis and details of this design are presented herein.

In working towards the achievement of the above-stated goals, a drogue slippage-measurement technique, employing high-resolution radar positioning, and appropriate computer programs for data analysis was developed. Furthermore, the usefulness of the FVR for measuring the dynamic environment of a window-shade drogue is demonstrated.

SECTION 2

WINDOW-SHADE-DROGUE DESIGN

The basic idea of a window-shade drogue is that of two large horizontal poles which are constrained by a flexible plastic material exactly like a home roll-up window shade. The shape will align itself normal to fluid flow if it is attached at the top in line with the center of the drogue and if weights on the bottom are balanced about the center. Additional design features of a large window-shade drogue to be used in the ocean are covered in this section.

2.1 Analysis

A simple analytical model of the static loads applied to a window-shade-drogue upper spreader bar can be derived by assuming the bar is uniformly loaded as shown in Figure 1. It is supported by two wires with vertical load components of R_A and R_B . There are two conditions which may lead to a static failure of the top spreader pole: an elastic instability (buckling) condition, and a tensile failure due to excessive bending stresses.

The buckling condition results from compressive loads in the support wires and is governed by the equation:

$$P_{crit} = \frac{\pi^2 EI}{l^2} \quad (1)$$

where P_{crit} is the critical compressive longitudinal load on the bar which results in buckling.

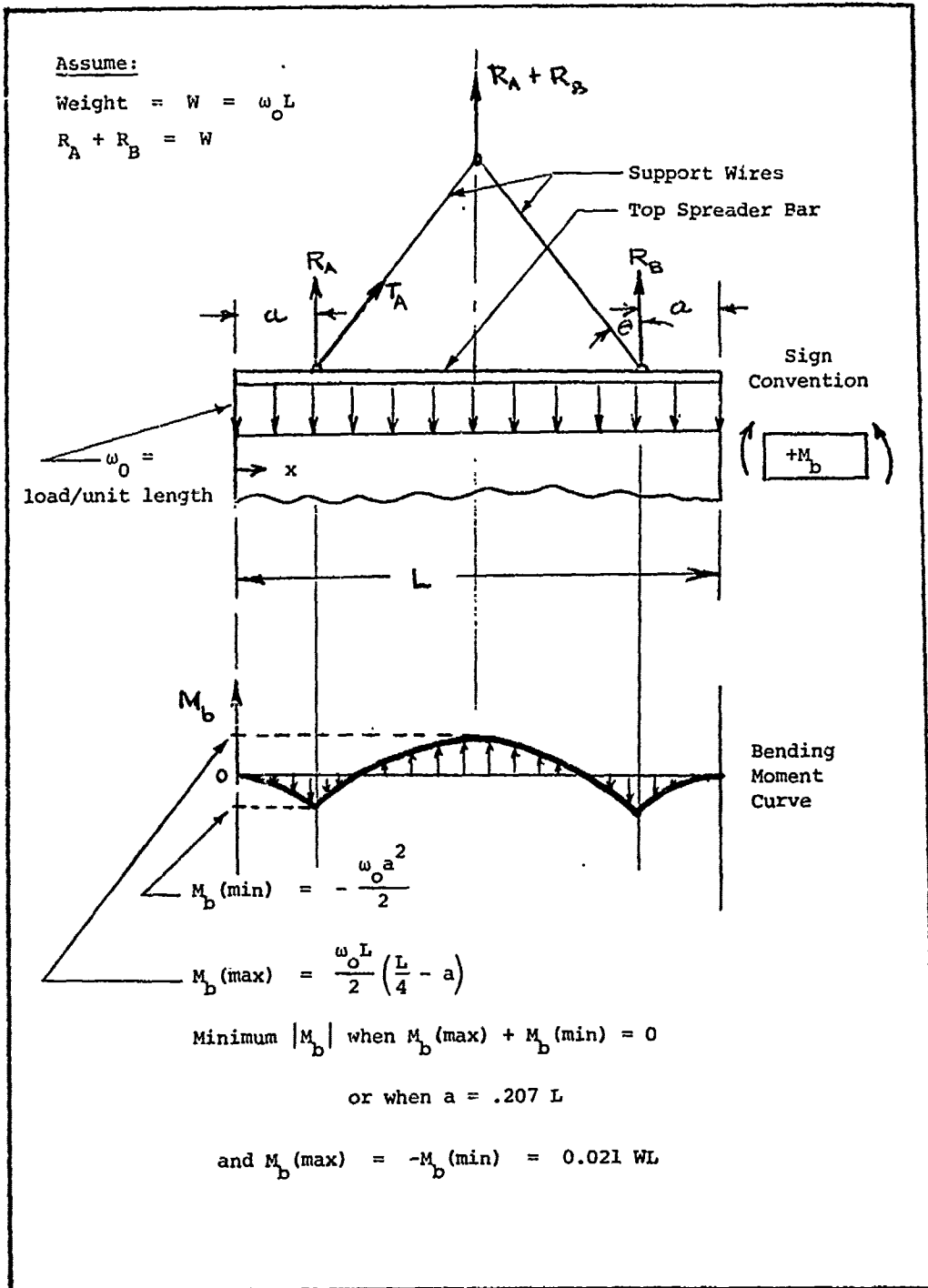


Figure 1. Window-Shade-Droge Spreader-Bar Bending Stresses

If the support wires are symmetrically mounted on the top spreader bar, and the weights within the bottom bar are uniformly distributed, then the tension values in each support wire T_A and T_B , will be equal. The loads which will theoretically give rise to a spreader bar buckling are then given by

$$P = T_A \sin\theta = R_A \tan\theta \quad (2)$$

In equation (1), for buckling in the plane of the drogue, I is the area moment of inertia of the spreader bar about the longitudinal axis in a horizontal direction ($I = .75 \text{ in}^4$). The value of Young's Modulus (E) in equation (1) is that for 6061 - T6 aluminum ($E = 10^7 \text{ lb/in.}^2$). Plugging the above parameters into equation (1), it was found that the compressive force which would bring about buckling was well above anything that could be encountered within the given design and loading.

As shown in Figure 1, the support points for the top spreader bar can be optimally located in order to minimize the bending stresses in the bar. If the force loading on the bar is given by w_0 (force/unit length), the stresses in the various components can be calculated.

The bending stresses in the top spreader bar of a window-shade drogue were calculated using the following equations:

$$\frac{\partial v}{\partial x} = -q \quad (3)$$

$$\frac{\partial M_b}{\partial x} = -v \quad (4)$$

where:

- q = load/unit length = $-w_0$
- v = shear force
- M_b = bending moment
- x = horizontal coordinate along bar as shown in Figure 1.

By using singularity functions and referring to Figure 1 it is possible to apply equations (3) and (4) to derive the general bending moment curve for the spreader bar. It should be pointed out that a family of singularity of functions can be defined as follows:

$P\langle x-a \rangle_{-1}$ = concentrated load of magnitude P
applied at $x=a$

$Q\langle x-a \rangle^0$ = Step in load of magnitude Q
beginning at $x=a$

$R\langle x-a \rangle^1$ = Ramp loading function of magnitude R
beginning at $x=a$

$S\langle x-a \rangle^2$ = Parabolic load function of magnitude S
beginning at $x=a$.

In general the above functions are related as follows:

$$\int_{-\infty}^x \langle x-a \rangle^n dx = \frac{\langle x-a \rangle^{n+1}}{n+1} \quad (5)$$

Equations (3), (4), and (5) are employed as follows (see Figure 1).

$$q(x) = -w_0 \langle x \rangle^0 + R_A \langle x-a \rangle_{-1} + R_B \langle x-(L-a) \rangle_{-1} \quad (6)$$

$$V(x) = w_0 \langle x \rangle^1 - R_A \langle x-a \rangle^0 - R_B \langle x-(L-a) \rangle^0 \quad (7)$$

$$M_b(x) = -\frac{w_0}{2} \langle x \rangle^2 + R_A \langle x-a \rangle^1 + R_B \langle x-(L-a) \rangle^1 \quad (8)$$

Equation (8) is plotted in Figure 1 for the case of a variable a . Two maxima in the bending moment (M_b) occur as shown in Figure 1. One is positive and the other is negative. If $a=0$ (i.e., the support wires are

suspended on the ends of the spreader bar), the bending moments are all positive and a maximum of $M_b(\text{max}) = \frac{1}{8} WL$ occurs at the center of the bar. If $a = \frac{L}{2}$, the bending is all negative and equal to $M_b(\text{min}) = -\frac{1}{8} WL$. Both positive or negative bending stresses are assumed to be equally bad for an assumed isotropic material in the spreader bar.

A condition of minimum bending stress exists when:

$$M_b(\text{max}) + M_b(\text{min}) = 0 \quad (9)$$

The parameter, a , which satisfies equation (9) is $a = .207 L$. In this case

$$M_b(\text{max}) = -M_b(\text{min}) = .021 WL \quad (10)$$

Equation (10) can be used in selecting the proper spreader-bar size and material.

2.2 Model Testing

A drawback to easy deployment of a window-shade drogue is that large dimensions on the spreader bars make drogue-launching a somewhat cumbersome and time-consuming operation. This is especially true for "ships of opportunity" which, it is hoped, will be able to launch drogued drifting buoys. In order to facilitate the handling and enable almost a drogue self-deployment when the buoy is put in the water, it is desirable to have a drogue whose width is on the order of 7 feet wide. With such a dimension the drogue can easily store alongside and attach to the lower cylindrical section of the Nova hull during deployment. It is felt that the drogue can then self-deploy within a few minutes by the dissolution of a fastener.

In order to keep the drogue area high in order to couple well to currents, a narrow drogue necessitates a long vertical dimension. Questions then arise as to whether a drogue, with a large length-to-width ratio, will align itself perpendicular to the flow. It is wondered whether the drogue may flutter like a ribbon in a breeze if it becomes too narrow.

In order to explore these questions, tow tank tests of five scale-model window-shade drogues of varying length-to-width (l/w) ratios were conducted in the MIT Ship Model Towing Tank.

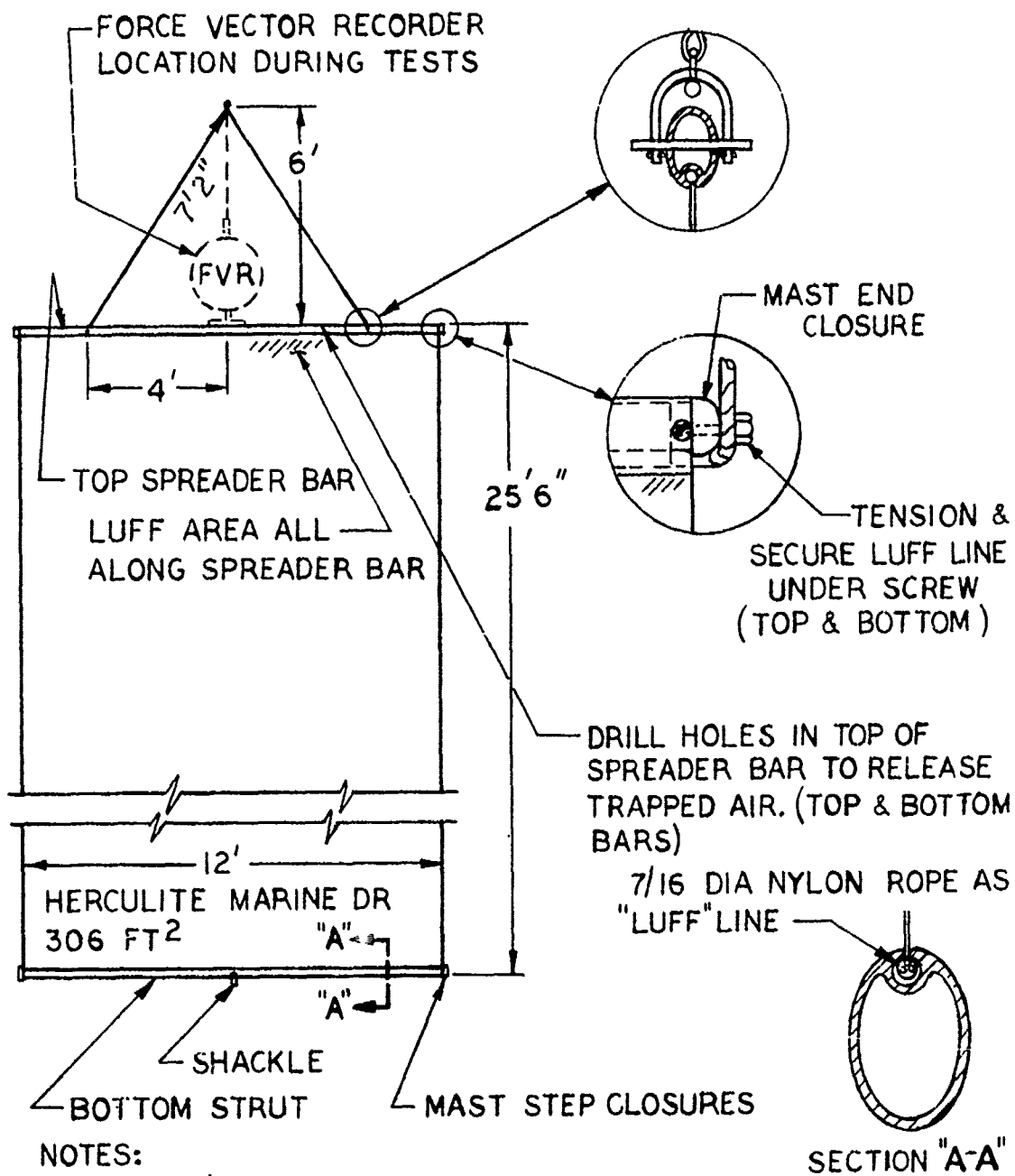
The l/w ratio was varied from 6 to 38 in model sizes whose vertical dimension did not exceed 38 inches. It was found that all models streamed normal to the flow at test speeds of 0.1 to 0.14 knots. Based on these brief tests, drogues were constructed at Nova University with dimensions of approximately 5 ft x 50 ft and tested in the Gulf of Maine by Dr. Bill Richardson.

2.3 Full-Scale Drogue Description

Over and above the basic desire to build a drogue that is cheap, easily fabricated, easy to deploy, and locks to the water mass, it is desirable that the drogue survive for a useful life in the ocean. This becomes a very practical engineering problem once the general drogue configuration and area is chosen.

Many points pertinent to the survivability of a drogued buoy were discussed in Vachon (1973). The appendices to that report endeavor to quantify conditions under which a drogue might swamp a buoy or alternatively lead to "shock" loading conditions in the buoy tether line.

A full-scale window-shade drogue was designed and built with the desire to maximize the strength, as analyzed in the previous section, and yet minimize drag due to motion in the vertical direction. Figures 2 and 3 give details of the window-shade-drogue design. Faired nautical spars were employed for the top and bottom poles of a 12 ft x 26 ft rectangular drogue. The faired poles give a maximum bending stiffness while minimizing drag to motion parallel to the plane of the drogue. This feature should reduce the drag coefficient to vertical motion and thus the dynamic loads on the buoy and tether line. The Herculite plastic was supported on a rope (7/16-inch dia.) which slides within a 9/16-inch-dia. groove in the spars. This feature distributes the stresses at the transition point between drogue and spar.



NOTES:

1. INSTALL BALLAST WEIGHTS WITHIN BOTTOM STRUT & CONTAIN WITH MAST STEP END CLOSURES.

Figure 2. Window-Shade-Drogue Design

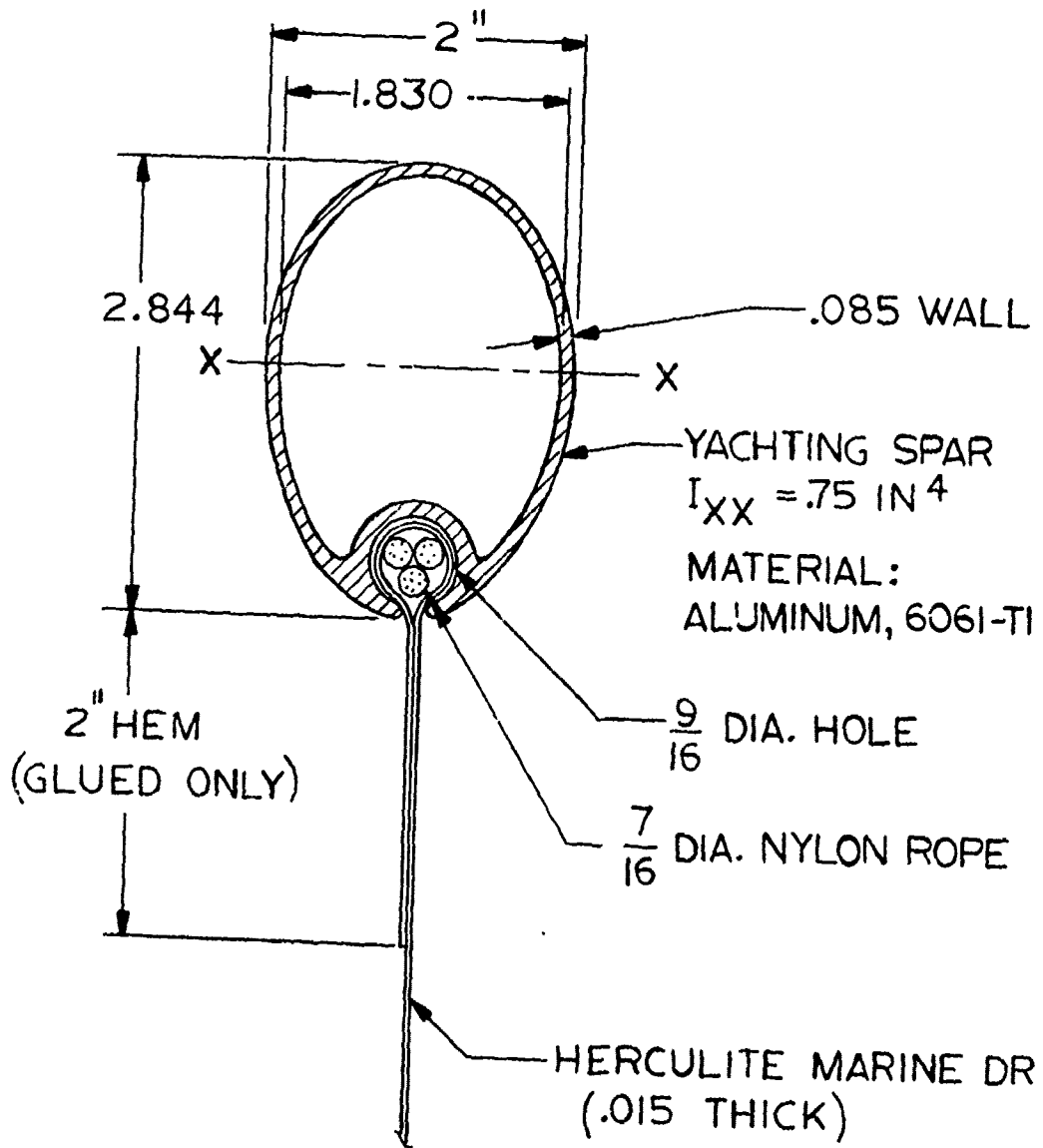


Figure 3. Window-Shade-Drogue Spreader Bar (Section Showing Herculite Mounting to Aluminum Spar)

The drogue design is straightforward and simple. The triangular area at the top of the drogue is not filled with plastic because it would, in general, cost more money to fabricate, while only adding a small percent to the total area, and would somewhat complicate the drag data analysis later. Standard nautical mast-step closures were used for the ends of the struts (both top and bottom). As shown in Figure 2, the mast-step closures close the ends of the bottom strut such that different ballast weights can be stowed safely within. The rope within the groove was left longer than the spar to enable one to pull tension in the drogue "luff" (i.e., the drogue area adjacent to the spar). The Herculite plastic was glued to the nylon rope as it was doubled back and glued to itself in order to make a secure hem at both top and bottom. The rope was thus secured within the hem such that tension in the rope pulled tension in the Herculite. The excess rope at the ends of the grooves was secured under screws tapped into the mast end closures.

The spars themselves, made of 6061-T6 aluminum, were distributed through the Zephyr Co. in Wareham, Mass. The spar size shown in Figure 3 cost \$3.80 per linear foot in the spring of 1974. As drogue widths are reduced, the spar lengths and strengths can be reduced, thus dramatically reducing this component of drogue cost.

2.4 Drogue Material

The Herculite plastic employed in the drogue was purchased in the spring of 1974. Its cost was then 18.5 cents per square foot (i.e., \$1.67/yd.²) It came in standard bolt widths of approximately 5 feet. Wider dimensions were easily fabricated with factory-glued joints at no extra cost. A 2-inch lapped and glued joint was avoided to develop the full strength of the fabric. The Herculite material chosen was the Marine DR grade because of its avoided better properties in sea water and substantial thickness (.015-inch thick). Other Herculite fabrics were available but most of them were thinner and not specifically designed for a marine environment.

Numerous samples of Herculite plastic sheet (PVC with nylon mesh reinforcement) were tested in the North Atlantic (location: approximately 28°N, 70°W) for extended periods of time. Only two types of Herculite were

placed in the ocean (Number 6 and Marine DR) along with samples of plastic coated nylon rip-stop, nylon cloth, and taffeta. All samples were returned in apparently the same condition in which they were installed. Only the Herculite samples were tested in the laboratory. The Herculite people in New York conducted a Mil Standard test CCC-T-191b free of charge on all samples whose history is summarized in Table 1. The breaking and tear strength of the materials was found to be unchanged. The only observed change was that the material was slightly stiffer. With these results in view of the lower cost per unit area of Herculite over the other fabrics tested, it was decided to construct the drogues of Herculite Marine DR fabric.

Table 1. Herculite Fabric Test Summary

<u>Sample No.</u>	<u>Depth (Meters)</u>	<u>Approx. Duration in Water</u>
1 (6 & DR)	500	June - December '73 - 165 days
2 "	500	March - June '73 - 100 days
3 "	1000	" "
4 "	1500	" "

It should be pointed out that more recent tests on the survivability of drogued buoys in the ocean were conducted in the Gulf of Maine under severe conditions by Dr. William S. Richardson of Nova University. The drogue design was essentially the same as that in the previous section although narrower (approximately 5 feet wide). The results of the tests are at present still very sketchy because Dr. Richardson and four other investigators were not officially seen again after they went to sea on Jan. 3, 1975 to retrieve drifting buoys and drogues. At that point in time the test data in substance showed that Herculite Marine DR fabric was not rugged enough to survive more than approximately 10 days while coupled to the Nova buoy. After testing many fabrics, it appears that a nylon canvas called "duck" is perhaps the most acceptable alternative. It is a rather heavy (9 oz. per square yard) sheet which, unlike Herculite, should support loads with nearly every fiber. It appears that Herculite supports nearly all its loads by a nylon cloth mesh which is imbedded in a matrix of polyvinyl chloride (PVC). Thus it is felt that Herculite is substantially weaker. The ocean materials tests described above indicate that under the given conditions nylon (as tested with nylon rip-stop) will survive as well as Herculite.

It was later decided that additional wires should be installed along the sides of the drogue between the top and bottom spreader bars in order to support the dynamic loads imposed by the ballast weight.

SECTION 3

FORCE VECTOR RECORDER (FVR) DESIGN

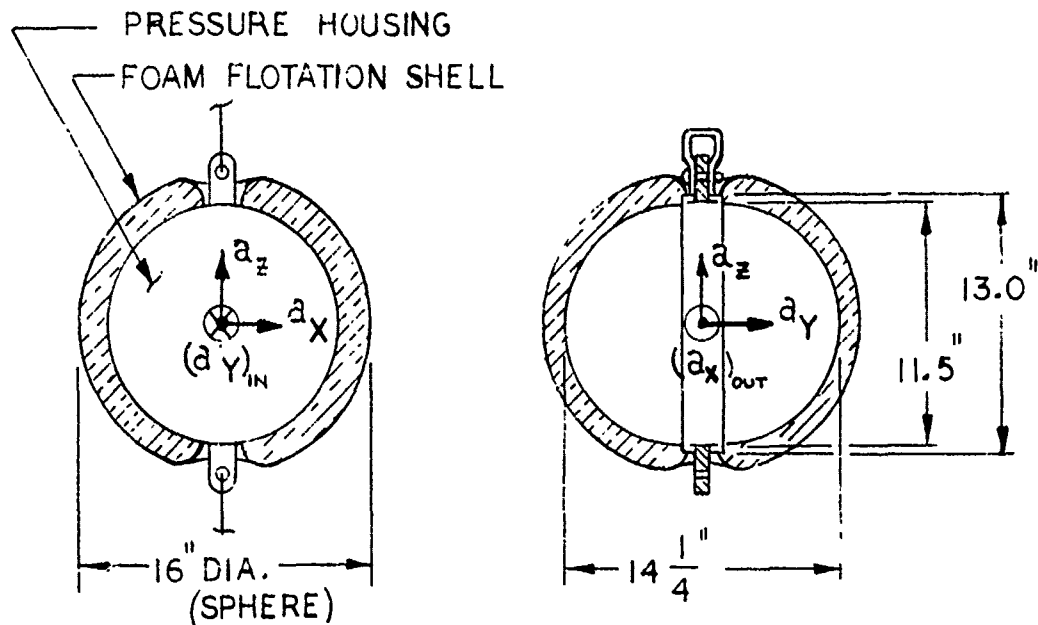
One method of measuring the drogue performance during the sea test was by an instrument mounted at the top spreader bar of the drogue. It was hoped that this instrument would, in essence, measure the horizontal component of drag force acting on the drogue as well as any dynamical input to the top of the drogue.

3.1 FVR Description

The FVR is a modified self-recording temperature/depth sphere, developed by the Draper Lab for the MODE program. The instrument package is altered in appearance and function in order to measure and record accelerations in three orthogonal directions, mooring line azimuth rotation angles, and pressure. Force balance accelerometers with a dynamic range of up to 1g are used to measure the accelerations. Two low-power-consuming magnetometers are used for the angle sensing devices. Finally, a high-sensitivity strain gauge pressure transducer is employed to measure absolute pressure.

The two accelerometers with their sensitive axes perpendicular to the mooring line are used to measure both the average as well as the dynamic excursions of the mooring line inclination angle under most circumstances. The pressure sensor, with a suitable pressure range, can measure the vertical excursions of the drogue in the water column. It was hoped that the data derived from the FVR, while mounted to a full-scale drogue in an ocean test, would provide valuable baseline data for future coupled dynamic math models of the buoy-tether line-drogue combination.

The instrument physically appears much like a sphere with a short cylinder interposed between hemispheres as shown in Figure 4. It contains all power, digitization, and recording capabilities within a pressure housing.



SPECIFICATIONS

<u>Measurement</u>	<u>Sensor</u>	<u>Max. Avail.</u>		<u>Resolution</u>
		<u>Range</u>	<u>Freq. Resp.</u>	
Acceleration (3 - axes)	Force Balance Accelerometer	±1 g	0-1 Hz	.001 g
Angular Change (2 - axes)	Magnetometer	0-360° Azimuth	0-1 Hz	~.1° (max.)
Pressure	Strain gage bridge	0-100 [†] psia	0-1 Hz	.0003 of full scale (**)
Tension (*)	Strain gage bridge	0-10,000 lbs.	0-1 Hz	.0003 of full scale (**)

CAPABILITIES

Pressure.....10,000 lb/in.² max. external working pressure
 Life.....To approximately 6 months on internal batt. pack
 Data recording..Burst or continuous mode @ max. rate of two 6-word scans/s (10-bit words)

(*) At present the inclusion of a tension measurement would necessitate sacrificing the pressure measurement. Tension sensor is readily adaptable but not included in the present design.

(**) Full-scale output selected for optimum accuracy and range in any application.

† Pressure sensors with ranges to 10,000 psig can be employed.

Figure 4. CSDL Neutrally Buoyant Force Vector Recorder (FVR)

3.2 FVR Capabilities

In order to understand how the FVR measures drogue drag force, it is necessary to define some basic equations relating to the sensor-drogue combination. If θ is the tilt angle of the tether line at the top of the drogue, ϕ the azimuth rotation angle of the inclined tether line, and ψ the azimuth angle of the top spreader bar of the drogue relative to north; the output of the two accelerometers normal to the mooring line in body-fixed coordinates for a static situation is the following (see Appendix D):

$$f_x = g \sin\theta \sin\phi \quad (11)$$

$$f_y = g \sin\theta \cos\phi \quad (12)$$

Equations (11) and (12) assume that the accelerometers are specific force receivers obeying the relation:

$$\vec{f} = \text{specific force} = \vec{a} - \vec{g} \quad (13)$$

where \vec{a} arises from linear accelerations and \vec{g} is the gravity vector, assumed to act vertically downward. The angle ϕ is defined as a rotation of the instrument x-y plane about its inclined body z-axis such that the positive x-axis rotates in the direction of the positive y-axis (i.e., a right-handed system, as shown in Figure 22).

By squaring and adding equations (11) and (12), the ϕ terms drop out leaving:

$$f_x^2 + f_y^2 = g^2 \sin^2\theta. \quad (14)$$

Therefore, the two accelerometer outputs, when properly combined in a simple electronic circuit (i.e., the square root of the sum of two squares) gives a measure of the inclination angle at the top of the drogue. This angle is related to the drag force through the following two relationships:

$$\tan \theta = \frac{F_D}{W-L} \quad (15)$$

and

$$L = F_D \tan\left(\frac{\theta}{2}\right) \quad (16)$$

where

F_D = horizontal component of tether line
tension = drag force

W = weight of drogue + ballast weight

L = lift force on drogue.

Equation (16) is an empirically derived relationship (Vachon, 1973) which seems to hold true for smaller values of θ . As θ approaches 90° , it is felt that equation (16) is not as valid as for values of θ up to approximately 40 to 60° . If properly designed and ballasted, a drogue tether line should never really reach high angles anyway. As a result, equation (16) is felt to be valid.

The combined weight of the drogue and ballast weight in equation (15) is the weight in water of everything below the tether line. It should be measured accurately because it is an error term in the drag measurement.

The combination of equations (15) and (16) results in the expression

$$F_D = W \left[\frac{\tan\theta}{1 + \tan\theta \tan\left(\frac{\theta}{2}\right)} \right] \quad (17)$$

This expression can be greatly simplified to the following:

$$F_D = W \sin\theta \quad (18)$$

This simple expression neglects tangential drag on the drogue, which should be small compared to the horizontal drag (F_D) for small values of θ . The tension in the tether line at the top of the drogue (T) also gives rise to a horizontal component of drag in a form $T \sin\theta = F_D$. By comparing this result with equation (18), it appears that to a good first approximation the tension in the tether line will be constant. This fact led to the selection of accelerometers instead of a tensiometer for measuring F_D because, to a first approximation, the line tension will be equal to the weight of the drogue in water.

A sensitivity analysis can be run on equation (18) for realistic values of W and θ which may be encountered in the test. An error in the drag force, F_D , as calculated by equation (17) is represented as follows:

$$dF_D = \left(\frac{\partial F_D}{\partial \theta} \right) W d\theta + \left(\frac{\partial F_D}{\partial W} \right) \theta dW \quad (19)$$

This gives:

$$dF_D = W \cos\theta d\theta + \sin\theta dW \quad (20)$$

The errors in the ability to measure θ and W are represented by $d\theta$ and dW . It is assumed at present that the weight of the drogue and ballast can be weighed to 1% off a dock (i.e., $dW = .01W$). Therefore $dW = 1$ pound for $W = 100$ pounds. The value of $d\theta$ derived by rewriting equation (14) as follows:

$$\sin\theta = \frac{1}{g} \left[f_x^2 + f_y^2 \right]^{1/2} \quad (21)$$

for which:

$$d(\sin\theta) = \frac{1}{g^2 \sin\theta} \left[f_x df_x + f_y df_y \right] \quad (22)$$

Substituting equations (11) and (12) in (22) gives:

$$d(\sin\theta) = \frac{1}{g} \left[\sin\phi df_x + \cos\phi df_y \right] \quad (23)$$

According to vendor catalogs the maximum total error in f_x and f_y is approximately .1% of the full scale reading. For this experiment lg accelerometers will be used, giving $df_x = df_y = .001g$. Equation (23) can be

further maximized if $\phi = 45^\circ$. Substituting these values in equation (23) gives:

$$d(\sin\theta) = .001414$$

or

$$d\theta = \frac{d(\sin\theta)}{\cos\theta} = \frac{.001414}{\cos\theta} \quad (24)$$

When equation (24) is substituted into (20) along with the relation $dW = .01W$, the following is derived:

$$dF_D = W(.001414 + .01 \sin\theta) \quad (25)$$

Equation (25) says that the maximum error in the drag force measurement is a linear function of the ballast weight. Table 2 summarizes dF_D as a function of θ for various values of W .

Table 2. Summary of dF_D as a Function of θ for Various Values of W

θ	dF_D (Pounds)		
	$W = 50$ lbs	$W = 100$ lbs	$W = 150$ lbs
2°	.085	.17	.26
4°	.105	.21	.317
6°	.125	.25	.37
10°	.155	.31	.47
15°	.2	.4	.6
20°	.24	.48	.72
30°	.32	.64	.96

By the suggested method of data handling [equation (21)], it is possible to get measurement errors due to linear accelerations of the sphere itself [see equation (13)]. If the problem is assumed to be planar with the drogue top spreader bar horizontal, accelerations of a_x , and a_z , in inertial space are assumed. The subscripts x' and z' refer to horizontal and vertical (down) respectively, both in the plane of the tether line. The specific force sensed by the accelerometers is as follows:

$$f_x = \sin\phi(-g\sin\theta + a_x\cos\theta - a_z\sin\theta) \quad (26)$$

$$f_y = -\cos\phi(-g\sin\theta + a_x\cos\theta - a_z\sin\theta) \quad (27)$$

When combined in the form of equation (21) and simplified, the following result is obtained:

$$f_x^2 + f_y^2 = g^2\sin^2\theta + (a_x^2\cos^2\theta - 2a_xa_z\sin\theta\cos\theta + a_z^2\sin^2\theta) \quad (28)$$

It can be seen that the signal being sought (i.e., $g^2\sin^2\theta$) is hidden amidst other signals arising from linear accelerations. If it is assumed that the accelerations are simple sinusoidal motion, those acceleration terms which are squared will still contribute to an increase in the time average of the whole equation.

As a result of this analysis it is shown that extreme care must be taken in designing the experiment. A minimum of dynamic excitation from the surface buoy is very important in order to make accurate measurements of mooring line inclination angle. In order to explore the sensitivity of FVR sensor errors to drogue motion, a mathematical computer simulation of buoy-drogue dynamics was created. It was assumed that an FVR was attached to the drogue-to-spreader bar. It was found that, for the assumptions of planar (two-dimensional) motion with zero mean acceleration, the Euler angles sensed by the FVR (after processing in the same manner as real data) were within a small part of a degree to the "real" simulated values from the dynamic response. Even at higher sea states, it is felt that the errors would still be small. The case being simulated was a 2-foot sea with the same conditions as the test to be described in Section 5.2.

3.3 FVR Design Considerations

In order to analyze the accelerometer outputs in a simple manner, as a means of measuring mooring line inclination, the FVR had to be very nearly neutrally buoyant with its center of buoyancy and center of gravity coincident. The desire for neutral buoyancy helps to ensure that the FVR mooring line attachment points will be in line with the mooring line for the case of moorings with low tension. This would not be such a strong consideration if mooring line tensions were greater than a few hundred pounds.

If the sphere is negatively buoyant (i.e., its normal condition) it will appear as a discontinuity in the mooring line which is proportional to the weight, line tension, and location of the CG. As the surface buoy moves up and down, the mooring line tension can change which would alter the discontinuity angle of the sphere. Such changes produce signals on the accelerometer output (due to pure angle change) which could be interpreted as accelerations. The opposite is true also. That is, vertical and horizontal accelerations at the sphere will be sensed as periodic ripples on top of the steady signals [equations (11) and (12)].

The CG and CB should be coincident because, when the sphere undergoes motion in response to buoy or tether line motion, the inertia and drag forces should act through the same point. The drag forces are assumed to act through the CG. If these points are separated, a force couple will be formed which will tend to rotate the sphere during accelerations. If the rotations of the sphere are at the same frequency as linear accelerations, a non-linearity can exist in the measurement system which can give rise to errors in the form of biases to the signal from an accelerometer sensitive to the direction of acceleration.

SECTION 4

CONTROLLED FULL-SCALE TESTS

The shallow water test of a window-shade drogue was conducted in a setting such that as many parameters as possible were controlled or measured. The primary goal of the test was to measure the drag coefficient of a full size window shade drogue and compare it with the value $[(C_D)_0 = 1.93]$ derived in the scale-model tests. Other goals of this experiment were the following:

- 1) Attempt to observe the dynamic angular response of the drogue to currents in different directions.
- 2) Check the performance of the Force Vector Recorder under steady and dynamic loads.
- 3) Calibrate the Force Vector Recorder as a device for measuring horizontal forces on the drogue.
- 4) Verify the mathematical model of a drogue inclination angle as a function of drag force.

4.1 Test Description

The tests were conducted in shallow water on a calm day in an attempt to minimize spurious effects. The overall test can be broken into four parts as shown in Figure 5. The first two parts are tests to ascertain the effects of wind and currents on the test. The first test involved ballasting the float with the same weight found in later tests such that the float was submerged by the same amount. This constraint provided the same wind and

Test Description

- (1) Test for presence of surface currents and wind drift
- (2) Test for deep currents
- (3) Calibrate drag of sphere and weight by measured tow (i.e. measure tension & \dot{R})
- (4) Calibrate drag of drogue by measured tow.

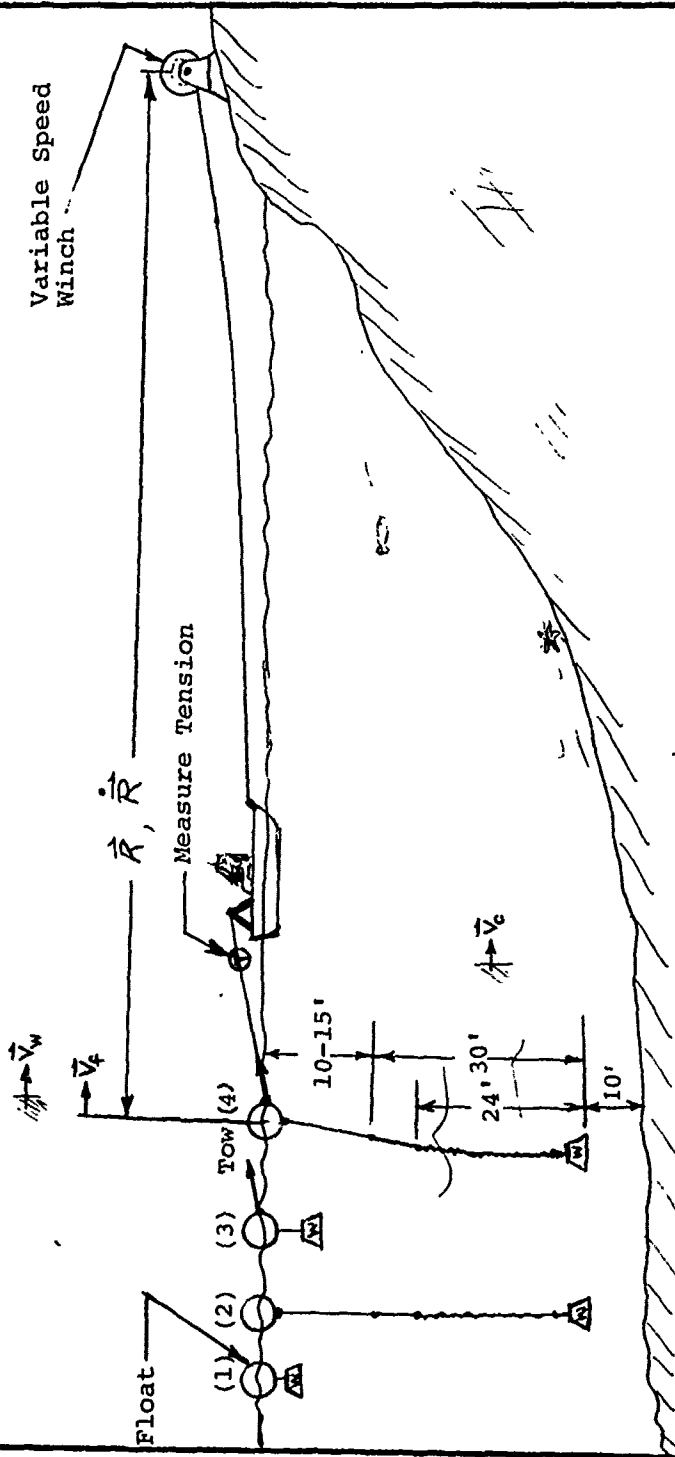


Figure 5. Shallow Water Tests of Window-Shadow Drogue

surface current coupling as in other tests. The float was a plastic barrel which minimized the surface drag. In the second test the drogue was ballasted and placed at its design depth in order to measure the true currents present. A comparison of the drift trajectories, as recorded by shore-based visual tracking in these two tests, gave insight into the conditions existing in the test basin, for which corrections must be included. It was found that in all tests wind and surface current effects were negligibly small.

Tests 3 and 4 were tests in which a drogued and undrogued float is towed through the water by a boat which in turn was towed at a constant speed by a shore-based winch. The tension required to tow each configuration is measured by a spring scale force gauge and visually recorded aboard the boat. The speed of the tow was measured by pulling a measurable amount of rope through the winch capstan over a measured period of time.

Test 3 was a calibration tow in which the drag force of the float and ballast weight were measured while riding at the same water depth as in test 4. Test 4 measured the drogue performance according to the equation:

$$F_D = \frac{1}{2} \rho V_{rel}^2 C_D A \quad (29)$$

for which all parameters are known except C_D .

It was found that low-speed towing tests could really only be conducted when wind conditions were very calm (5-10 knots). This was true because higher wind velocities would, when not directly on the bow or stern of the towing boat, cause the boat to veer from its towing path. Such motion would cause the drag force measurements to be erratic. Therefore, for all tests in which the data were valid, the effects of wind and also surface currents were negligible.

The final test shown in Figure 5 is that of towing the full-scale drogue at a measured speed with the application of a measured horizontal force in a body of water whose wind and current effects are negligibly small. If the float and drogue combination shown in test 4 of Figure 5 is pulled by a tension force, T , at a velocity, \vec{v}_f , the following equation applies:

$$\vec{T} + \frac{1}{2} \rho_{\text{air}} (C_D A)_{\text{float above}} (\vec{v}_w - \vec{v}_f) |\vec{v}_w - \vec{v}_f| + \frac{1}{2} \rho_w (C_D A)_{\text{float below}} (\vec{v}_s - \vec{v}_f) |\vec{v}_s - \vec{v}_f| + \frac{1}{2} \rho_w (C_D A)_{\text{drogue}} (\vec{v}_c - \vec{v}_f) |\vec{v}_c - \vec{v}_f| = 0 \quad (30)$$

All items in equation (30) should be known except $(C_D)_{\text{drogue}}$. The induced drag forces in relation to the ballast weight and drogue area were in most cases not small enough to assume that C_D is constant. In these cases the drag coefficient is governed by the relation:

$$C_D(\theta) = (C_D)_0 \cos^3\left(\frac{\theta}{2}\right) \quad (31)$$

In this equation, the value of θ is determined from equation (18), where F_D is measured on the stern of the towboat and W , the weight of all drogue elements beneath the top spreader bar, is measured independently.

In the last controlled full-scale drogue test (i.e., quarry test 2) the FVR is connected to the top spreader bar in order to measure θ . The validity of employing equations (18) and (31) as a model of the drogue performance as a function of θ is then verified.

4.2 Walden Pond Test

On 11 and 12 April 1974, a series of towing tests was conducted on a 312-square-foot full-size window-shade drogue. The tests were conducted from the main dock of Walden Pond in Concord, Massachusetts. Walden was selected because of the desired depth in close proximity to a dock. The availability of electrical power and a row boat were also strong site advantages.

On the first day the test apparatus and drogue were assembled on site and checked out. A weighted line was used to explore the bottom topography of Walden and find the proper spot with adequate water depth. A pothole with a 59-foot depth reading was found approximately 175 feet from the dock at about a 25 degree angle from the front of the dock.

Brief tests were conducted but no meaningful data was derived because of the weather conditions. A 20-30 knot wind out of the west combined with severe chop to produce impossible test conditions.

On the second day the wind was very light and the water flat calm. Approximately seven meaningful towing tests were conducted on that day as described in Table 3. Other test results are not reported because either the drogue azimuth angle was very bad or the drogue ran aground.

It can be seen in Table 3 that the test data cover a Reynolds number range of 1.6 to 3.8×10^5 . The Reynolds number $\left(\frac{VL}{\nu}\right)$ in all cases is based on the drogue width (i.e., $L = \text{Width}$). The average drag coefficient, C_D , is computed using equation (29) where A is the full drogue area of 312 ft². Table 3 also shows that there is considerable scatter in the drag coefficient data. It is felt that part of the scatter, on the low side, is due to the drogue progressing through the water at an acute angle to the drag direction. In these cases it is felt that if the drogue were towed a greater horizontal distance it would have straightened out. Such was not possible because the drogue would soon run aground if towed very far. The area within Walden pond which contained water of adequate depth was not as extensive as desired. It was found that the horizontal dimensions to the test area were limited to a circle of approximately a 100-foot diameter.

The average value of the drag coefficient of a window-shade drogue, derived in tow-tank tests, was approximately 1.93. This value seems to

Table 3. Test Results—Shallow-Water Test of Window-Shade Drogue

Shallow-Water Window-Shade Drogue Test Results - Walden Pond Concord, Mass. April 11, 12, '74						
Ave. Velocity Knots	Ave. Velocity ft/sec	Width Reynolds Number	Ave. Drag Force (Pounds)	Float Drag (est.) (Pounds)	Ave. Drag Coef. C_D	Comments
.148	.25	2.7×10^5	31.5	.2	1.65	May have had angle off of normal.
.188	.318	3.4×10^5	22	.3	0.71	Bad angle during test.
.13	.22	2.4×10^5	30	.15	2.04	Gradual buildup to 30 lb drag after which it held. 82-second tow.
.115	.195	2.1×10^5	33	.15	2.87	Ave. values over 73 second tow after reaching "steady state".
.09	.152	1.6×10^5	20	.10	2.85	56-second tow.
.096	.162	1.7×10^5	22.5	.12	2.51	51-second tow.

Note: All tests conducted with total weight of 80 lbs (in water), 70 lbs at bottom.

agree in general with values reported in Hoerner (Fluid Dynamic Drag). In the tests reported herein, it was hoped that a value close to 1.9 would be derived. In Table 3 only the fourth test is close to this value. The last three are considerably higher, yet close to each other in value. It is felt that the inertia from the extremely high added mass for horizontal motion of a window-shade drogue may have contributed to the high values of C_D . It was observed in some cases that the drag force would climb rapidly to a high value for many seconds. It would subsequently diminish to a force level of approximately two thirds the maximum. This is felt to be the added mass effect. The horizontal dimensions of the test area did not permit acquiring much data after the diminution of drag force. Much of the data shown averages the drag force during this period of diminishing force.

After a test run was conducted the row boat would be rowed by hand back to the far extremities of the test pothole. Such was required because motors are not allowed on Walden Pond. Rowing a small boat with a large drogue attached was, needless to say, a futile effort at best. Progress was very slow. As a result the tests were very long and tiring.

Insufficient data were derived and a subsequent series of tests were conducted in a water-filled quarry. Such a test site afforded a larger test area with better ability to pull the drogue back towards the far shore after the conclusion of a test run.

4.3 Quarry test No. 1

On May 13, 14, and 15 a series of controlled tests were conducted on a full-scale window-shade drogue. The tests were conducted in a deep, abandoned, water-filled quarry whose dimensions afforded sufficient space for prolonged towing tests. The data derived were, in general, far superior to those derived in phase 1 tests (in Walden Pond). The results indicated that the full scale window shade drogue has on the average approximately 35% more drag (i.e., $(C_D)_O \approx 2.6$) than the scale model.

The drogue tested was the same one as reported in the phase 1 test results. It was noticed during the tests that a portion of the ballast weight, placed within the bottom horizontal pole, had shifted to one side. As will be discussed later, this weight unbalance in the drogue resulted in an acute angle at the drogue and a sideward thrust in the direction of the more heavily weighted side. Therefore, for these tests, all weights were mounted externally on the ends of the bottom pole, taking care to prevent a weight unbalance. A total of approximately 90 pounds of weight (in air) was used on the bottom bar. When implanted in the water the total drogue weight, including all hardware, was approximately 82 pounds, 76 pounds of which was assigned to the bottom bar area.

The general test setup was essentially the same as in the previous test. Figure 5 outlines the basic setup. A level spot approximately 1 foot above the water was found on which the winch was mounted. It was secured to two pipes pounded into a convenient crack in the rock in a manner analogous to mountaineers' pitons. After a failure of the power winch gearbox early in the tests, the boat and drogue were pulled by hand. A convenient timed rhythm was set up whereby a fairly constant rate of pull was established which was nearly independent of the force applied. The drag force measured off the stern of the boat and the drogue orientation were radioed to shore every 5 seconds and recorded. The test was conducted over a time span of 2 to 6 minutes such that long-term average values were measured. Once the azimuth angle of the drogue became stable the drag force values did not vary more than 10% over the duration of a given test.

The effects of surface and deep currents were checked by setting a ballasted surface float and drogued float freely adrift. It was determined that there were negligible, if any, deep currents at the depth of the drogue. Wind effects varied from one test to another but in all cases were negligible due to the low profile of the surface float.

The measured data were the total horizontal force on the drogue and float at 5-second intervals and the average tow velocity over a given test run. By knowing the full drogue area these data can be used in equation (29). What would truly be necessary in order to apply equation (29) to derive an average drag coefficient would be a knowledge of the average drag force and the average of the velocity squared. In this way, variations in the velocity during the test run would be analyzed properly.

In order to tailor equation (29) to the manner in which data were derived it is necessary to take the square root as follows:

$$\sqrt{\overline{F_D}} = \left(\frac{1}{2} \rho C_D A \right)^{\frac{1}{2}} \overline{v}_{rel} \quad (32)$$

where bars over the quantities represent ensemble averages. Thus, it is necessary to take the average value of the square root of the individual drag measurements taken every 5 seconds. The average velocity on the right side of equation (32) is a direct output of the measurement. Therefore, the drag coefficients for these tests, in which velocity was not necessarily constant, are calculated from equation (32) and tabulated in column 5 of Table 4.

The data are analyzed in order to determine the value of drag coefficient if the drogue were hanging straight down (i.e., $(C_D)_0$). In order to do this, equation (18) from the math model of the drogue is applied in order to determine an angle, θ , at the top of the drogue (Column 5, Table 4.) This value is then employed in equation (31) along with the measured value of C_D (Column 5, Table 4) in order to determine an equivalent value of $(C_D)_0$ for a given run (Column 7).

The best value for $(C_D)_0$ based on the data given in Table 4 is calculated by minimizing the total mean-square difference between the measured values of C_D , at a given angle, and the theoretical values determined by equation (31). Therefore, it is necessary to minimize the expression:

$$\sum_{i=1}^8 \left[(C_D)_i - (C_D)_0 \cos^3 \left(\frac{\theta_i}{2} \right) \right]^2 \quad (33)$$

In order to minimize equation (33) with respect to $(C_D)_0$, a derivative is taken with respect to $(C_D)_0$ and the expression set equal to zero. This gives the following expression for choosing $(C_D)_0$ in terms of the measured data,

$(C_D)_i$:

$$\sum_{i=1}^8 \left[(C_D)_0 \cos^6 \left(\frac{\theta_i}{2} \right) - (C_D)_i \cos^3 \left(\frac{\theta_i}{2} \right) \right] = 0 \quad (34)$$

Table 4. Shallow Water Window-Shade Drogue Tow Test Results—Phase 2

Shallow Water Window Shade Drogue Phase 2 Tow Test Results		Manships Quarry Gloucester, Mass. May 13-15, 1974					
Ave. Velocity Knots	Ave. Velocity ft/sec	Width Reynolds No. (VW/V)	Ave $(\sqrt{F_D})^2$ (Pounds)	Ave. Drag Coef., (C_D)	$\theta =$ $\sin^{-1}(F_D/W)$	Equiv. (C_D)	Comments and Observations (*)
.085	.143	1.29×10^5	16.8	2.73	12.7°	2.78	Total drogue wt.=82 lbs. in water(76 lbs at bot.) 355 - second run
.097	.164	1.48×10^5	20.2	2.52	15.3°	2.59	290 - second run
.099	.167	1.5×10^5	22.4	2.63	17.1°	2.72	235 - second run
.099	.167	1.5×10^5	23.4	2.81	17.8°	2.91	220 - second run
.134	.226	2.03×10^5	33.8	2.20	26.3°	2.38	80 - second run
.154	.261	2.35×10^5	44.5	2.15	35.6°	2.49	95 - second run
.187	.316	2.84×10^5	57.6	1.94	49.0°	2.55	225 - second run
.189	.32	2.88×10^5	59.8	1.94	51.5°	2.66	50 - second run

(*) Drogue Dimensions: 25.8' l. x 12.0' w., Herculite Marine DR material.

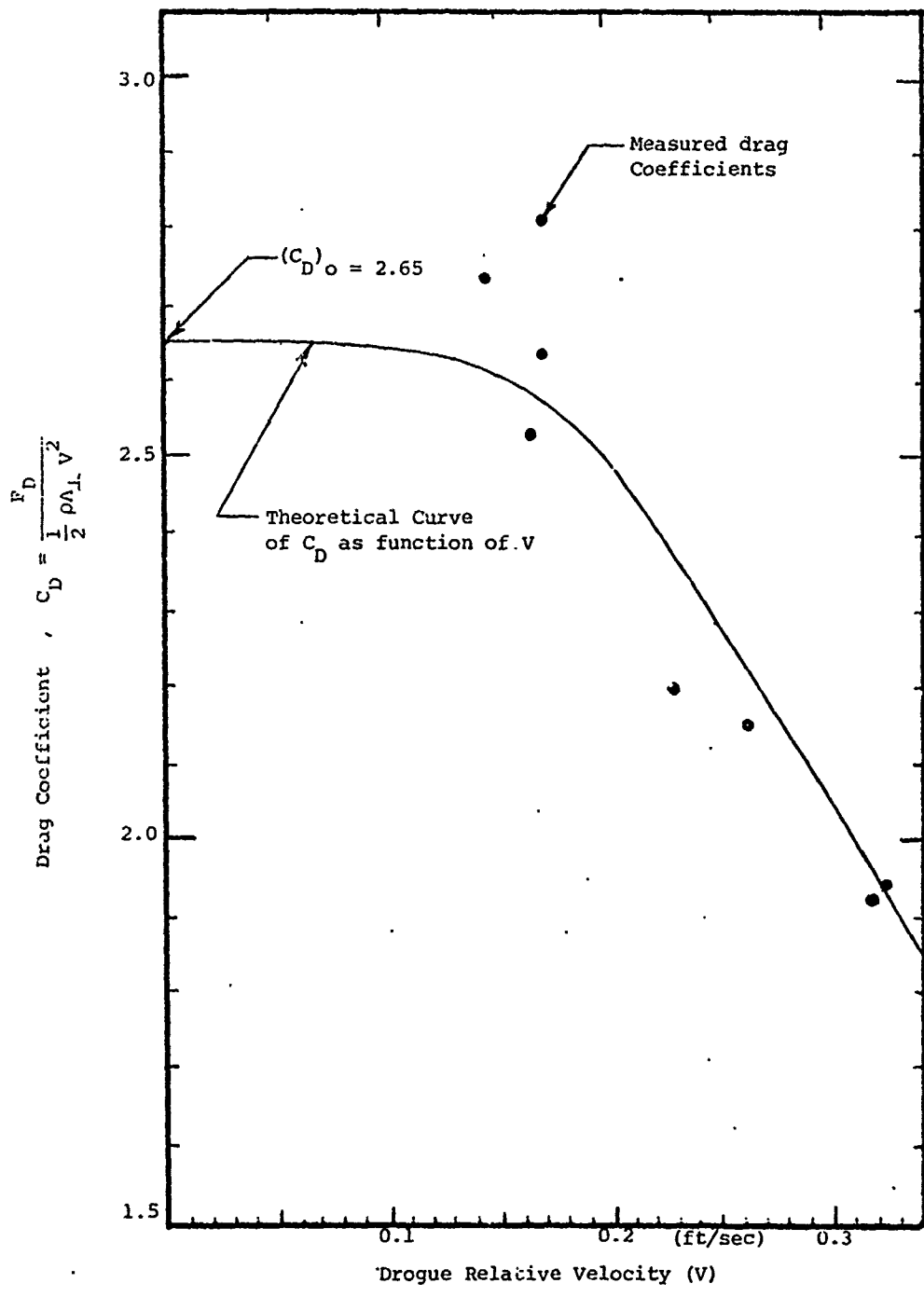


Figure 6. Window-Shade Drogu, Test Results From Full-Scale Quarry Test No. 1

Based on the data shown in Table 4, the value of $(C_D)_0$ derived by an application of equation (34) is: $(C_D)_0 = 2.65$. Based on this value of $(C_D)_0$, a theoretical curve of the C_D as a function of relative velocity, employing equation (31), is plotted in Figure 6. Also included in this figure are actual measured values of C_D . It can be seen that over the measured velocity range the theoretical curve describes the decreasing drag coefficient with increasing speed rather well.

Other more qualitative tests were also run at the same time. As mentioned earlier, a weight unbalance at the bottom of the drogue caused the drogue to stream at an acute angle with respect to the flow. The flow impinging on the drogue caused it to develop a sideways lift force in the direction of the weight unbalance. This problem can be best visualized by referring to Figure 7. This sketch shows a front view and

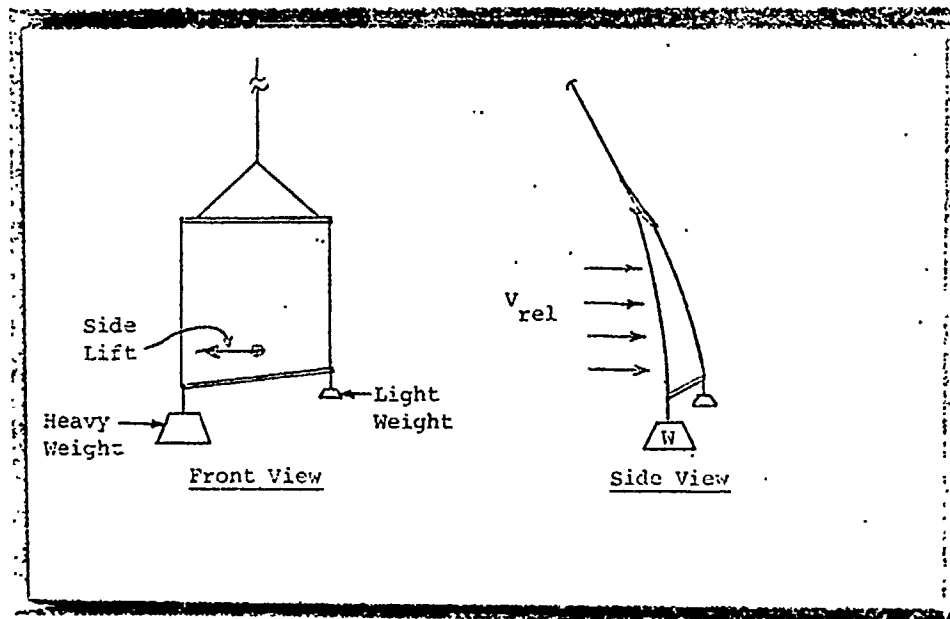


Figure 7. Effect of Unbalanced Weight on Window-Shade Drogue

a side view of a drogue. The side of the drogue with the heaviest weight will not stream as far back in the flow as the lighter side. The acute angle to the flow, thus produced, gives the side lift force shown. In order to avoid this problem which produces unwanted errors, care must be taken to ensure that ballast weights on the bottom of the drogue are at all times balanced.

A second result of a qualitative nature was observed while the drogued float was set adrift under the influence of wind and surface currents only. At the beginning of the test the drogue was lined up pointing in the direction of the wind. The 15-inch diameter \times 23-inch long float shown in Figure 5 exhibited only about 6 inches of freeboard to be acted on by a wind of between 10 and 20 knots. After 1 hour of test the drogue had moved approximately 75 feet in the direction of the wind while at the same time the drogue had begun swinging around such that it was approximately at a 45° angle to the wind and drift direction. After another 20 minutes the drogue had rotated approximately another 20 degrees and drifted another 25 feet downwind.

If a truly zero value of current existed at the drogue depth, as believed from other tests with no wind blowing, the wind force acting on the buoy caused a relative velocity by the drogue of approximately 0.01 knots (0.5 cm/s). It is believed from this test, at which time drogue ballast weights were balanced, that the drogue angular response in quiet water is sufficient to ensure that it will eventually rotate normal to the flow. Questions still remain, however, on how a drogue angular response will be affected by the wave-induced dynamics of a surface buoy coupled to the drogue.

4.4 Quarry Test No. 2

On 18 and 19 November 1974, a third series of full-scale shallow-water drogue tests were conducted. Again they were conducted in the Gloucester quarry.

It was especially important that the orientation of the tow be known relative to magnetic north because magnetometers within the FVR were used as the angle sensing devices. Therefore, a hand-held compass was employed as a reference sensor to measure the angle between magnetic north and the direction of tow.

The magnetometers were calibrated at the field site in order to obtain the magnitude of the magnetic vector and the local dip angle.

The towing test results are evaluated and displayed in Table 5 and Figure 8. The drag data, plotted in Figure 8, also display a theoretical curve of drag coefficient as a function of relative velocity. This curve is based only on the data derived in the last quarry test (test 3). It was determined based on a least-squares fit to the given data. It can be seen that the maximum value of drag coefficient, $(C_D)_0 = 2.58$, is very close to the value of $(C_D)_0 = 2.65$ derived in the previous quarry test.

Two drag data points in Figure 8 are conspicuously different from the body of other data presented. At present no firm explanation is available to explain the low drag coefficient. It is felt that because of the low force values during these runs (3.6 pounds and 7 pounds), a force measurement error due to stiction in the spring scale may have been the source of the problem. This problem did not, however, show itself in other test runs as the spring scale was able to move smoothly from one force value to another with no sudden "jumps" which might be expected if undue stiction were present. In general, it is felt that the spring scales had a force resolution of less than 1 pound.

Figure 9 shows the drogue fully deployed while being pulled by large forces getting into position for a test. This configuration is not what one would expect to find in the ocean. Figure 10 shows the drogue and FVR (a sphere) suspended stationary beneath the float. The float is attached to the stern of a boat, ready for a towing test. Drag forces are measured on the stern of the boat and values radioed to shore in real time. Tow velocities are measured at the shore-mounted winch.

Table 5. Shallow Water Window-Shade Drogue Tow Test Results—Test 3

Ave. Velocity		Width Reynolds No (VW/ν)	Ave. ($\sqrt{F_D}$) ² (Pounds)	Ave. Drag Coef. (C_D) _i	$\sin^{-1}(F_D/W)$	Equiv. (C_D) _o	Comments and Observations (*)
ft/sec	cm/sec						
.068	2.08	6.1×10^4	3.27	2.39	2.93°	2.39	344 sec. run
.069	2.09	6.2×10^4	4.12	2.87	3.7°	2.89	200 sec. run
.086	2.61	7.7×10^4	5.73	2.62	5.1°	2.63	307 sec. run
.087	2.64	7.8×10^4	3.59	1.61	3.2°	1.61	240 sec. run
.094	2.87	8.5×10^4	6.59	2.53	5.9°	2.54	360 sec. run
.10	3.05	9.0×10^4	7.11	2.40	6.4°	2.41	240 sec. run
.12	3.66	1.08×10^5	12.31	2.88	11.1°	2.92	290 sec. run
.122	3.72	1.10×10^5	10.12	2.24	9.1°	2.26	360 sec. run
.125	3.81	1.13×10^5	9.97	2.14	9.0°	2.16	462 sec. run
.125	3.81	1.13×10^5	7.01	1.55	6.3°	1.56	360 sec. run
.126	3.83	1.13×10^5	12.45	2.66	11.2°	2.70	155 sec. run
.144	4.39	1.3×10^5	16.53	2.65	15.0°	2.72	208 sec. run
.183	5.59	1.65×10^5	26.33	2.64	24.3°	2.83	300 sec. run
.193	5.89	1.74×10^5	25.84	2.33	23.8°	2.38	300 sec. run
.397	12.1	3.57×10^5	63.45	1.35	82.5°	3.18	161 sec. run

(*) Drogue Dimensions: 25.7' l. x 11.9' w.; Weight: 64lbs. (in water) at drogue bottom, Hercules Marine DR material.

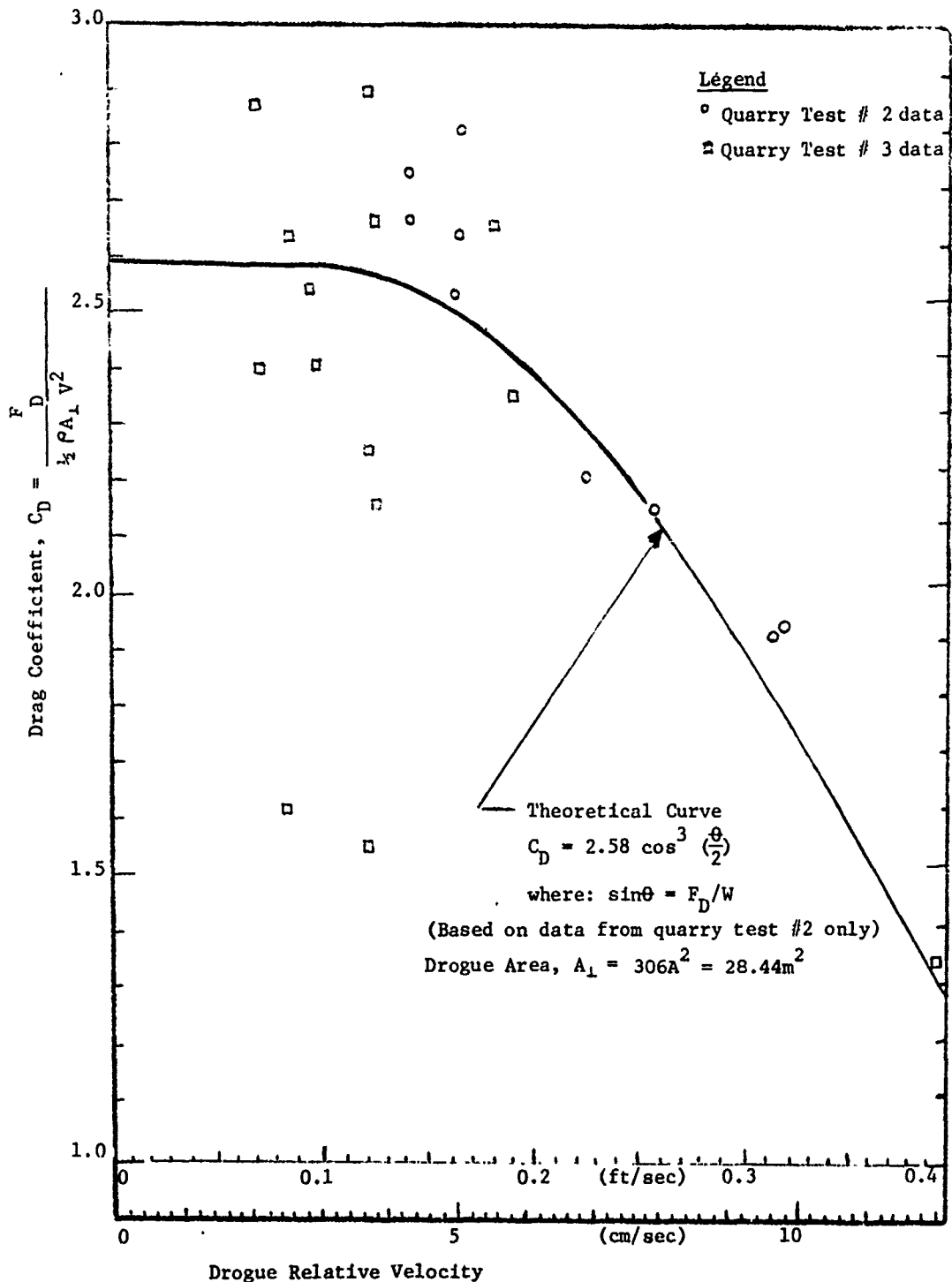




Figure 9. Drogue under Heavy Tow



Figure 10. Window-Shade Drogue Stationary in Water

The inclination angle of the top of the drogue is monitored by the accelerometers on the FVR acting as inclinometers. The two accelerometers sensitive to accelerations in a horizontal plane (when drogue hangs straight down) give outputs f_x and f_y which are employed in equation (21) in order to determine tilt angle θ . The value of the inclination angle, θ , derived from the FVR data used in equation (21) was compared with the value derived from a knowledge of the drag force F_D , and weight at the bottom of the drogue, W , employed in equation (18).

Some of the values of θ derived in the above manners during quarry test 2 were compared as shown in Tables 6 and 7. The subscripts to the θ -column refer to the equation numbers by which the values were calculated. The value of θ , and the calculated drag force in Table 6 were determined assuming a weight, W , equal to the sum of the full drogue and ballast weight (both are in-water weights). The values displayed in Table 7 were, however, calculated assuming a weight, W , equal to the sum of only one-half of the drogue weight and the full ballast weight (in-water weights). In these calculations the weight of the top spreader bar, bridle, and FVR are neglected in that they do not appreciably contribute to a moment balance which would keep the drogue vertical in the water column.

The last column in Tables 6 and 7 shows the percentage difference between the measured drag force and a calculated drag force based on the inclination angle measured by the FVR. It can be seen that, in general, the calculated drag force tends to be too high if the full drogue material weight is employed in calculating the total ballast. If, however, only one-half of the drogue material weight is employed in the calculation (Table 7), the calculation scheme, based on equation (18), predicts drag forces whose average difference with the measured forces is nearly zero. Therefore, it is felt that, in the future, when equation (18) is applied the value of W should be evaluated as the sum of the wet weights of the ballast and one-half the drogue material weight.

Table 6. Quarry Test 2 Results Compared with Results Calculated from Force Vector Recorder when Full Weight of Drogue Material (in Water) is Employed in Calculations

Test No.	Relative Velocity (cm/sec)	C _D	(F _D) _{meas} (Newtons)	θ ₁₇ [*]	θ ₂₀ ^{**}	(F _D) _{calc} (Newtons) [†]	% Diff. $\frac{(F_D)_{calc} - (F_D)_{meas}}{(F_D)_{calc}}$
10B	2.09	2.87	18.3	3.4	4.6°	24.6	25.6%
4	2.61	2.62	25.5	4.8	6.3°	33.7	24.3%
10A	3.05	2.40	3.17	5.9°	6.9°	36.8	13.8%
3	3.66	2.88	54.8	10.3°	10.6°	56.4	2.8%
5	3.81	2.14	44.3	8.3°	9.4°	49.9	11.2%
9B	4.39	2.65	73.6	13.9°	12.7°	67.0	-9.9%

* θ₁₇ = sin⁻¹ [(F_D)_{meas}/W] where W = 305.6 Newtons (68.7 pounds)

** Measured by FVR accelerometers, θ₂₀ = sin⁻¹ $\left[\frac{(f_x^2 + f_y^2)^{1/2}}{g} \right]$

† (F_D)_{calc} = W sin θ₂₀

Table 7. Quarry Test 2 Results Compared with Results Calculated from Force Vector Recorder when One-Half of Weight of Drogue Material (in Water) is Employed in Calculations

Test No.	Average Relative Velocity (cm/sec)	Meas. C_D	$(F_D)_{meas.}$ (Newtons)	θ_{17}^*	θ_{20}^{**}	$(F_D)_{calc.}$ (Newtons)	Percent Difference $\frac{(F_D)_{calc.} - (F_D)_{meas.}}{(F_D)_{calc.}}$
10B	2.09	2.87	18.3	3.7°	4.6°	22.7	19.4%
4	2.61	2.62	25.5	5.2°	6.3°	31.0	17.7%
10A	3.05	2.40	31.7	6.4°	6.9°	34.0	6.8%
3	3.66	2.88	54.8	11.2°	10.6°	52.0	-5.4%
5	3.81	2.14	44.3	9.0°	9.4°	46.2	4.1%
9B	4.39	2.65	73.6	15.1°	12.7°	62.2	-18.3%

* $\theta_{17} = \sin^{-1} \left[\frac{(F_D)_{meas.}}{W} \right]$ where $W = 282.9$ Newtons (63.6 pounds)

** Measured by Force Vector Recorder Accelerometers, $\theta_{20} = \sin^{-1} \left[\frac{(f_x^2 + f_y^2)^{1/2}}{g} \right]$

+ $(F_D)_{calc} = W \sin \theta_{20}$

4.5 Check on Quality of FVR Data

The quality of the data derived by the FVR during the quarry test were checked in three different ways in order to gain insight into the capabilities and limitations of the instrument. First, the pressure sensor was employed to find on a printed record if the drogue was hanging straight down. The output resolution of the pressure sensor was .07 ft/count. With this sensitivity it would sense when the drogue streamed up vertically during a towing test. The tilt angle, θ , based only on the output of the pressure sensor was evaluated employing the relation:

$$\theta = \cos^{-1}\left(1 - \frac{\Delta Z}{\ell}\right) \quad (35)$$

where: ΔZ = change of height in water column

ℓ = tether line length

Equation (35) assumes that the tether line is straight from the buoy pivot to the sensor. Attempts at getting good correlation between results obtained by equations (21) and (35) were somewhat heartening, although the values predicted by equation (35) were always larger. For example, tests number 5 (average velocity = 3.41 cm/s) and 9B (average velocity = 4.39 cm/s) predicted tilt angles of 12.2 and 17.0 degrees, respectively. These values were 30% and 34% higher than the values predicted by the accelerometers. It is felt that three factors may have contributed to the poor agreement. First, the tether line length was relatively short (approximately 8 ft.), leading to a θ value very sensitive to ΔZ . Secondly, equation (35) is dealing with a cosine function near zero values for θ which necessitates the greatest sensitivity on the ΔZ measurement in order to know θ well. Lastly, the surface float supporting the test reduces its submergence as relative velocity and drogue lift forces increase. This fact leads to another uncertainty which it is hoped will be calculated at a later time in order to get a better correlation. In summary, the pressure transducer was of immeasurable value in pinpointing key occurrences in the data which are sometimes more obscure in the accelerometer data.

A good method of checking the data quality was to plot the data from the accelerometers as a function of time as a visual check on the data for noise and drift. Figure 11 is a plot of the accelerometer data recorded during towing test 10B. The sensitivities of each axis and the bias value of f_x , f_y , and f_z are also shown. These values should pertain when the relative velocity at the drogue is zero.

It can be seen in Figure 11 that the noisiest axis, the y-axis, displays a peak-to-peak amplitude variation of approximately 20 counts, which when divided by the sensitivity, amounts to a signal variation of .026 g. If all the change were in the y-axis only this would amount to a 1.5-degree angle change. This change in value is felt to be reasonable in the presence of an average angle of approximately 4.6°.

A third method of checking data quality is to see if the square root of the sum of the squares from the three accelerometer axes measures local gravity. Table 8 is a summary of accelerometer data from the six tests shown in Tables 6 and 7.

Table 8. Quarry Test Accelerometer Data

Test	f_x	f_x^2	f_y	f_y^2	f_z	f_z^2	$(f_x^2 + f_y^2 + f_z^2)^{1/2}$
10B	.057	.0032	.057	.0032	.996	.992	.9988
4	.054	.003	.096	.0092	.994	.988	1.0006
10A	.059	.0035	.103	.011	.994	.988	1.003
3	.056	.0031	.175	.031	.988	.977	1.011
5	.051	.0026	.156	.024	.988	.977	1.003
9B	.046	.0021	.215	.046	.998	.996	1.044

It can be seen from Table 8 that the square root of the sum of the squares of the average accelerometer signals differs from 1g by a maximum of 4.4%. Most of the other values are within 1% of 1g. This fact adds great confidence to the data derived. It may be that test 9B, which was at the fastest speed and had the most error in the sum of accelerometer signals was sensitive to a non-linear dynamically-induced error. This cannot be determined at present. The technique of measuring drogue tilt angle with the FVR does, however, look adequate for the purposes of the ocean test. The effects of ocean dynamics on these conclusions may be assessed later.

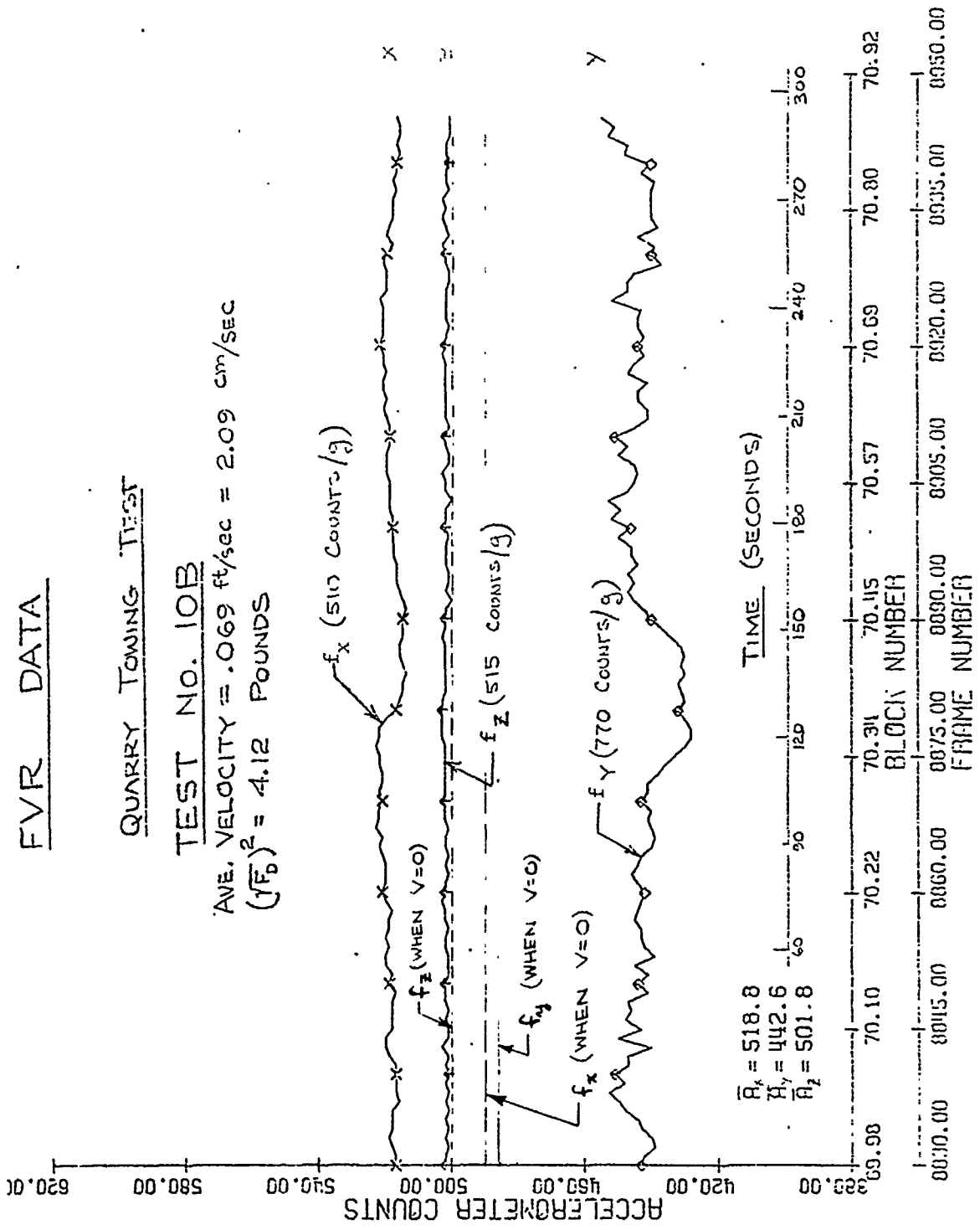
FVR DATA

QUARRY TOWING TEST

TEST NO. 10B

AVE. VELOCITY = .069 ft/sec = 2.09 cm/sec

$(\overline{V_D})^2 = 4.12$ POUNDS



$\bar{A}_x = 518.8$
 $\bar{A}_y = 442.6$
 $\bar{A}_z = 501.8$

Figure 11. Force Vector Recorder Data—Computerized Plot from Quarry Test No. 2

4.6 Interpretation of Quarry Test Data

A comparison between the drag coefficient of a window-shade drogue measured in the scale model towing tests (i.e., $(C_D)_0 \approx 1.93$, Vachon (1973)) and the full-scale towing tests is somewhat puzzling. The average full scale measured drag coefficient of $(C_D)_0 \approx 2.6$ is approximately 35% higher than that measured in the model tests. First, a precedent for believing the very high value of drag coefficient measured in the quarry tests is found in the vertical drag coefficient of a gliding parachute. Secondly, it is believed that difficulties inherent in the hydrodynamic scale model testing may have led to some of the measured differences between model and full-scale test results. Lastly, it is felt that the test configuration in the quarry may have also given rise to some of the measured differences.

When the window-shade-drogue scale-model test data are closely examined (Vachon, 1973, Figures 16-19, and Appendix A) a few interesting observations help to understand some of the measured differences. First, the modified Froude scaling tests, in which the model relative velocity was equal to the full-scale relative velocity, were conducted at Reynolds numbers much lower than the full-scale model. This points out one of the basic difficulties in any hydrodynamic model testing; that is, that it is not possible to conduct Froude and Reynolds scaling tests simultaneously. For the Froude scale model tests, the Reynolds number range was 1.3 to 6.6×10^4 , while, for the full-scale model, the Reynolds number based on drogue width ranged from 1.3 to 3.0×10^5 , or about one decade higher. At the low speeds found in both tests, the drogue did not oscillate due to vortex shedding. Therefore, from this viewpoint, the tests are analogous although at different Reynolds numbers.

It is, however, believed that, on the basis of the higher Reynolds numbers only, the higher drag coefficient of the full-scale model can be somewhat attributed to an adverse pressure gradient on the back side of the drogue caused by flow separation at the edge of the drogue. At the higher Reynolds numbers the water has more difficulty moving around the drogue edges and filling in the back side. The result is a lower pressure on the back of the drogue and a higher drag force.

Attempts were made in the scale model tests to conduct Reynolds scaling tests (i.e., model Reynolds no. = full-scale Reynolds no.) in which the drogue angle and shape were kept the same as in the equivalent Froude scaling tests. Reynolds numbers between 1 and 3.3×10^5 were achieved with the models. It should be noted that this range corresponds to the full-scale test Reynolds numbers (see Tables 4 and 5). Because the Reynolds scaling velocities were higher than Froude scaling velocities by the dimensional scale factor (approximately 10) the model had to be very heavily ballasted in order to maintain the same shape. As pointed out in Vachon (1973), this heavy weight at the high velocities lead to two problems.

- 1) Vortex shedding from the drogue caused large lateral and rotational oscillations of the model drogues; and
- 2) the heavy weight suspended from the bottom of the drogue picked up and stored some of the vortex shedding oscillatory energy and appeared to reinforce the pendulum mode of drogue and weight oscillation.

As the relative velocity by the drogue was increased, the drogue began to oscillate in a manner similar to a "sculling" motion. Sculling motion is named after the manner in which a single oarsman propels a small boat from the stern by thwart-ship oar rotation coordinated with rotation about its longitudinal axis. With the drogue, such motion appeared as a pendulum mode of oscillation combined with an abrupt change of drogue azimuth angle at the extreme positions of the pendulum motion. It is felt that this oscillation of the models at Reynolds speeds caused the adverse pressure gradient across the drogue to be "spilled." As a result the measured drag force and drag coefficient of the models were less than a non-oscillatory condition. This effect is believed to account for some of the difference between the model Reynolds tests as compared to the full-scale tests.

Slight oscillations of the models were first noticed at Reynolds numbers of 6×10^4 in the Froude scaling tests. Oscillations first appeared at Reynolds numbers of approximately 2×10^5 in the heavily-ballasted Reynolds tests and became more severe as the relative velocity was increased. At a relative velocity of 0.813 knot ($Re = 2.7 \times 10^5$), a pendulum angle of approximately ± 15 degrees at a frequency of approximately .3 Hz was observed in the model tests. No such oscillations were observed at similar Reynolds numbers during the full-scale tests.

The lower drag coefficient measured during scale-model Froude tests is believed to be partly due to the lower Reynolds number (one decade lower than full scale). A similar phenomenon is shown in Figure 8 of Vachon (1973) wherein the drag coefficient of a cylinder or sphere at intermediate Reynolds numbers ($Re \approx 10^3-10^4$) is reported to be approximately 20% less than the value at a Reynolds number of approximately 10^5 (i.e., just below the critical Reynolds number). It is felt that the window-shade drogue exhibits a similarly lower drag coefficient at lower relative velocities. It is hoped that future tests may more fully explore this phenomenon and that the theoretical curve at low relative velocities in Figure 8 may be refined in order to reflect a variation in C_D with Reynolds number.

It is felt that another problem existed in the quarry tests which may have given rise to test error. The drogue itself was suspended approximately 8 feet beneath the surface of the water in order to enable one to view its angular response during a test. The vertical and horizontal dimensions of the drogue were, however, 26 and 12 feet, respectively. It is felt that the relatively close proximity of the drogue to the surface resulted in a small flow "blocking" effect. As the drogue is pulled water piles up on the front surface which ultimately must leak around the edges in order to establish a steady flow condition. In such a situation the surface will appear much like a solid boundary to flow trying to leak over the top surface, possibly resulting in a higher drag coefficient.

This effect is felt to be small compared to the total measurement difference. It is, however, a test parameter which was different from that employed in the scale-model tests in which the drogue was submerged a distance approximately equal to one drogue length. It also had a similar clearance to the bottom of the tow tank. Future towing tests of the full-scale drogue in still bodies of water should attempt to place the drogue at least 26 feet from the surface and bottom of the body of water. The quarry in which the past tests were conducted is approximately 90 to 100 feet deep in certain areas. Such depths should permit the type of test desired.

In addition to differing with the scale-model test results, the quarry test drag coefficients are at first glance well above the values reported in Hoerner (1965) for a stable, descending full-scale parachute. Hoerner (Section 13.8) reports that the drag coefficient of a stable chute in straight vertical descent will be approximately 1.4. If, however, the chute is unstable due to its design, such that it glides laterally through the air as it descends, it will develop a lift force which augments its apparent vertical drag as shown in Figure 12. This phenomenon is more fully explored for various chute designs in Knacke and Hegele (1949). They found that for vertically descending model chutes in the Reynolds number range of 1.5 to 5×10^5 , the drag coefficient increased with decreasing velocity. It was assumed that air vortices more readily attached themselves preferentially to one side of the canopy at lower velocities causing lateral streaming motion and a lift force.

The lift force, F_L (shown in Figure 12), will act normal to its total velocity vector, V , which is the sum of the glide (V_g) plus the descent (V_d) velocities. In such a case, the lift force resolves into a vertical (upward) and a horizontal component. The horizontal component causes the chute to glide while the vertical lift component augments the chute drag.

The angle, α , at which the chute streams is approximately 45° for a material with zero porosity. In such cases a computation of C_D based on the total weight, W , and the total velocity, V , gives a drag coefficient as high as 1.65. This value is computed from equation (29). If, however, the true descent velocity (i.e., $V_d = V \cos \alpha$) normal to the chute area were put in equation (29), the drag coefficient would be as high as 3.3 for streaming angles of 45° .

When one examines the literature for reported values of drag coefficients of flat plates and other similar shapes, it is difficult to find a shape with a value as high as that for the window-shade drogue. It is reported in Hoerner (p. 3-17, Figures 32 and 33) that three-dimensional flat disc has a C_D of 1.17. For a two-dimensional flow, in which the shape is held between flat walls parallel to the flow, the reported drag coefficients

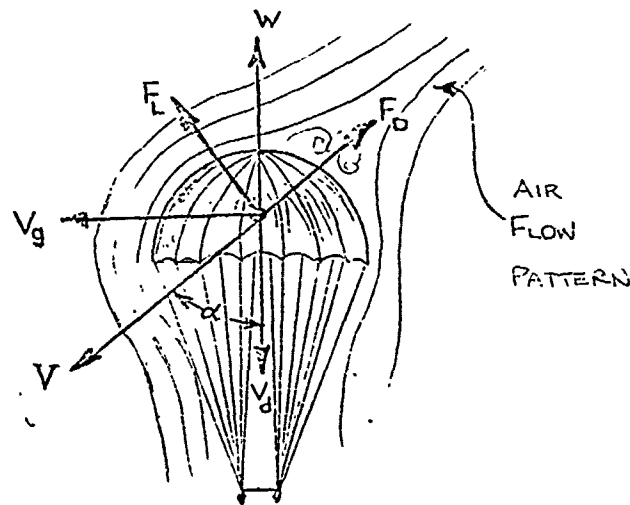


Figure 12. Forces on an Unstable or Gliding Parachute

are higher. A flat plate exhibits a C_D of 1.98 while flow into the open portion of a semicircular cylinder exhibits a C_D of 2.3. The Reynolds numbers for these values is in the range of 10^4 to 10^5 . Two other sources of comparative drag coefficient data are available. Terhune (1968) developed a window shade drogue buoy for following water masses. He

employed a drogue drag coefficient of 2 in his velocity correction estimates because it is the value given for flat plates. In addition, Pritchard and Burt (1951) measured the drag coefficient of a "Chesapeake Bay drogue" as equal to 2.4. This drogue was a bi-planar crossed vane approximately 2 feet on a side. This value leads one to believe that a value of $(C_D)_o = 2.6$ is realistic for a window shade drogue undergoing steady relative velocity and so constructed and balanced that it weathervanes in a manner perpendicular to the relative velocity. If, however, the drogue were subject to buoy-induced vertical and horizontal dynamics or installed in a manner so close to the buoy that it receives dynamic relative velocity from wave-motion, the drag coefficient may be drastically altered. It may even be found that near the surface wave zone a window shade drogue does not reliably weathervane as designed. This aspect should be investigated more fully by further tests. The variation of drag coefficient in the presence of dynamics is explored more fully in section 5.2.2 in which the ocean slippage test data are discussed.

4.7 Recommended Window-Shade-Drogue Drag Coefficient

It is felt that the true drag coefficient of a window-shade drogue in the non-dynamic quarry test configuration may be slightly less than 2.6. This might be true primarily because the value of 2.6 that was repeatedly measured may have been somewhat high due to surface interference effects. It is further felt, though, that drogue dynamics caused by coupling to buoy motion would raise the effective drag coefficient. Therefore the drag coefficient of a full scale window shade drogue will be specified as follows in all subsequent analyses:

$$(C_D)_o = 2.6$$

This value will be degraded with an increasing tilt angle of the top of the drogue in accordance with equation (31).

SECTION 5

DROGUE OCEAN TESTS

During the months of February and March of 1975, a few relatively calm days were sought during which two types of drogue ocean tests were conducted. The first test entailed the measurement of the vertical drag coefficients (parallel to drogue surface) of two different window-shade drogues. The second test involved the conduct of a drogue slippage test. Both tests required the proper functioning of the FVR.

5.1 Measurement of Drogue Vertical-Drag Coefficient

On February 15, 1975, a series of 14 at-sea tests were conducted on two different drogues in order to ascertain the value of the vertical-drag coefficient of a window-shade drogue (i.e., parallel to the drogue surface). The value of this parameter is important in analytically predicting buoy-drogue dynamics. The values were determined by releasing drogues ballasted with a known amount of weight, from near the surface; allowing them to drop free in water and obtain their terminal velocity. The drop tests were conducted on a 7.33 x 32.25-foot (2.23 m x 9.83 m) Nova University-built nylon canvas (9½ oz duck) drogue and an 11-¾ foot x 25-¾ foot (3.58 m x 7.85 m) Herculite (Marine DR grade) Draper Lab-built drogue. Both drogues were instrumented with the FVR in order to measure drogue dynamics and the drop rate (using a pressure transducer).

A 74.5-foot piece of 3/8-inch nylon line was loosely coupled between the apex of the drogue and a shock cord suspended from the ship's A-frame. Prior to the drop, the drogue apex was supported by a pelican hook whose trip rope was cut in order to begin the test. The drogue was then allowed to freely descend approximately 74 feet before being restrained by the nylon rope.

Seven drop tests were conducted on the Nova-built drogue, employing three different weights to explore the variation of $C_D A$ with velocity. Seven tests were also conducted with the Draper Lab drogue, employing two different weights. The results of the drop tests are summarized in Table 9. The main results are listed in columns 5 and 7 in which the total drag area for the whole drogue and for the drogue material alone are listed. The values listed are computed based on the total weight in water of the drogue material and ballast weight exclusive of the top spreader bar. The FVR is neutrally buoyant such that only its drag force is a factor in determining the terminal descent velocity. Rough calculations show that the net weight of the spreader bar and bridle is offset by the drag of the 16-inch-diameter FVR sphere as the drogue descends.

The overall or average vertical-drag coefficient measured during each test, shown in column 5 of Table 7, combines the effects of all elements in the drogue as shown in the following equation:

$$\overline{(C_D)}_{//} = \frac{\sum_i [(C_D)_{//}]_i A_i}{A_{TOT}} \quad (36)$$

Where A_{TOT} is the total frontal area of drogue material and frontal areas of the spreader bars to vertical flow. The numerator in equation (36) is made up basically of three elements; the $C_D A$ of each spreader in the presence of vertical flow and the $(C_D)_{//} A$ of the drogue material itself. The drogue design, described in Section 2 of this report, endeavored to minimize the $C_D A$ of each spreader bar, by using faired nautical spars, and yet maximize the bending stiffness of the bars to vertical loads. Column 7 of Table 7 is derived by subtracting the calculated buoyant drag force of the lower spreader bar from the weight of the drogue material and ballast (column 2). The drag and weight of the upper spreader have been assumed to cancel during the test and are thus neglected in the calculation.

Table 9. Summary of Drogue Drop Tests for the Purpose of Measuring the Vertical-Drag Areas of Window-Shade Drogues

Test No.	Weight of Drogue plus Lower Ballast Weight (in water) (Newtons)	Ave. Descent Terminal Velocity from FVR data (cm/sec)	Total $(C_D) // A$ of Drogue based on FVR Data (meter) ²	Total Vertical Drag Coefficient $(\overline{C_D}) //$	Buoyant Drag Force on Bottom Spreader Bar (Newtons)	Vertical Drag Coefficient of Drogue Only $(C_D) //$	Comments
NOVA DROGUE TEST RESULTS - A (drogue) = 22.1 meter ²							
1	282.5	82.9	.80	.036	29.1 (*)	.032	Top rolled over.
2	282.5	86.9	.73	.033	32.0	.029	" " "
3	282.5	89.6	.69	.031	34.1	.027	Slight roll over.
4	399.0	104.5	.71	.032	46.4	.028	" " "
5	399.0	106.7	.69	.031	48.3	.027	" " "
6	515.1	127.1	.62	.028	68.5	.024	" " "
7	515.1	119.5	.70	.032	60.6	.028	" " "
CSDL TEST RESULTS - A (drogue) = 28.2 meter ²							
8	300.7	83.5	N.G.	-	19.9 (§)	N.G.	Lines fouled around bridle.
9	300.7	88.4	.75	.027	22.3	.025	Top rolled over.
10	300.7	78.3	.95	.034	17.5	.032	" " "
11	225.5	63.1	N.G.	-	11.3	N.G.	Lines fouled.
12	225.5	59.4	1.25	.044	10.1	.042	Top rolled over.
13	225.5	60.0	N.G.	-	10.3	N.G.	Lines fouled.
14	225.5	58.8	1.27	.045	9.9	.043	Top rolled over.

* C_D (cylinder with wake splitter) = 0.59 (see Roshko, 1953), § $C_D \approx .3$ (Hoerner, 1965, p.2-3 & p. 3-11).

By a careful inspection of the output of the FVR during the drop tests it is apparent that to varying degrees the top of the drogue curled over. Such an effect was probably caused by the presence of a negatively buoyant bridle attached to the top spreader bar. The effect was especially pronounced at the lower descent velocities where viscous and pressure drag on the bridle and upper portion of the drogue were inadequate to keep the drogue planar.

It can be seen in Table 9 that the last column qualitatively alludes to the "roll-over" problem. The descent velocities encountered in the CSDL drogue tests were, in general, less than those for the Nova drogue due mainly to a greatly reduced ballast weight in the lower spreader bar. As a result the roll-over problem was more pronounced, as borne out by a qualitative look at the FVR accelerometer and magnetometer data. This fact could lead to higher apparent values of $(C_D)_{//}$ (column 7).

For the drogues employed in the tests it is safe to assume an overall vertical-drag coefficient of .03 for analysis purposes. For calculating the submerging forces on buoys the .03 value may be high because the drogue is in considerable tension when it imparts submerging forces. In such a situation it is felt that drogue "flutter" and lateral "roll-over" would be held to a minimum, leading to a lower overall drogue vertical drag force.

For the case of analyzing the drogue tether line zero tension condition, a value of $(C_D)_{//} = .03$ is very realistic at the onset of the slack line condition. After the line has gone slack the top of the drogue may roll over, as was observed in the described tests, leading to an effective increase of $(C_D)_{//}$. The really important point is still, however, when the slack line condition begins.

For the same reasons as just described, it is recommended that the value of drag coefficient of the drogue material alone be given as $(C_D)_{//} = .026$. Appendix E employs $(C_D)_{//}$ in analytical estimates of both the drogue-induced buoy submerging forces and the tether line zero tension condition as a function of drogue area, ballast weight, and sea state.

5.2 Drogued Ocean Test

Three different buoys, including a Nova minibuoy, were employed in a drogued ocean drift test in order to get as much information as possible for measuring the relative or slip velocity at the drogue. In addition, the Force Vector Recorder (FVR) was mounted to the top spreader bar of the

drogue beneath the Nova buoy in order to measure the dynamics and inclination angle of the drogue. As shown in equation (18), the inclination angle at the drogue should afford an estimate of the drogue drag force, F_D . By a knowledge of F_D , and a value for the drag coefficient, C_D , for the drogue, the slip velocity can be estimated from equation (20) provided the window shade drogue weathervanes perpendicular to the drogue relative velocity. The drag coefficient of the full scale drogue will be that inferred from the quarry towing tests and the scale model towing tests (i.e., $(C_D)_0 \approx 2.6$).

A direct measurement of the drogue slip velocity by employing a current sensor was not attempted because the state-of-the-art of current sensing technology did not permit such a measurement with a satisfactory degree of precision. The main problem encountered in making such measurements is due to wave and buoy-induced dynamic errors as described by McCullough (1974). For drogued buoys in which the drogue is directly and strongly coupled to a surface-following buoy, a horizontal current sensor attempts to measure a relatively small relative velocity in the presence of oscillatory velocities approximately an order of magnitude larger. Future measurements such as this may be more feasible due to continuing improvements on present sensors and the development of new sensors.

The three buoys employed in the drogued ocean test are shown in Figs. 13-15. All of the pertinent dimensions of each buoy are shown. Table 10 lists the assumed drag areas of each buoy above and below water. It was assumed that all elements on the Nova minibuoy and cylindrical portions of the floats exhibited a drag coefficient of 1.0 or 1.1. The drag coefficient of the buoyancy element of the floats and lights shown in Figures 14 and 15 is assumed to be that of a sphere (i.e., $C_D \approx .5$). The drag coefficient of the flags is assumed to be 0.1 (Hoerner, 1965, p. 3-25). That portion of the buoys above water is assumed to be acted on by wind forces only. The portion below water is assumed to be subject to forces from waves and surface currents, but modelled as purely a surface current. The drag area of the tether line, which cannot be neglected, is apportioned equally between the buoy and the drogue with a drag coefficient of 1.7 assumed. Figures 16 and 17 are plots of wind and current forces respectively on the buoys based on the assumed drag areas listed in Table 10.

Figure 18 depicts the area of the ocean drift test and the location of lighthouses employed for mounting the radar navigation transponders. The area shown was chosen for a number of reasons. First, the water was of adequate depth (50-65 meters) to accommodate the buoys and drogues.

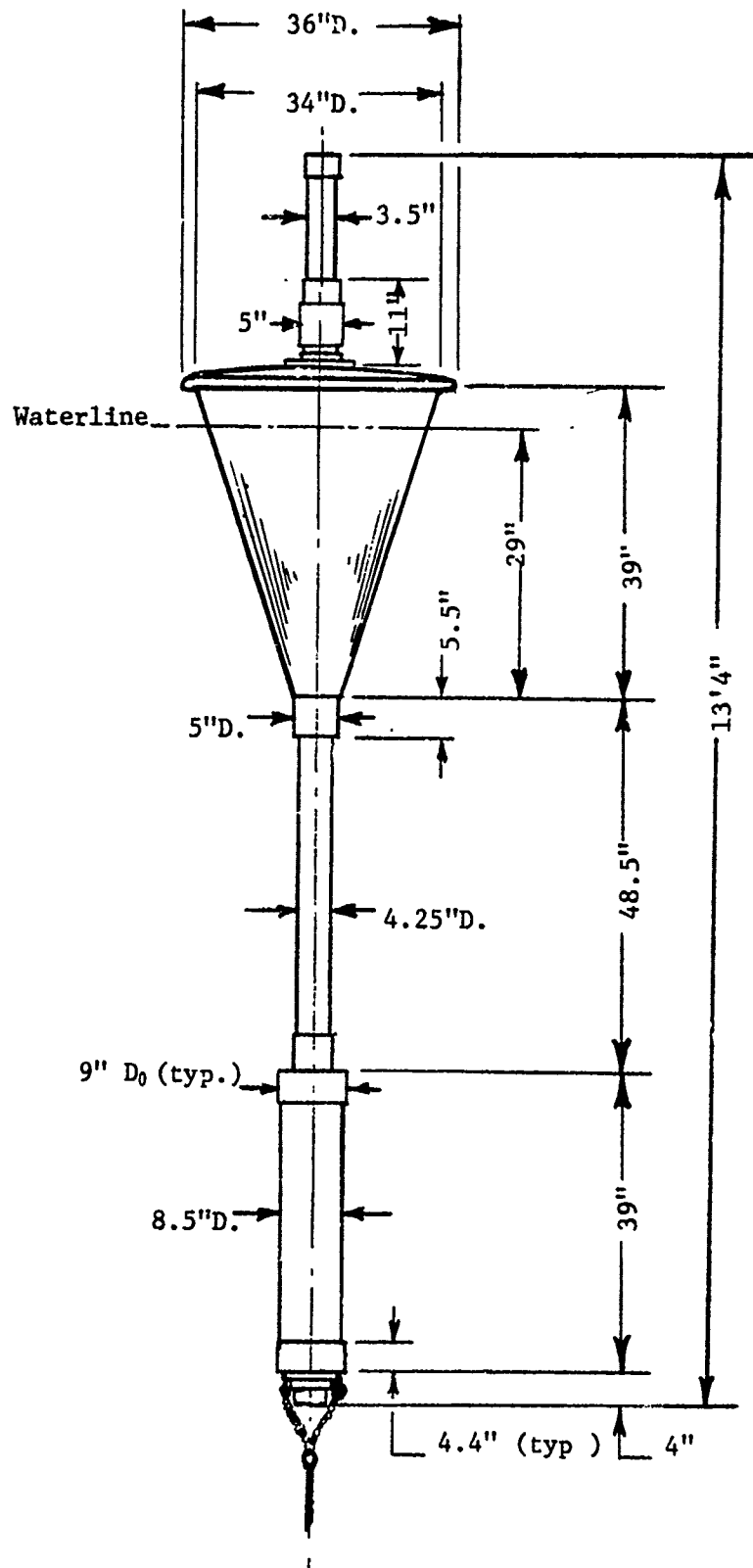


Figure 13.

NOVA Minibuoy Outline, Including Major Dimensions

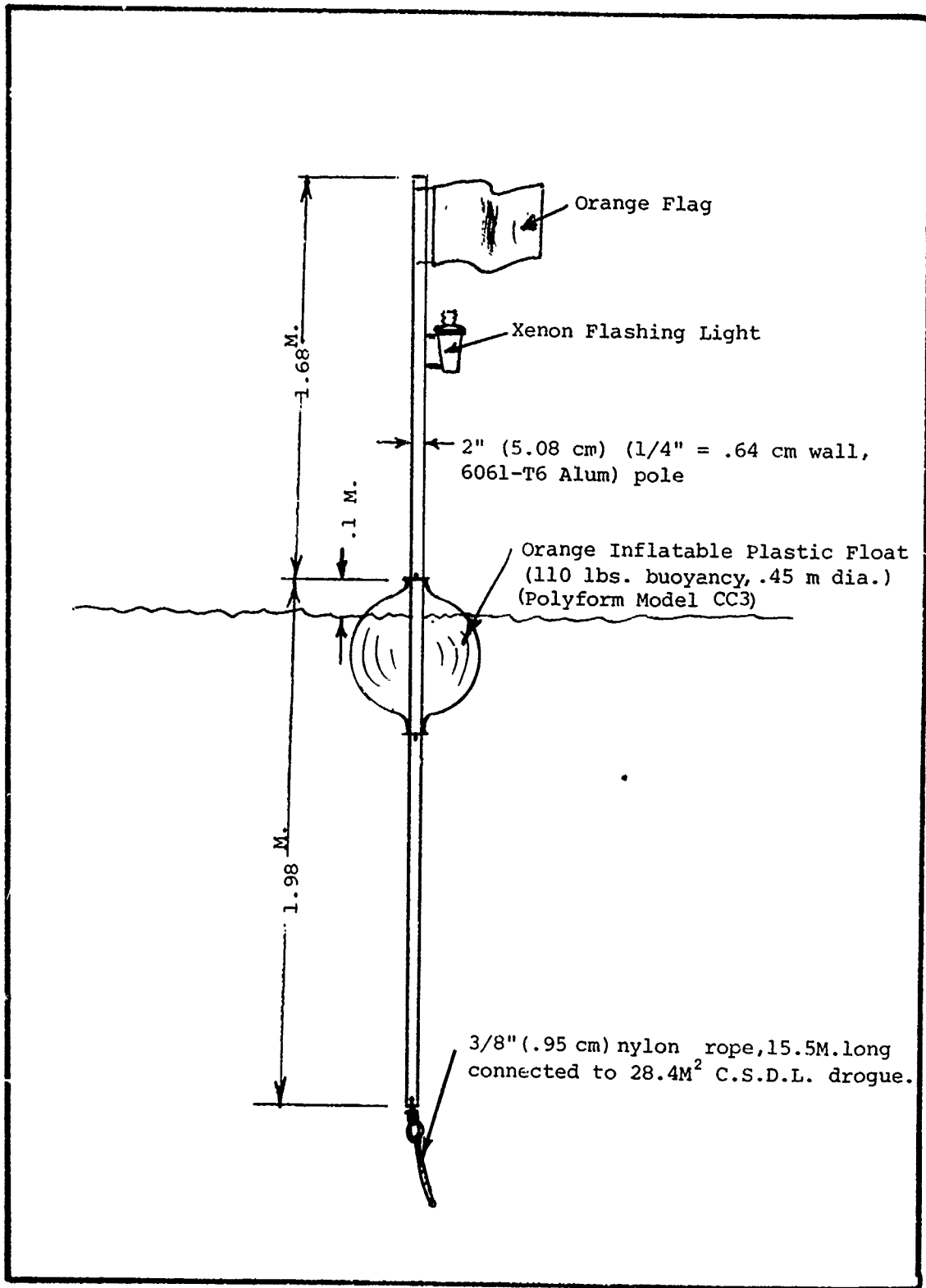


Figure 14. Drogued float configuration employed during drogued ocean test.

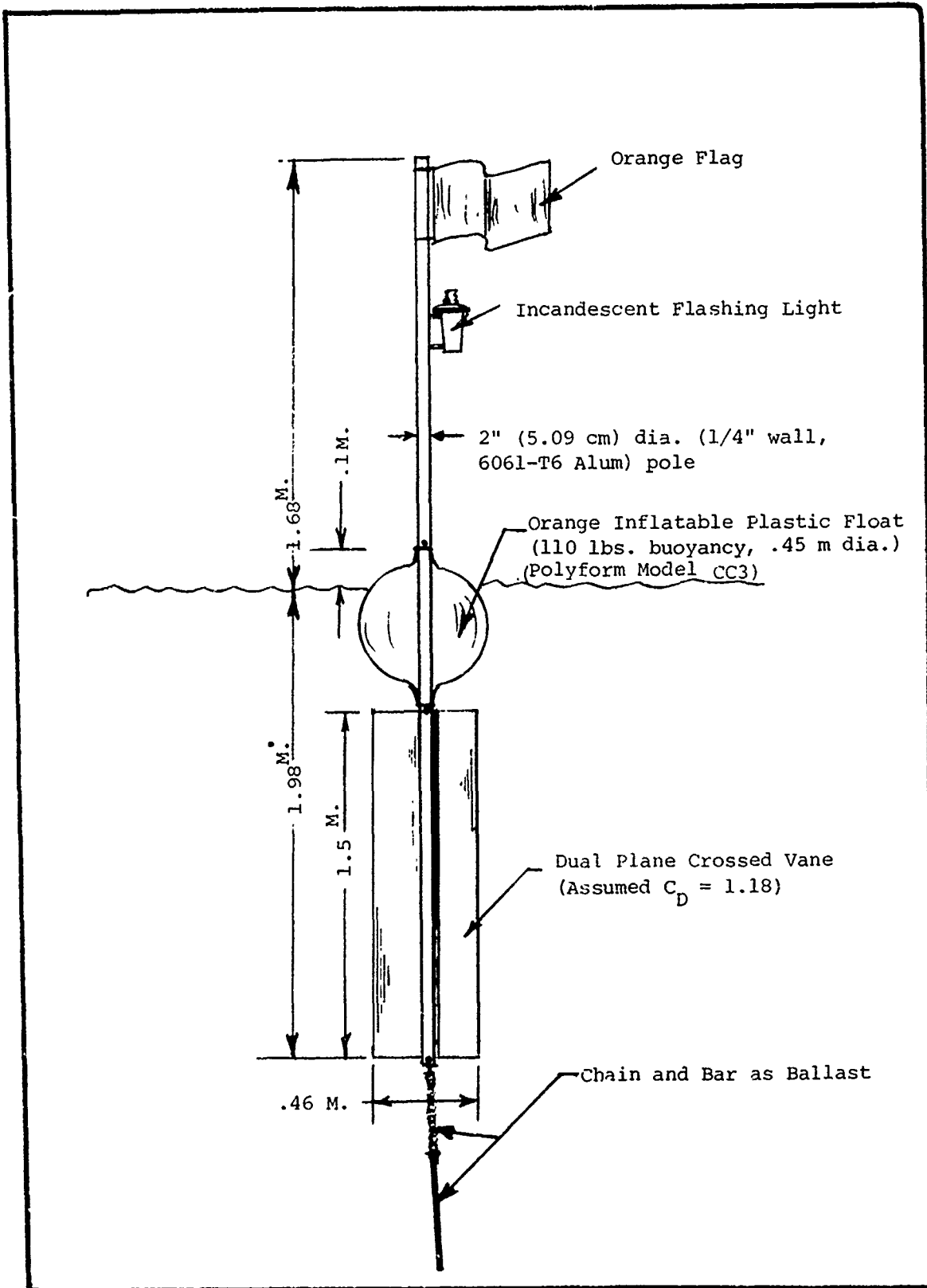


Figure 15. Surface Drogued Float Employed for Measuring Surface Currents During Drogued Ocean Test.

ABOVE WATER VALUES									
Buoy	Areas (m ²) and Assumed Drag Coefficients								Total Drag Area (m ²) Above water-Line = $\sum C_D A$
	Mast	C _D	Flotation	C _D	Flag	C _D	Light	C _D	
NOVA Minibuoy #1	.096 m ²	1.1	.19 m ² (cone)	1.0	0.18 m ²	.1*	.025 m ²	.6	0.329 m ²
Surface Floats (#2 & #3)	.085 m ²	1.1	.017 m ² (plastic float)	0.5	0.18 m ²	.1*	.025 m ²	.6	0.135 m ²
VALUES FOR WETTED PORTION OF BUOYS									
Buoy	Portion of buoy, Area (m ²), and Assumed Drag Coefficient								Total Drag Area Including 1/2 of Tether Line = $\sum C_D A (m^2)$
	Flotation	C _D	Cylinder	C _D	Tether Lines (total)		C _D		
NOVA Minibuoy #1	.3 m ² (cone)	1.0	0.37 m ²	1.1	2, 3/8" dia. x 12.2 m. long = 0.23 m ²		1.7	0.903 m ²	
Drogued Float #2	.11 m ² (plastic float)	0.5	0.08 m ²	1.0	1, 3/8" dia. x 15.5 m. long = .15 m ²		1.7	0.263 m ²	
Surface Float #3	.11 (m ²) (plastic float)	0.5	0.69 m ² crossed vanes	** 1.18	---		--	0.87 m ²	

(*) See Hoerner (1965) p. 3-25

(**) See Vachon (1973) p. 38

TABLE 10. Description, Areas, Drag Coefficients, and Drag Areas of Test Buoys and Tether Lines

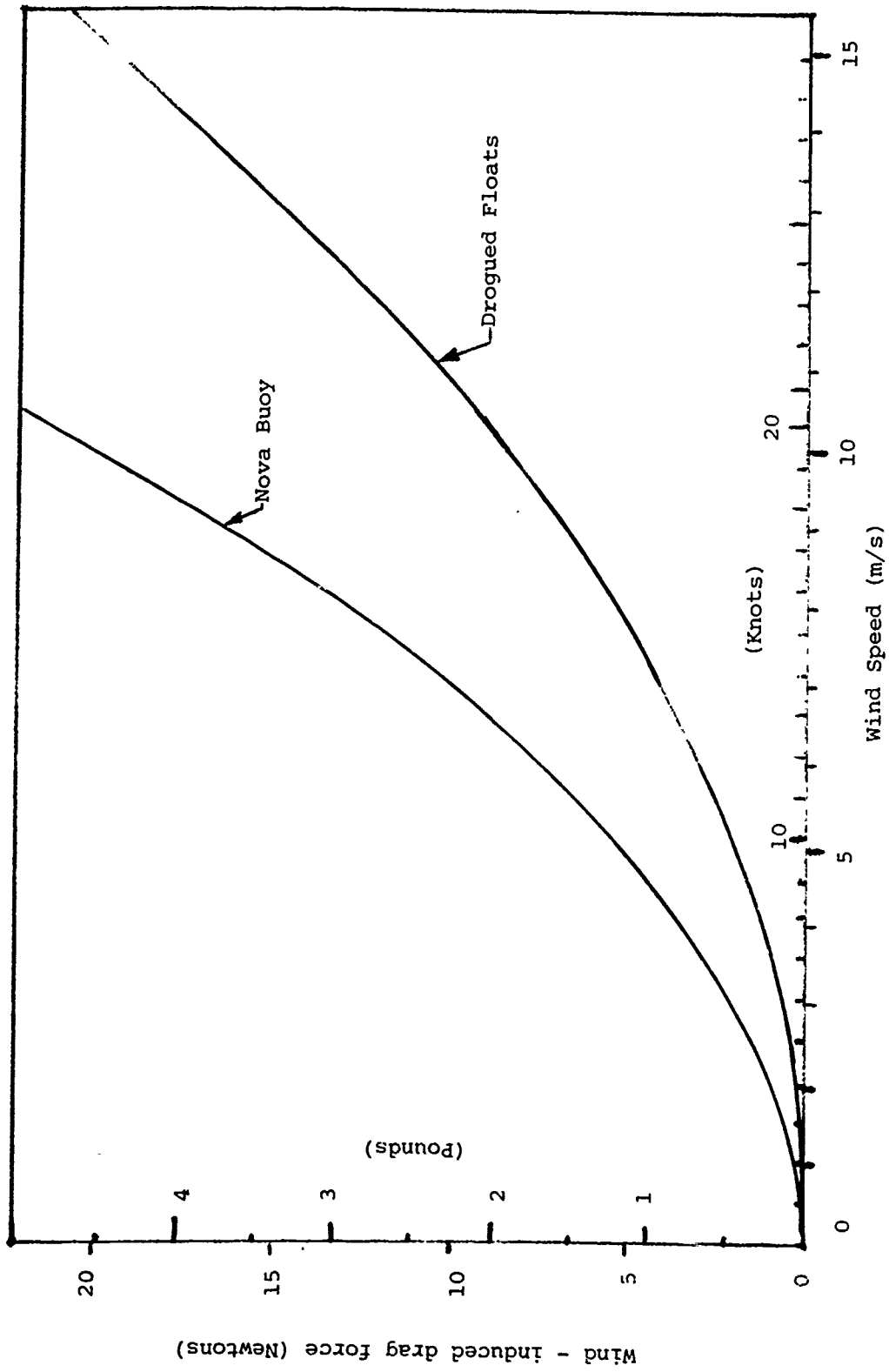


Figure 16. Estimated wind forces on test buoys as function of wind speed.

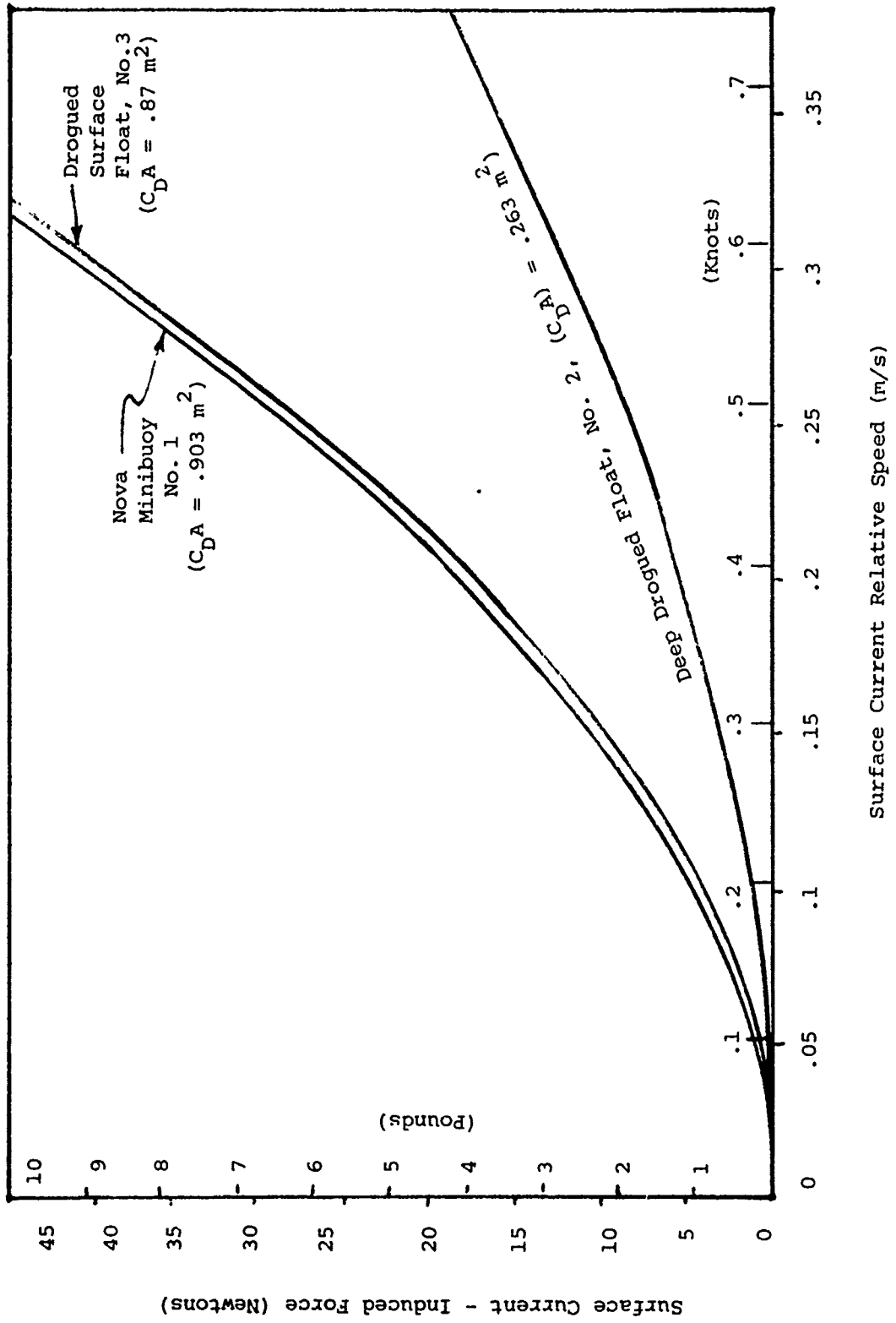


Figure 17. Estimate of forces acting on test buoys as a result of buoy velocity relative to the surface current only.

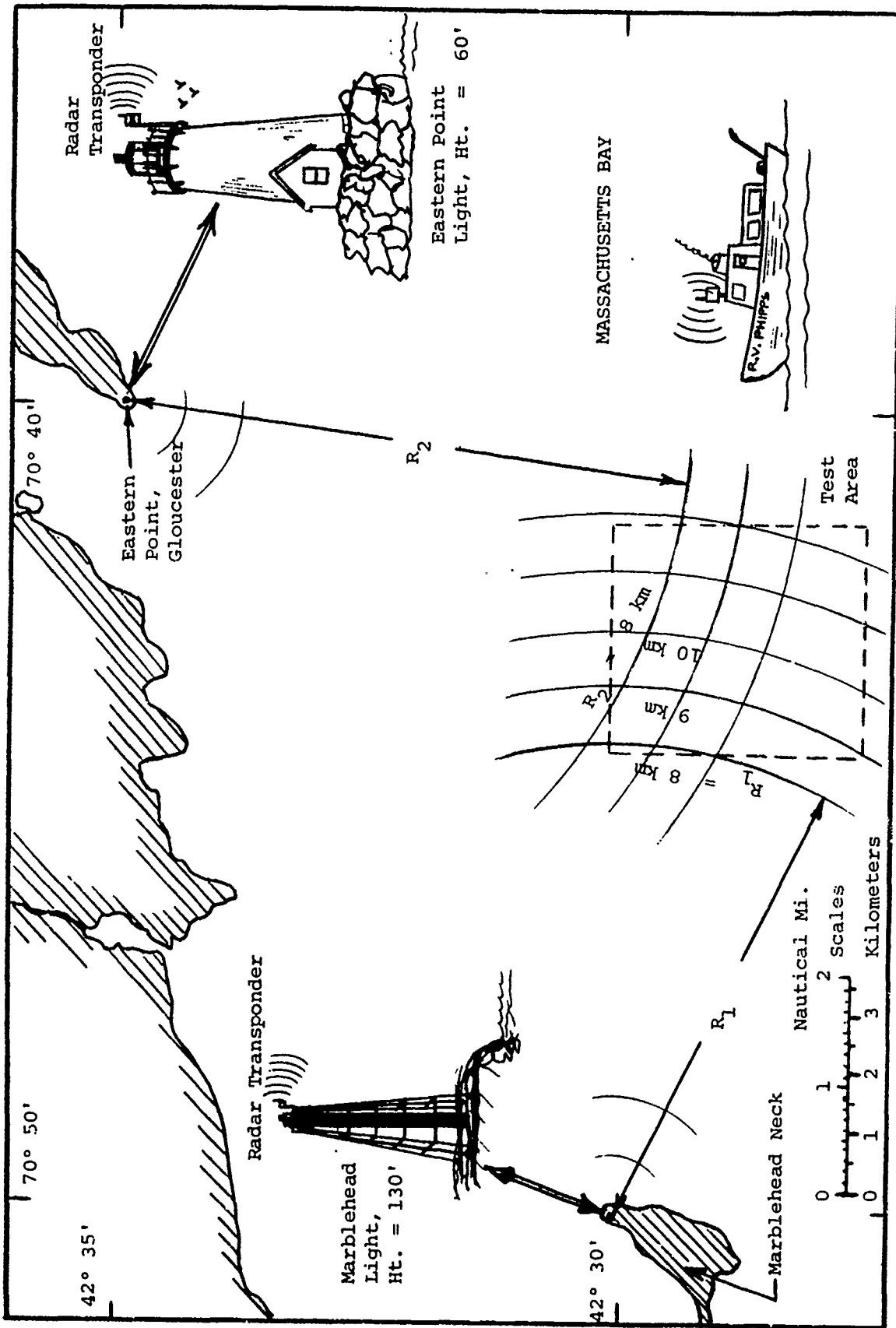


Figure 18 Description of ocean drift test site and location of radar navigation transponders.

Secondly, the location was half way to Boston (approximately 20 nautical miles northeast) yet was out of the main shipping channels. Lastly, the existing lighthouses afforded excellent bases for installing the Decca Trisponder navigation transponders employed as the main navigation scheme for tracking the buoy trajectories.

A mobile transponder mounted to the research vessel allowed the vessel position to be monitored to an accuracy of approximately ± 3 meters. Each time a buoy fix was desired the vessel would come alongside the buoy and a person would visually read the trisponder system output and hand-record the data. An omni-directional antenna on the vessel permitted position readings independent of ship heading. The relative distance and geographic bearing between the ship and buoy was also logged during a fix as a means of enhancing the data. The data listed in Appendix A have already corrected for the relative distance between the ship and buoys during a position fix.

In addition to radar transponder position data taken during the test, each time a buoy position was taken on the ship, a LORAN C ship position was also taken as a backup. The LORAN C data were also of very high accuracy (better than 200 feet) owing to the phase-tracking system employed. Both an automatic Epsco and a Simrad/Internav Loran C system were used with separate antennas for each. The readings agreed when compared. A detailed list of both the radar and LORAN C (using Simrad output) position data are presented in Appendix A and buoy trajectories derived from differential LORAN C described and plotted in Appendix B.

The sizes of the drogues employed during the sea test are summarized in Table 11. The mean depth of the drogues (i.e., drogue middle) was approximately 24 meters if no relative velocity at the drogue were present which would cause it to stream upward in the water. The drogue beneath the Nova buoy (Buoy (1)) was fabricated by Nova University. It was made of 9 1/4 oz. nylon canvas or nylon "duck" material. The drogue beneath Buoy (2) (i.e., the float), made at the C. S. Draper Lab, was fabricated of Herculite Marine DR fabric (i.e., a PVC over nylon mesh) with a weight of approximately 15 oz. per square yard. The total drag area attributed to the drogue includes the remaining half of the drag area of the tether lines not included with the buoys in Table 10.

Buoy Number	Drogue Dimensions & Area (m ²)	Drogue Drag Area, (C _D) ₀ A (m ²)	Drag Area of 1/2 of Tether Line, C _D A (m ²)	Total Drag Area (m ²)
1 (Nova)	2.25 m. (wide) x 9.83 m. (long) = 22.1 m ²	57.46	.39	57.85
2 (CSDL)	3.59 m. (wide) x 7.85 m. (long) = 28.3 m ²	73.32	.26	73.58

Table 11.

Summary of Drogue Size, Drag Areas, and Total Drag Area
(including 1/2 of Tether Line Drag Assigned to Drogue)

Note: (1) Drogue (C_D)₀ = 2.6, (when hanging straight)

(2) Assumed Tether Line Drag Coef., C_D = 1.7

5.2.1 Details of Slippage Test

Figure 19 describes some of the velocity parameters which will be used to describe the slippage test. Buoy (1), the NOVA buoy is shown in this figure. Two other parameters of interest are the velocities of the two other buoys. V₂ is defined as the measured velocity of the drogued float while V₃ is the measured velocity of the surface drogued float.

The velocity of the deep current and the surface current were sampled by the deep drogued float (with window shade drogue) and the drogued surfact float with designations \bar{v}_2 and \bar{v}_3 respectively. It was hoped that buoy-2 would sample the deep current and buoy-3 would sample the surface current. Their trajectories will not, however, be true indicators of the desired velocity because they will in both cases be acted on by forces due to wind and surface currents. The best way to understand how the data are used is to write the force balance equations of each buoy-drogue system in terms of vector relative velocities. The constants K_i, which appear in the following equations are contractions of the parameter group $1/2\rho(C_D)_i A_i$, which is assumed to be a constant.

Deep Drogued Nova Buoy (1)

$$\Sigma F = 0 = K_1(\bar{v}_w - \bar{v}_1) |\bar{v}_w - \bar{v}_1| + K_2(\bar{v}_s - \bar{v}_1) |\bar{v}_s - \bar{v}_1| + K_3(\bar{v}_c - \bar{v}_1) |\bar{v}_c - \bar{v}_1|$$

(37)

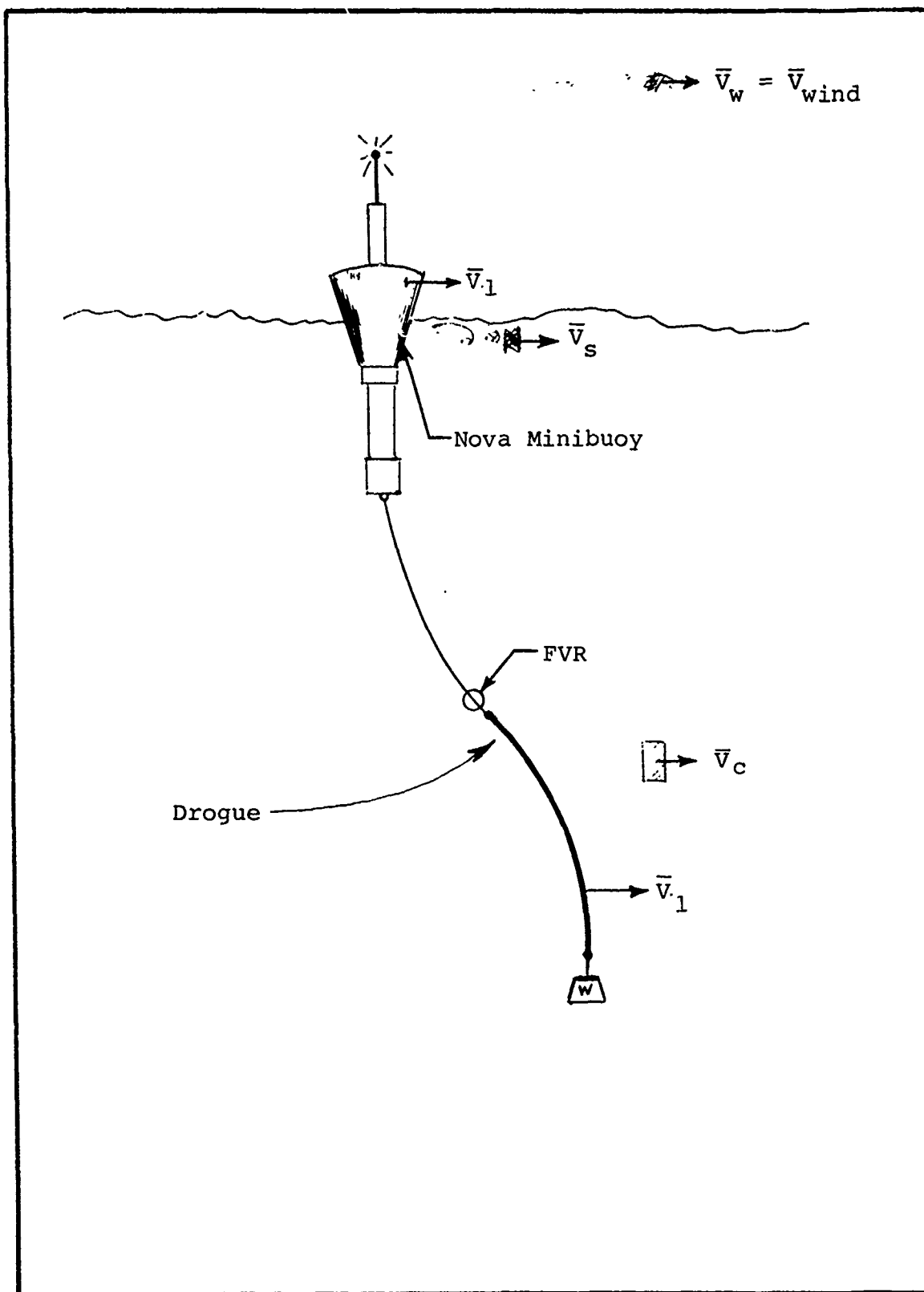


Figure 19. Drogue Slippage Test Velocity Definitions.

Deep Drogued Float (2)

$$\Sigma F = 0 = K_4(\bar{V}_w - \bar{V}_2) |\bar{V}_w - \bar{V}_2| + K_5(\bar{V}_s - \bar{V}_2) |\bar{V}_s - \bar{V}_2| + K_6(\bar{V}_c - \bar{V}_2) |\bar{V}_c - \bar{V}_2|$$

Surface Drogued Float (3) (38)

$$\Sigma F = 0 = K_4(\bar{V}_w - \bar{V}_3) |\bar{V}_w - \bar{V}_3| + K_7(\bar{V}_s - \bar{V}_3) |\bar{V}_s - \bar{V}_3| \quad (39)$$

It should be recognized that equations (37) and (38), pertinent to buoy-1 and buoy-2 respectively, are the same basic equations with different drag areas on the buoys and drogue. By so doing it is hoped that the smaller surface drag area of buoy-2 will result in drogue-2 being more nearly coupled to the deep current, \bar{V}_c .

The 7 constants in equations (38) to (39) are calculated based on the drag area values ($\Sigma C_D A$) listed in Tables 10 and 11, and densities for air and water of 1.29 Kg/M^3 and 1027 Kg/M^3 respectively. The resulting values are derived and employed in subsequent analyses:

$$K_i = 1/2\rho(C_D A)_i \text{ (generally)}$$

$$K_1 = 0.212 \text{ Kg/M}$$

$$K_2 = 463.2 \text{ Kg/M}$$

$$K_3 = 29,677 \text{ Kg/M}$$

$$K_4 = 0.087 \text{ Kg/M}$$

$$K_5 = 135.9 \text{ Kg/M}$$

$$K_6 = 37,746 \text{ Kg/M}$$

$$K_7 = 446.3 \text{ Kg/M}$$

The manner in which the data are used is as follows:

- (1) Employ buoy-3 trajectory and a measure of \bar{V}_w in equation (39) in order to get an estimate of \bar{V}_s .
- (2) Use above estimate of \bar{V}_s and measurements of \bar{V}_w and \bar{V}_2 in equation (38) in order to get an estimate of \bar{V}_c .
- (3) Use above estimate of \bar{V}_s and measurements of \bar{V}_w and \bar{V}_1 in equation (37) in order to get an estimate of the true current, \bar{V}_c , as measured from the NOVA buoy.

- (4) Compare the values of \bar{V}_c derived by (2) and (3) above.
- (5) Employ the above estimate of \bar{V}_c (as derived from buoy-2 corrected trajectory) and \bar{V}_s along with measurements of \bar{V}_w and \bar{V}_1 in equation (37) to ascertain an estimate of the NOVA buoy drag areas which would make the corrected trajectory of the Nova buoy agree with that of the drogued float. This includes changing drag areas ($C_D A$) both above and below water, K_1 and K_2 respectively. A computer program was written for this purpose.
- (6) A separate estimate of K_1 and K_2 pertinent to the NOVA hull based purely on hydrodynamic drag information can then be compared with (5) above as a crude indication of the augmented hull drag forces caused possibly by wave forces and non-linear rectifying effects caused by buoy motion.

In addition, based on the previous measurements, it is possible to predict the drag force acting on the Nova buoy drogue. This force is the sum of the first two terms in equation (37). Calculation checks may then be done with this force data in order to see if the value agrees with that estimated by the Force Vector Recorder on buoy-1 through a measure of drogue tilt and the use of equation (18).

In the future it is hoped that additional at-sea slippage tests can be conducted with independent moored current sensors. These tests should be conducted under varying sea conditions in order to arrive at a model which allows one to correct for drogue slippage as a function of winds, waves, currents, and swells. The data to be described herein presents a scheme for estimating slippage under one given set of conditions in which the effects of waves, currents, and swells on the buoys are lumped together as if they were a current only. Such a simplifying assumption is expeditious for this empirical study but neglects the details of such effects as a water mass transport current arising from a wind-drive wave field (i.e., Stokes drift), unique non-linear wave-buoy interaction forces which can be highly empirical, and any progressive buoy motion resulting from a rectification of the orbital motion of the surface gravity wave field. Such effects are not necessarily scalable from tests under other conditions. In order to properly model their effects, many at-sea tests

should be conducted under varying conditions and the results correlated with dynamic math models of buoy and drogue performance.

Additional assumptions are also required in order to estimate the drag forces due to wind and currents acting on buoy-2. The drag coefficients employed are the best estimates based on previously reported data. These data were, however, primarily derived from non-dynamic tests. Therefore, their validity is also questionable when the dynamic effects of waves, nonlinearities of orbital motion, and strumming are taken into account.

5.2.2 Analysis of Slippage Data

Tables 12 and 13 are lists of the important velocity vectors measured during the sea test, illustrating magnitude and direction (in Cartesian coordinates) as well as x and y components. They are broken down into one-hour averages except for the hours 16:00 to 24:00 on 6 March 1975. During this period the ship was disabled because its rudder came loose. The ship was towed to port, the rudder fixed, and the test continued at 24:00 hours. The one-hour vector averages of all velocities and forces (in later figures) are shown occurring at 30 minutes past the hour. For example, the vector average velocity between 1000 and 1100 is shown as the average velocity at 1030 hours.

During the period that the rudder was inoperable, the 3 buoys drifted freely. After the repairs, the ship returned to the test site and ultimately reacquired the positions of all buoys. The position reacquisition, occurring at night, was very difficult on buoy-3 because its flashing light was not working. It was later determined that its ON/OFF switch had been bumped (off) during one of the many deployment/retrieval operations during the first day.

The weather during the test is best shown by that recorded by the Coast Guard during the test. Table 14 is the weather recorded approximately 6.5 nautical miles north of the test area at Eastern Point Lighthouse, a manned station. This is the same light that supported one of the radar transponders. Table 15 lists the weather recorded at the Boston Liteship approximately 10 nautical miles south of the test area and in open water. It can be seen that the records do not differ substantially. The wind information in Table 15 is the direction from which the wind is blowing in geographic coordinates (i.e., 0° = true north). The wind information recorded on the research ship also agrees well with Tables 14 and 15.

Date & Time	NOVA Buoy Velocities, V_1 (m/s)				Drogued Float Velocities, V_2 (m/s)			
	$ V_1 $	$\theta_1 = \angle V_1$	$ V_1 \cos \theta_1$	$ V_2 \sin \theta_1$	$ V_2 $	$\theta_2 = \angle V_2$	$ V_2 \cos \theta_2$	$ V_2 \sin \theta_2$
March 6 & 7, 1975								
10:30	.133	48°	.089	.099	.133	48°	.089	.099
11:30	.152	45.3°	.107	.108	.155	50.5°	.099	.12
12:30	.132	58.6°	.069	.113	.178	58.8°	.092	.152
13:30	.099	74.8°	.026	.096	.078	81.1°	.012	.077
14:30	.084	90.5°	-.0008	.084	.082	87.4°	.0037	.082
15:30	.079	118.8°	-.038	.069	.059	122.2°	-.0315	.05
16:00 to 24:00	.049	148.2°	-.042	.026	.052	147.5°	-.0477	.0198
00:30 (3/7/75)	0.64	81.9°	.0089	.063	.06	101.5°	-.012	.059
01:30	.066	104.9°	-.017	.064	.07	138.7°	-.044	.055
02:30	.054	111.8°	-.02	.05	.084	144.2°	-.068	.049
03:30	.066	135°	-.047	.047	.099	141.2°	-.077	.062
04:30	.069	153.4°	-.062	.031	.083	161.1°	-.079	.027
05:30	.074	174.9°	-.074	.0066	.076	-173.2°	-.075	-.009
06:30	.058	-164°	-.0557	-.016	.060	-150°	-.052	-.03
07:30	.033	-172.1°	-.033	-.0046	.035	-175.1°	-.035	-.003
08:30	.025	121.8°	-.013	.021	.028	140.7°	-.022	.018
Average Velocities	Scalar .069 (M/S)	—	-.017	.045	Scalar .074 (M/S)	—	-.025	.042

Table 12. Drogued buoy velocity vectors during drogue sea test.

Date & Time	Drogued Surface Float Velocities V_3 (M/S)				Wind Velocities, V_w (M/S)				
	$ V_3 $	$\theta_3 = \angle V_3$	$ V_3 \cos \theta_3$	$ V_3 \sin \theta_3$	$ V_w $	$\theta_w = \angle V_w$	$ V_w \cos \theta_w$	$ V_w \sin \theta_w$	
March 6-7, 1975									
10:30	.219	71.4°	.07	.208	7.73	112°	-2.89	7.17	
11:30	.219	71.4°	.07	.208	8.24	112°	-3.09	7.64	
12:30	.218	77.3°	.048	.213	8.76	112°	-3.3	8.12	
13:30	.218	77.3°	.048	.213	8.76	112°	-3.3	8.12	
14:30	.216	78.5°	.043	.212	9.27	112°	-3.45	8.6	
15:30	.247	82.1°	.034	.245	10.3	112°	-3.86	9.55	
16:00 to 24:00	.127	34.8°	.108	.072	6.66	59°	4.46	7.42	
00:30	.093	-18.8°	.088	-.03	5.67	0°	5.67	0.0	
01:30	.048	-7.1°	.048	-.006	5.67	0°	5.67	0.0	
02:30	.042	-55.6°	.024	-.035	5.67	0°	5.67	0.0	
03:30	.085	-2.7°	.086	-.004	5.15	0°	5.15	0.0	
04:30	.065	-120.5°	-.033	-.056	4.63	-15°	4.48	-1.18	
05:30	.071	-125.3°	-.041	-.058	4.11	-30°	3.56	-2.06	
06:30	.059	-125.3°	-.034	-.048	3.56	-45°	2.52	-2.52	
07:30	.040	-106.2°	-.011	-.038	3.56	-45°	2.52	-2.52	
08:30	.075	52.1°	.046	.059	3.08	-52°	1.91	-2.42	
Average Velocities	.187 (M/S)	—	.108	.107	Scalar 7.1 (M/S)	—	2.3	3.9	

Table 13. Velocity vectors of drogued surface float and wind during sea test.

Date & Time	Sky Conditions	Visibility	Wind Direction	Wind Speed (Knots)	Sea Conditions	Sea Period	Temp. (°F)	Barometric Pressure (in Hg)
3/6, 07:00	Cloudy	Hazy, 8 mi.	SSE	6	Calm	—	29	30.19
3/6, 10:00	Cloudy	Hazy, 9 mi.	SSE	15	1'	3 sec.	33	30.19
3/6, 13:00	Cloudy	Hazy, 5 mi.	SSE	17	2'	3 sec.	35	30.12
3/6, 16:00	Cloudy	Hazy, 5 mi.	SSE	20	2'	3 sec.	37	30.03
3/6, 19:00	Cloudy	Hazy, 5 mi.	SSE	22	2'	4 sec	36	29.99
3/6, 22:00	Cloudy	Hazy, 5 mi.	W	8	2'	4 sec.	35	29.98
3/7, 01:00	Clear	Clear, 10 mi.	W	11	1'	5 sec.	36	30.00
3/7, 04:00	Clear	Clear, 10 mi.	W	10	1'	5 sec	35	30.01
3/7, 07:00	Cloudy	Hazy, 6 mi.	NW	7	Calm	—	33	30.02
3/7 10:00	Cloudy	Hazy, 6 mi.	NNW	5	Calm	—	34	30.04

Table 14. Weather conditions recorded at Eastern Point, Gloucester, during sea test.

Date & Time	Visibility (miles)	Wind Direction (Geographical)	Wind Speed (Knots)	Sea Conditions	Sea Period	Barometric Pressure	
						Millibars	Inches of Mercury
3/6/75							
07:00	10	160°	10	Calm	-	1017.6	
10:00	10	160°	18	2 ft.	5 sec.	1017.3	
13:00	10	180°	20	1-2 ft.	5	1015.9	
16:00	10	160°	22	1-2 ft.	5	1011.2	
19:00	5	170°	21	1-2 ft.	5	1009.5	
22:00	10	310°	8	Calm	-	1011.5	
3/7/75							
01:00	10	260°	12	Calm	-	1011.2	
04:00	10	280°	14	Calm	-	1011.2	
07:00	10	290°	14	Calm	-	1012.5	
10:00	10	240°	12	Calm	-	1012.9	

Table 15. Weather conditions recorded at Boston Lightship (18 kilometers south of test area) during sea test.

The tracks of the three test buoys are shown in Figures 20 and 21. It should be observed in Figure 20 that buoys 1 and 2 began to diverge only after 16:00 hours on 6 March, during which time the ship was in port. Figure 21 shows the paths of the surface drogue along with appropriate times.

The implementation of a solution to equations (37) to (39) is carried out in the subsequent tables. Each table portrays vectors in both magnitude-direction as well as component forms.

Table 16 is a computation of the wind forces on the test buoys. It portrays a value for the first term in equations (37) to (39). Table 17 employs the wind force on buoy 3 to solve for the slip velocity of buoy 3 with respect to the wind and also the true surface current, V_s , by the application of equation (39). A plot of the estimated "true" surface current trajectory is shown in Figure 22 along with the uncorrected estimated trajectory of the drogued float (buoy-3) if it were allowed to drift freely and not periodically retrieved and brought alongside the Nova buoy.

Table 18 lists the vector slip velocities of the surface buoys with respect to the true surface current while Table 19 lists the associated forces from the surface current. These forces are the second terms in equations (37) and (38). Table 20 tabulates the sum of the wind and surface current forces on buoys 1 and 2. That is the sum of the first two terms in equations (37) and (38) that give rise to a drogue slip velocity. Table 21 lists the drogue slip velocity vectors arising from the forces listed in Table 20.

It can be seen that the maximum slip velocity for each drogue is .028 m/s and .016 m/s for buoys 1 and 2 respectively. This maximum, occurring during the hour 1500 to 1600 on March 6, 1975, was due primarily to wind forces as shown by a comparison of Tables 16 (wind forces) and 20 (surface current forces).

Table 22 takes the slip velocities of buoys 1 and 2, shown in Table 21 and adds to them the measured buoy velocities from Table 12 in order to arrive at an estimate of the true current at the drogue depth. Figure 23 is a plot of the measured drogued drifting buoy trajectories (buoys 1 and 2) and the estimated trajectories if corrections are made for error influences of wind and surface current. The corrections shown in this plot are derived in a manner based wholly on drag data appearing in Tables 10 and 11. The

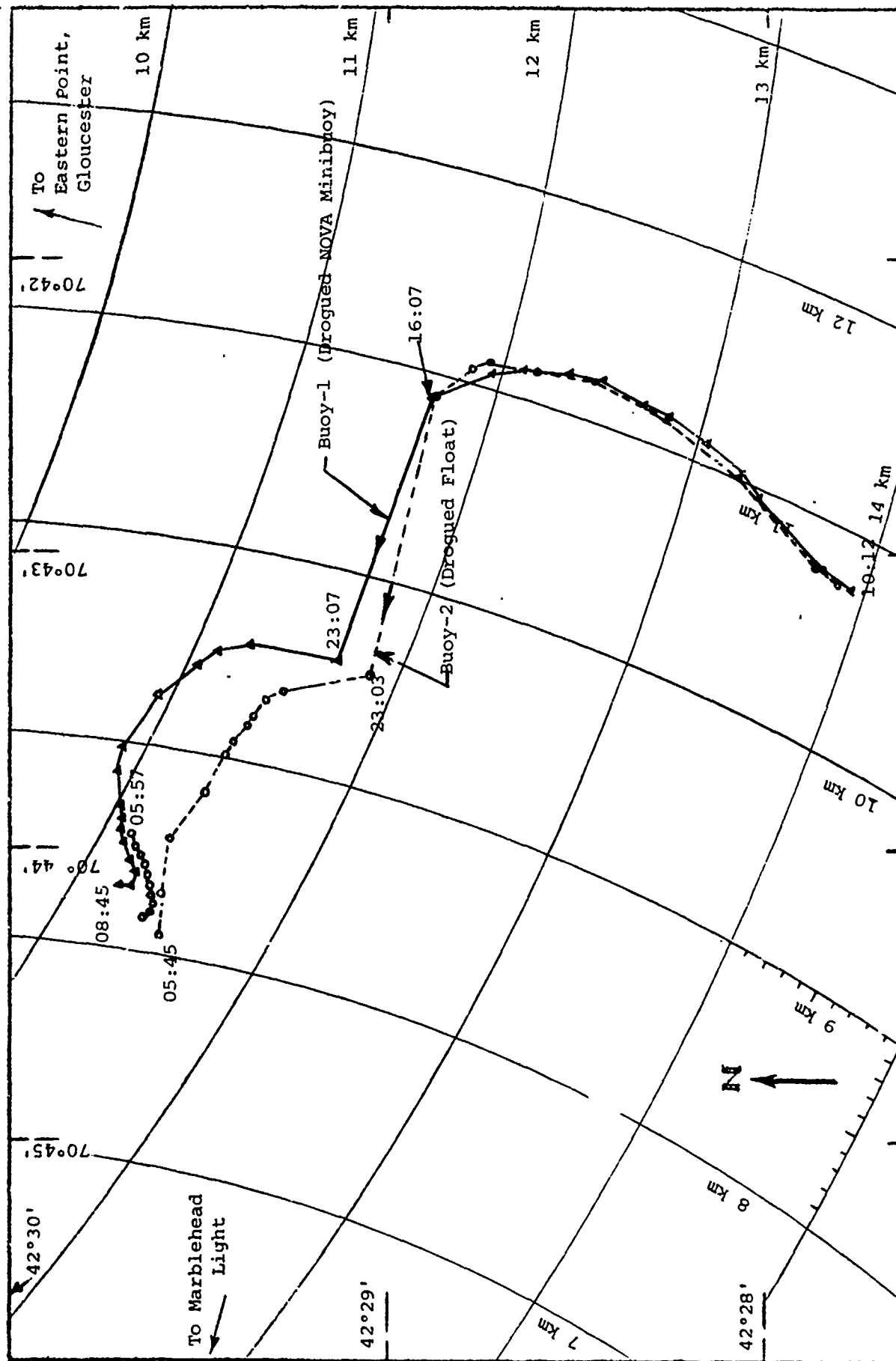


Figure 20. Path of drogued buoys during ocean test of 6-7 March, 1975.

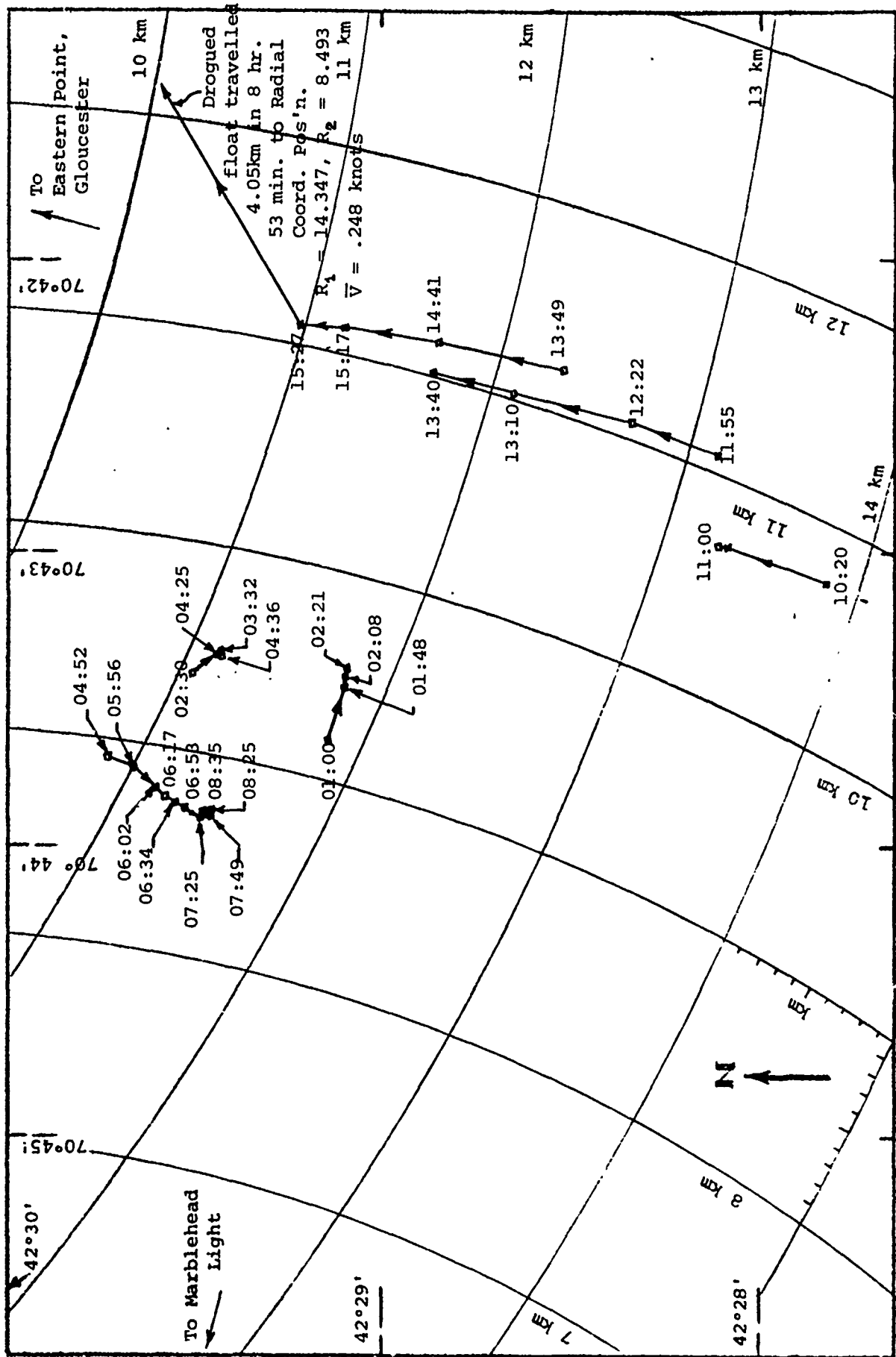


Figure 21. Tracks of surface-drogued float during ocean drift test of 6-7 March, 1975 in Massachusetts Bay.

Date & Local Time March 6, 7 1975	Force on Nova Buoy (1) Due to Wind $F_{1/w}$ (Newtons)			Force on Floats (2) and (3) Due to Wind $F_{2/w} = F_{3/w}$ (Newtons)				
	$ F_{1/w} $	$\theta_{1/w}$	$ F_{1/w} \cos \theta_{1/w}$	$ F_{1/w} \sin \theta_{1/w}$	$ F $	θ	$ F \cos \theta$	$ F \sin \theta$
1030	12.48	112.9°	-4.85	11.5	5.12	112.9°	-1.99	4.72
1130	14.2	113.0°	-5.55	13.07	5.80	113.0°	-2.27	5.34
1230	16.0	112.8°	-6.2	14.75	6.53	113.1°	-2.56	6.00
1330	16.0	112.5°	-6.1	14.75	6.58	112.4°	-2.51	6.09
1430	17.9	112.1°	-5.72	16.6	7.35	112.1	-2.76	6.81
1530	22.2	112.0°	-8.3	20.55	9.13	112.0°	-3.41	8.47
1600 to 2400	15.9	58.7°	8.3	13.6	6.53	58.7°	3.4	5.58
0030	6.8	-6°	6.8	-0.8	2.81	-6°	2.81	-0.3
0130	6.9	-6°	6.9	-0.8	2.841	-5°	2.84	-0.3
0230	6.9	-5°	6.9	-0.8	2.86	-5°	2.86	-0.2
0330	5.7	-5°	5.7	-0.8	2.38	-7°	2.38	-0.3
0430	4.7	-14.9°	4.5	-1.2	1.94	-14.8°	1.87	-0.5
0530	3.7	-29.6°	3.3	-1.8	1.52	-29.4°	1.32	-0.74
0630	2.8	-44.2°	2.0	1.9	1.12	-44.1°	.8	-0.78
0730	2.7	-44.6°	1.9	-1.9	1.12	-44.6°	.8	-0.79
0830	2.1	-51.8°	1.3	-1.6	0.84	-51.6°	.52	-0.66
Average FORCES	8.8	70.5°	2.9	8.3	3.62	70.5°	1.21	3.41

Table 16. Effective wind forces on test buoys during ocean test of 6-7 March 1975 (Hourly averages except 1600-2400 hrs, 3/6/75)

Date & Local Time March 6, 1975	Slip Velocity of Buoy 3 due to Wind $\vec{V}_{3/w}$ (m/s)			True Surface Current Velocity $\vec{V}_s = \vec{V} - \vec{V}_{3/w}$			
	$ \vec{V}_{3/w} $	θ	$ \vec{V}_{3/w} \cos \theta$	$ \vec{V}_s $	θ_s	$ \vec{V}_s \cos \theta_s$	$ \vec{V}_s \sin \theta_s$
1030	.106	112.9°	-.041	.157	44.9°	.111	.111
1130	.113	112.9°	-.044	.155	42.4°	.114	.104
1230	.12	113.1°	-.047	.14	47.3°	.095	.103
1330	.12	113.1°	-.047	.14	47.3°	.095	.103
1430	.127	112.7°	-.049	.132	46.1°	.092	.095
1530	.141	112.6°	-.054	.145	52.5°	.088	.115
1600 to 2400	.119	59.0°	.06	.069	-11.2°	.067	-.013
0030	.078	0°	.078	.0322	-71.0°	.0105	-.0304
0130	.078	0°	.078	.0312	-168.2°	-.0305	-.0064
0230	.079	0°	.079	.0654	-147.7°	-.0552	-.035
0330	.071	0°	.071	.0158	-14.9°	.0153	-.0041
0430	.065	-14.3°	.063	.104	-157.3°	-.096	-.0401
0530	.058	-29.2°	.05	.0956	-161.7°	-.0908	-.03
0630	.050	-44.2°	.036	.071	-169.1°	-.0697	-.0135
0730	.049	-45.0°	.035	.0464	-176.5°	-.0463	-.0028
0830	.043	-53.4°	.026	.0951	78.1°	.0196	.0931
Average Velocities	.0978	Angle 61.9°	x-Veloc .031	Slip speed .086	Angle 30.3°	x-Veloc .034	y-Veloc .020
		y-Veloc .058					

Table 17. Slip velocity of wind relative to surface buoy (3) and corrected true surface current during ocean test.

Date & Local Time March 6, 1975	Uncorrected Nova buoy (1) slip velocity relative to surface current; $\vec{V}_1/s = \vec{V} - \vec{V}_s$ (m/s)			Drogued float (2) slip velocity relative to surface current, $\vec{V}_2/s = \vec{V} - \vec{V}_s$ (m/s)				
	$ \vec{V}_1/s $	θ	$ \vec{V}_1/s \cos \theta$	$ \vec{V}_1/s \sin \theta$	$ \vec{V}_2/s $	θ	$ \vec{V}_2/s \cos \theta$	$ \vec{V}_2/s \sin \theta$
1030	.025	27.9°	.022	.012	.025	28.6°	.022	.012
1130	.008	-27.9°	.007	-.004	.022	-46.8°	.015	-.016
1230	.028	-22.0°	.026	-.01	.049	-86.5°	.003	-.049
1330	.07	5.5°	.069	.007	.087	17.4°	.083	.026
1430	.09	7.0°	.093	.011	.089	8.4°	.088	.013
1530	.13	20.0°	.126	.046	.136	28.4°	.12	.065
1600 to 2400	.116	-19.8°	.11	-.039	.12	-16.0°	.115	-.033
0030	.093	-89.0°	.002	-.093	.092	-76.1°	.022	-.089
0130	.072	100.9°	-.014	-.07	.063	-56.7°	.014	-.061
0230	.092	-112.5°	-.035	-.085	.085	-81.2°	.013	-.084
0330	.081	-39.3°	.062	-.0511	.113	-35.7°	.092	-.066
0430	.079	-115.6°	-.034	-.071	.069	-104.2°	-.017	-.067
0530	.04	-114.6°	-.017	-.037	.026	-127.3°	-.016	-.021
0610	.014	169.8°	-.014	.003	.024	135.0°	-.017	.017
0730	.013	172.5°	-.013	.002	.011	180.0°	-.011	0.0
0830	.079	65.7°	.033	.072	.086	60.6°	.042	.075
Average Velocities	.08	-28.7°	.046	-.025	Speed .084	-17.8°	.06	-.019

Table 18. Drogued buoy slip velocities relative to true surface current before computerized iterations to make Buoy-1 virtual displacement agree with that of Buoy-2.

Date & Local Time	Force on Nova Buoy (1) due to Surface Current, \vec{F}_1/s (Newtons)			Force on float (2) due to Surface Current, \vec{F}_2/s (Newtons)				
	$ \vec{F}_1/s $	θ	$ \vec{F}_1/s \cos \theta$	$ \vec{F}_1/s \sin \theta$	$ \vec{F}_2/s $	θ	$ \vec{F}_2/s \cos \theta$	$ \vec{F}_2/s \sin \theta$
March 6: 1975								
1030	.295	27.9°	.26	.14	.087	27.9°	.08	.04
1130	.03	-27.9°	.03	-.01	.065	-46.2°	.04	-.05
1230	.36	-22.0°	.33	-.13	.333	-86.8°	.02	-.33
1330	2.21	5.5°	2.20	.21	1.02	17.2°	.97	.3
1430	4.03	7.0°	4.00	.49	1.08	8.6°	1.07	.16
1530	8.38	20.0°	7.87	2.87	2.53	28.5°	2.22	1.21
1600 to 2400	6.27	-19.8°	5.9	2.12	1.95	-16.1°	1.88	-.54
0030	4.04	-89.0°	.07	-4.04	1.15	-76.1°	.28	-1.12
0130	2.38	100.9°	-.45	-2.34	.53	-77.6°	.12	-.52
0230	3.92	112.5°	-1.5	-3.62	.99	-81.4°	.15	-.98
0330	3.01	-39.3°	2.32	-1.90	1.75	-35.6°	1.42	-1.02
0430	2.88	-115.6°	-1.24	-2.60	.64	-104.3°	-.16	-.62
0530	.75	-114.6°	-.31	-.68	.096	-127.1°	-.06	-.08
0630	.093	169.8°	-.09	.02	.078	136.6°	-.06	.05
0730	.084	172.5°	-.08	.01	.017	180.0°	-.02	0.0
0830	2.9	65.7°	1.19	2.64	1.00	61.0°	.48	.88
Average Forces	3.72	0.7°	2.69	0.35	1.17	-16.6°	.94	-.28

Table 19. Surface Current Forces on Drogued Buoys

Date & Local Time	Sum of Wind and Surface Current Forces on Nova Buoy, $\vec{F}_1 + \vec{F}_{1/w}$ (Newtons)				Sum of Wind and Surface Current Forces on Drogued Float, $\vec{F}_2 + \vec{F}_{2/w}$ (Newtons)			
	$ \vec{F}_1 $	θ	(Fx) slip	(Fy) slip	$ \vec{F}_2 $	θ	(Fx) slip	(Fy) slip
March 6, 1975								
1030	12.51	111.5°	-4.58	11.64	5.13	111.9°	-1.91	4.76
1130	14.17	112.9°	-5.52	13.05	5.74	112.8°	-2.22	5.29
1230	15.75	111.9°	-5.87	14.61	6.21	114.1°	-2.54	5.67
1330	15.49	104.7°	-3.93	14.99	6.57	103.5°	-1.53	6.39
1430	17.29	99.1°	-2.72	17.08	7.18	103.7°	-1.70	6.98
1530	23.42	91.0°	-4.1	23.42	9.74	97.0°	-1.19	9.67
1600 to 2400	18.21	38.9°	14.17	11.45	7.29	43.7°	5.27	5.04
0030	8.00	-31.0°	6.86	-4.12	3.29	-20.4°	3.08	-1.15
0130	6.85	20.6°	6.41	-2.41	3.01	-10.5°	2.96	-0.55
0230	6.50	34.5°	5.36	-3.68	3.17	-18.4°	3.01	-1.00
0330	8.28	-13.7°	8.05	-1.96	3.94	-15.4°	3.80	-1.05
0430	5.02	-49.2°	3.28	-3.8	2.04	-33.1°	1.71	-1.11
0530	3.84	-40.9°	2.91	-2.52	1.51	-33.1°	1.26	-0.82
0630	2.66	-45.3°	1.87	-1.89	1.04	-44.1°	.75	-0.72
0730	2.67	-45.7°	1.86	-1.90	1.11	-45.2°	.78	-0.79
0830	2.67	22.8°	2.46	1.03	1.03	12.1°	.029	.22
Average Forces	12.64	51.9°	5.63	7.18	5.17	56.1°	2.11	3.14

Table 20. Drogue Slippage Forces on Nova Buoy and Float Before Computerized Iterations to Make Buoy-1 Virtual Displacement Agree with that of Buoy-2

Date & Local Time	Slip Velocity at Nova Buoy (1), $(V_{slip})_1 = \vec{V}_1 - \vec{V}_c$ (m/s)				Slip Velocity at Drogued Float, $(V_{slip})_2 = \vec{V}_2 - \vec{V}_c$ (m/s)			
	$ V_{slip} _1$	θ	$(V_x)_{slip}$	$(V_y)_{slip}$	$ V_{slip} _2$	θ	$(V_x)_{slip}$	$(V_y)_{slip}$
	March 6, 1975							
1030	.021	111.5°	-.008	.020	.012	111.9°	-.004	.01
1130	.022	112.9°	-.008	.020	.012	112.8°	-.005	.009
1230	.023	111.9°	-.008	.021	.013	114.1°	-.005	.013
1330	.023	104.7°	-.006	.022	.013	103.5°	-.003	.012
1430	.024	99.1°	-.004	.024	.014	103.7°	-.003	.014
1530	.028	91.0°	0.000	.028	.016	97.0°	-.002	.016
1600 to 2400	.025	38.9°	.019	.016	.014	43.7°	.01	.009
0030	.016	31.0°	.014	.008	.009	-20.4°	.008	-.001
0130	.015	20.6°	.014	.005	.009	-10.5°	.008	-.002
0230	.015	34.5°	.012	.008	.009	-18.4°	.009	-.003
0330	.017	-13.7°	.017	-.004	.01	-15.4°	.01	-.003
0430	.013	-49.2°	.008	-.01	.007	-33.1°	.006	-.004
0530	.011	-40.9°	.008	-.007	.006	-33.1°	.005	-.003
0630	.01	-45.3°	.007	-.007	.005	-44.1°	.004	-.003
0730	.01	-45.7°	.007	-.007	.005	-45.2°	.004	-.004
0830	.009	22.8°	.008	.003	.005	12.1°	.005	-.001
Average Velocities	Speed .02	50.7°	.009	.011	Speed .011	45.5°	.0051	.0052

Table 21. Drogued Buoy Slip Velocities Prior to Computerized Iterations
on Buoy-1 Virtual Trajectory

Date & Time	True Current at Drogue as Measured by Nova Buoy, $\vec{V}_3 = \vec{V}_1 - (\vec{V}_1 - \vec{V}_2) = \vec{V}_2 - (\vec{V}_1 - \vec{V}_2)$ (M/S)				True Current at Drogue as Measured by Drogued Float, $\vec{V}_c = \vec{V}_2 - (\vec{V}_2 - \vec{V}_c)$ (M/S)			
	$ V_c $	θ	$(V_x)_c$	$(V_y)_c$	$ V_c $	θ	$(V_x)_c$	$(V_y)_c$
March 6 & 7, 1975								
1030	.125	39.6°	.096	.08	.128	43.4°	.093	.088
1130	.145	37.3°	.116	.088	.15	40.3°	.104	.109
1230	.12	49.7°	.078	.092	.171	55.3°	.097	.140
1330	.08	66.7°	.032	.074	.066	76.8°	.015	.064
1430	.06	87.2°	.003	.06	.069	84.2°	.007	.069
1530	.056	132.5°	-.037	.041	.045	130.9°	-.029	.034
1600 to 2400	.062	170.4°	-.061	.01	.059	170.0°	-.058	.010
0030	.072	94.2°	-.005	.071	.066	108.2°	-.020	.062
0130	.076	114.2°	-.031	.07	.077	133.1°	-.053	.056
0230	.067	118.9°	-.032	.058	.093	145.8°	-.077	.052
0330	.081	141.2°	-.063	.051	.108	143.3°	-.087	-.065
0430	.082	149.9°	-.071	.041	.090	160.3°	-.085	.030
0530	.084	170.4°	-.083	.014	.08	-176.2°	-.08	-.005
0630	.063	171.6°	-.062	-.009	.062	-154.8°	-.056	-.026
0730	.04	176.9°	-.040	.002	.039	+178.5°	-.039	+0.001
0830	.028	141.5°	-.022	.017	.032	148.1°	-.027	.017
Average Velocities	Speed .073 m/s	126.8°	-.027	.036	Speed .076 m/s	135°	-.030	.030

Notes: Low Tides, Boston: 12:21 (3/6/75) & 00:35 (3/7/75); High Tides: 18:36 (3/6/75) & 06:57 (3/7/75)

Table 22. Estimate of True Current at Drogue Depth (24m.) as Measured by Buoys 1 and 2 Before Computerized Iteration on Buoy-1 Virtual Trajectory to Make it Agree with that of Buoy-2.

corrected trajectories are derived by making a progressive vector diagram of the hourly estimates of the true current at the depth of the drogue. These values are given in Table 22. The mathematical corrections that are employed in order to arrive at these estimates assume that a negligible amount of horizontal variability in winds and currents existed between where the buoys actually were and where they would be after the correction is taken into account. Figure 23, which is much like a progressive vector plot for a moored current meter, cannot be really made accurately because of these variations over the test area. As pointed out by Kirwan and McNally (1975) and others, the error-inducing effects of wind and surface currents can push a drogued drifter into an area of the ocean in which the currents, and even the wind field, may bear no relation to the parcel of water originally tagged. In reality, corrected hourly velocity vectors at the buoy location would be a more appropriate manner in which to display such drifter data. One would then obtain a series of 1-hour streamlines in the direction of the estimated true current, displaced from each other by the wind and surface current-inducing errors arising during that hour.

Figure 23 is very useful for illustration purposes. It is very easy to see the amount of velocity correction required in order to bring the corrected trajectory of each drogued buoy into closer agreement with each other. A computerized solution to equations (37) to (39) will be shown which will allow one to place the computerized estimate of each buoy at the same virtual location at the end of the test by varying the $C_D A$ of the Nova buoy both above or below water (lumped with 1/2 of tether line). It is, however, interesting to note that by employing "standard" drag coefficient shown in Tables 10 and 11 the corrected virtual destination of the Nova buoy differs from the virtual destination of the drogued float (assumed to be the true destination) by only 25% of the total correction for the Nova buoy.

Figure 23 also shows that the deep current (at 24 meters) was closely following the surface current for approximately the first 6 hours of the test. During this period the wind was blowing strongly in the same general southerly direction as the deep current. Then the wind dropped abruptly and came from the northwest. During this period the surface and deep currents stopped tracking each other. The value of the surface current dropped sharply

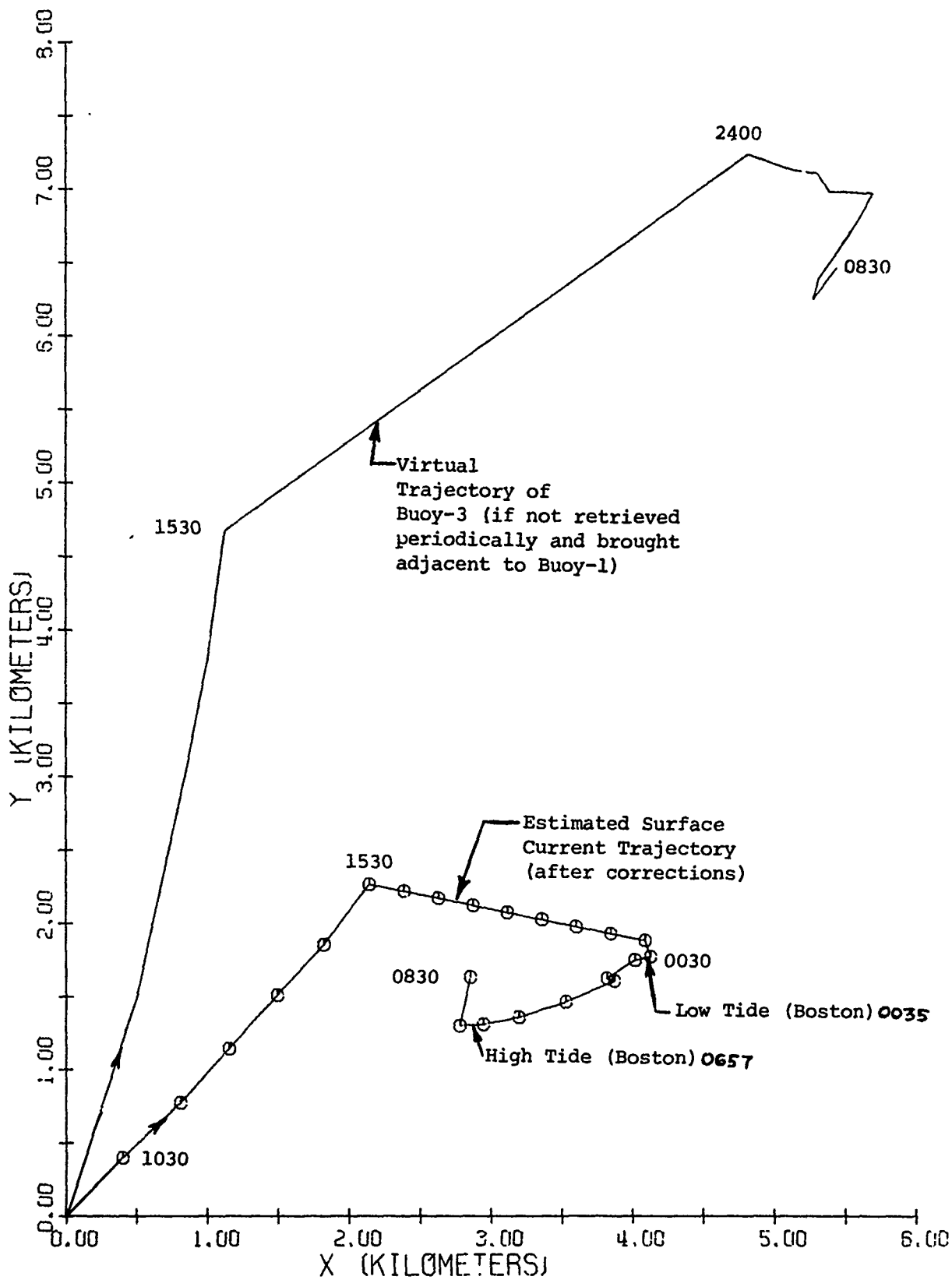


Figure 22. Virtual trajectory of surface drogued buoy and estimated surface current trajectory.

Legend

- Buoy-2 Measured Trajectory
- Buoy-2 Corrected Trajectory
- ▲—▲ Buoy-1 Measured Trajectory
- +—+ Buoy-1 Trajectory after standard correction
for wind and surface current forces

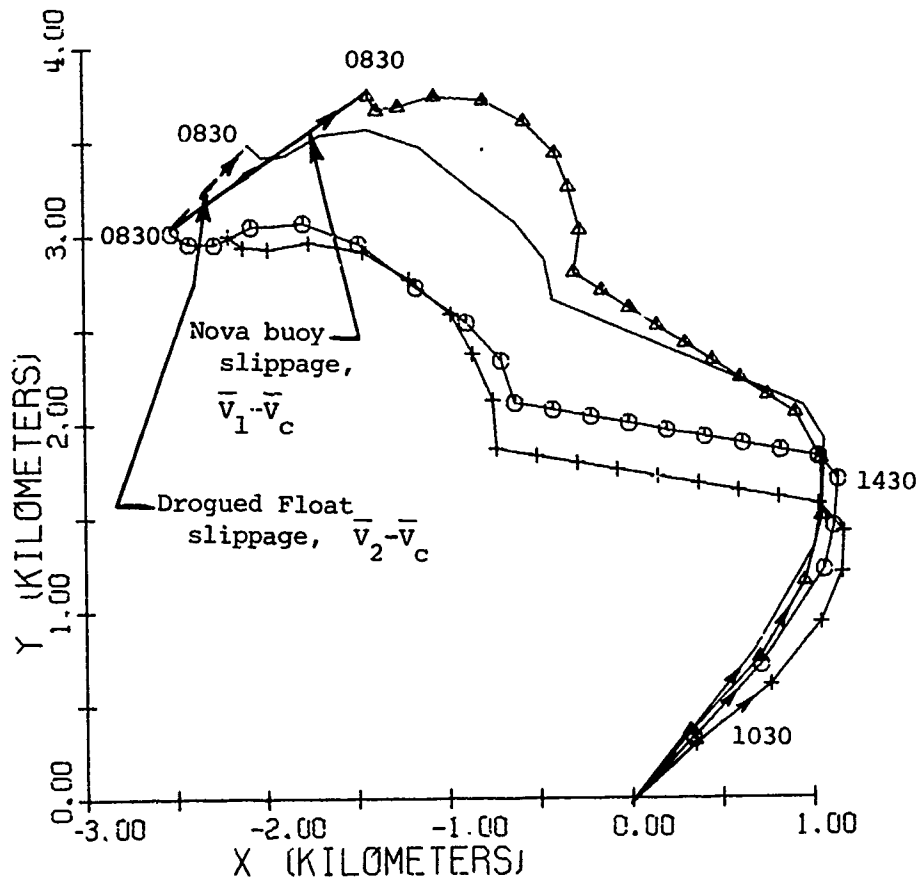


Figure 23. Corrected and uncorrected (measured) trajectories of drogues buoys showing estimated slippage for each drogue buoy.

(see Table 17) and went into a small clockwise circular motion. The corrected surface current trajectory shown in Figure 22 shows a strong correlation with the high and low tides in nearby Boston (see also bottom of Table 22). The deep current, on the other hand, maintained most of its velocity and began turning to the west (i.e., left) and never went into a circular motion. The reason for this apparent shear between the surface and 24 meters is not understood nor is there an explanation for the fact that current at 24 meters is larger than that at the surface.

In order to explore the information contained in Tables 16 through 21 more fully, time series plots of much of the data are shown. Figure 24 is a plot of the North-South (N-S) and East-West (E-W) components of wind force on buoy-2 as well as the sum of the wind and surface current forces as given in Tables 16 and 20 respectively. It can be seen that for the first 6 hours the error-inducing forces were building up leading to the greatest slip velocity occurring just prior to the loss of the ship's rudder at hour 6. Secondly it can be seen that the predominant error force is from the wind. Figure 25 contains plots of the simultaneous components of the buoy-2 slip velocity during the test taken from Table 21. It can again be seen that the peak estimated slippage value is about 1.6 cm/sec just prior to the 6th hour as expected from the force history.

Figures 26 through 29 are plots of the time history of estimates of error-inducing forces and drogue slippage at the Nova buoy. Figures 26 and 27 are values which are calculated, based on the standard drag coefficients given in Tables 10 and 11 and listed in Tables 16, 20, and 21. Figure 26 contains calculated histories of the N-S and E-W components of both the estimated wind and the sum of wind and surface current forces on buoy-1. Figure 27 is the time history of the N-S and E-W components of estimated slip velocity. By comparing Figures 26 and 27 it can be seen that the general shape of the components of slippage in Figure 27 is the same as that for the same component of wind only in Figure 26. Small differences arise due to the role of surface current-induced forces.

Figures 28 and 29 are revised versions of Figures 26 and 27, respectively, based on a computerized iterative solution which mathematically allowed a variation in the drag area of the Nova buoy (buoy-1) both above and below water in order to cause the terminal point of its trajectory to closely coincide with that of buoy-2 (see Figure 23). The solutions were carried out

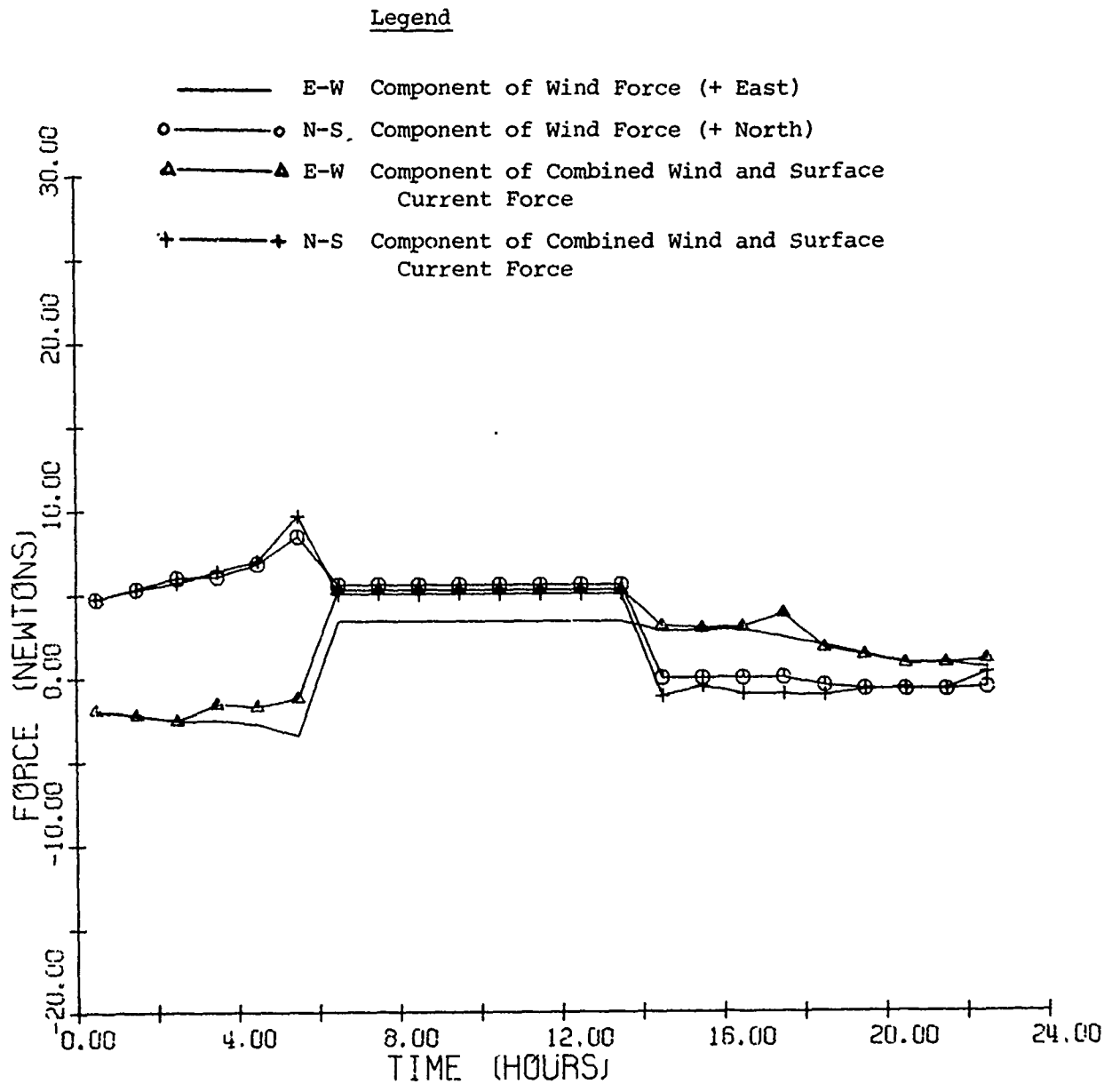


Figure 24. Plot of estimated error-inducing forces on Buoy-2 as function of time.

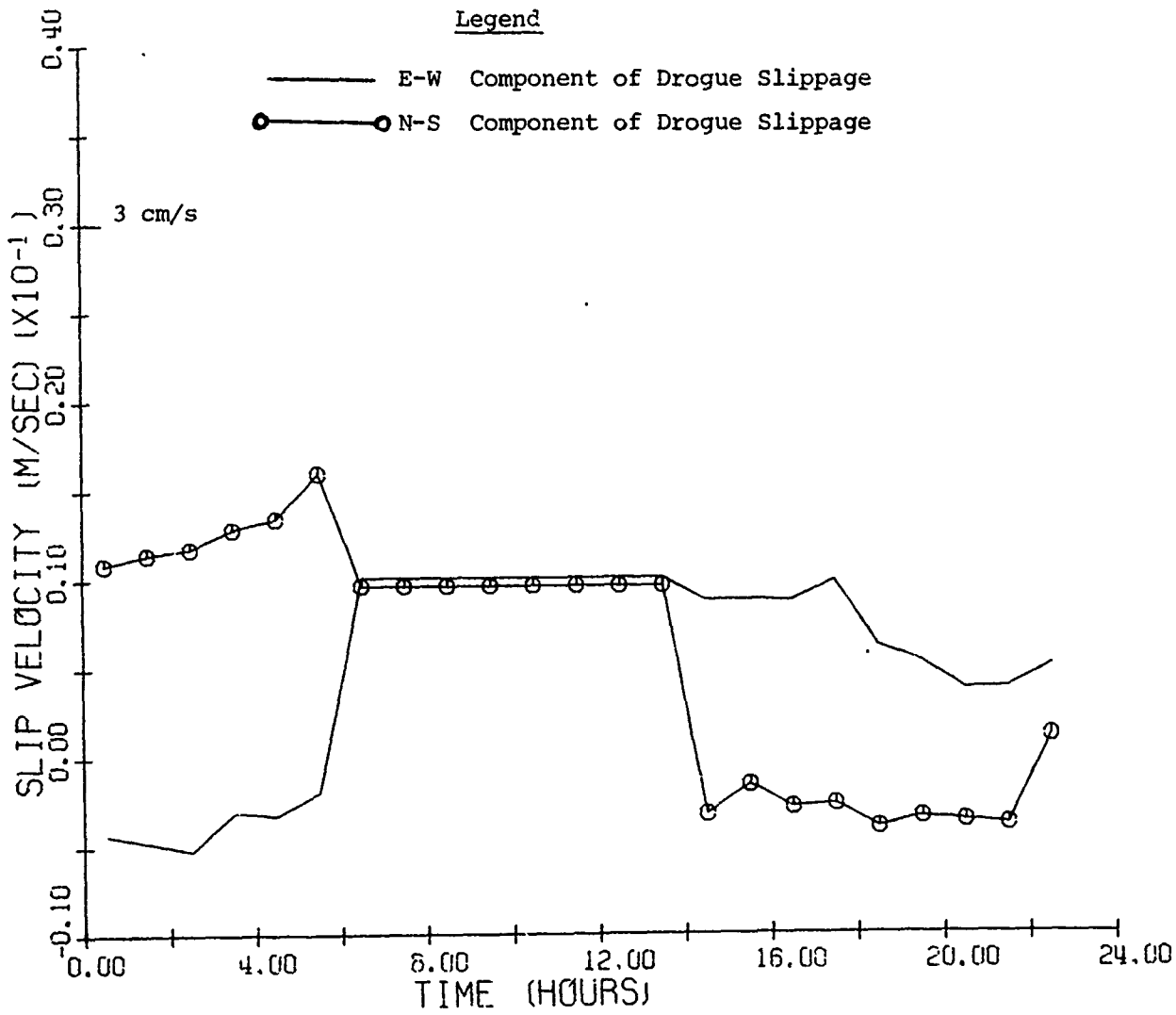


Figure 25. Estimated components of buoy-2 drogue slippage velocity.

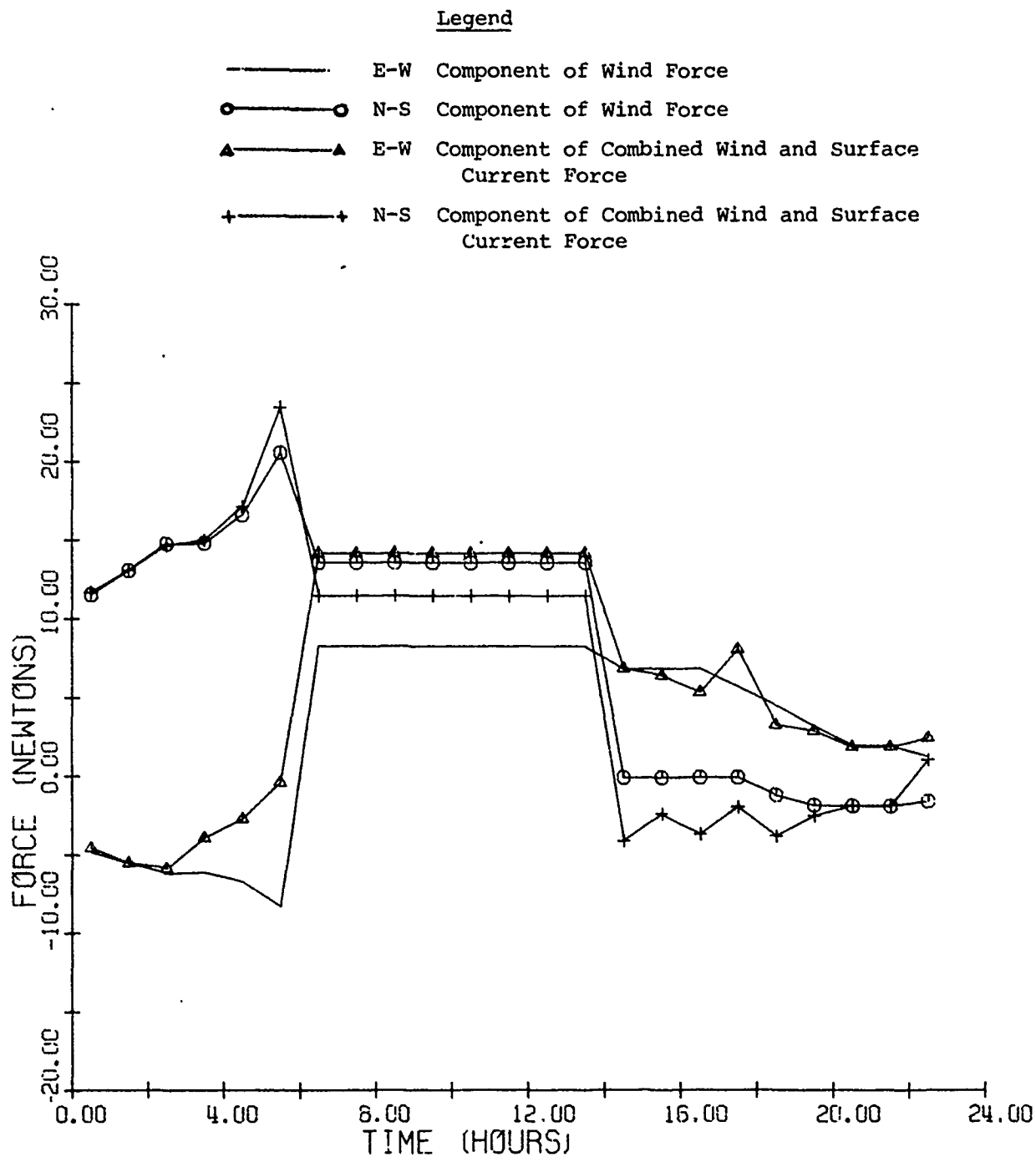


Figure 26. Estimated history of error-inducing forces on buoy-1 (Nova Buoy) before iterating on drag coefficients in order to make estimated trajectory agree with that of buoy-2.

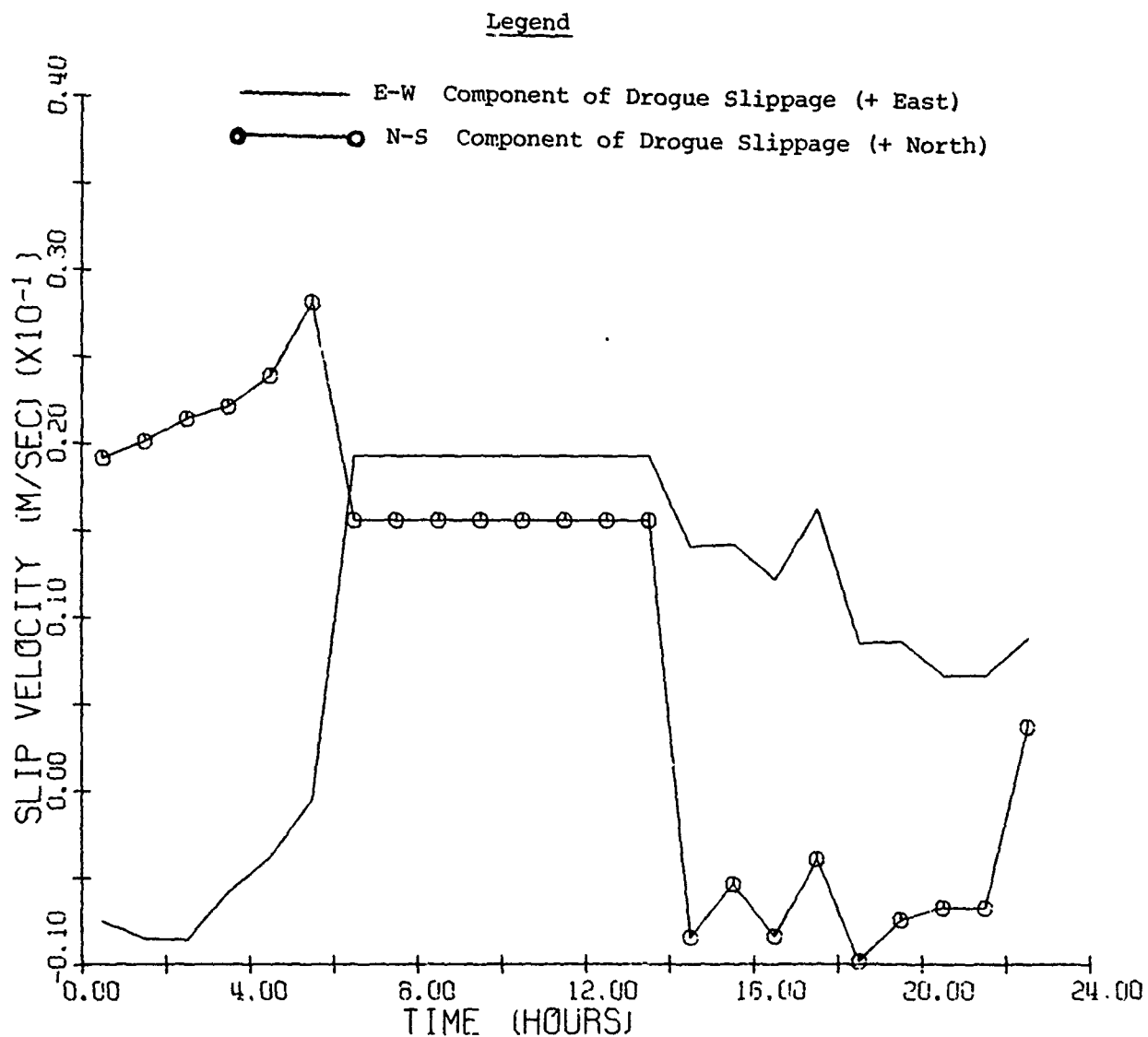


Figure 27. Estimated components of buoy-1 (Nova Buoy) drogue slip velocity before iterating on buoy-1 drag coefficients in order to make estimated current trajectory agree with that of buoy-2.

Legend

- E-W Component of Wind Force (+ East)
- N-S Component of Wind Force (+ North)
- ▲—▲ E-W Component of Combined Wind and Surface Current Force
- ✦—✦ N-S Component of Combined Wind and Surface Current Force

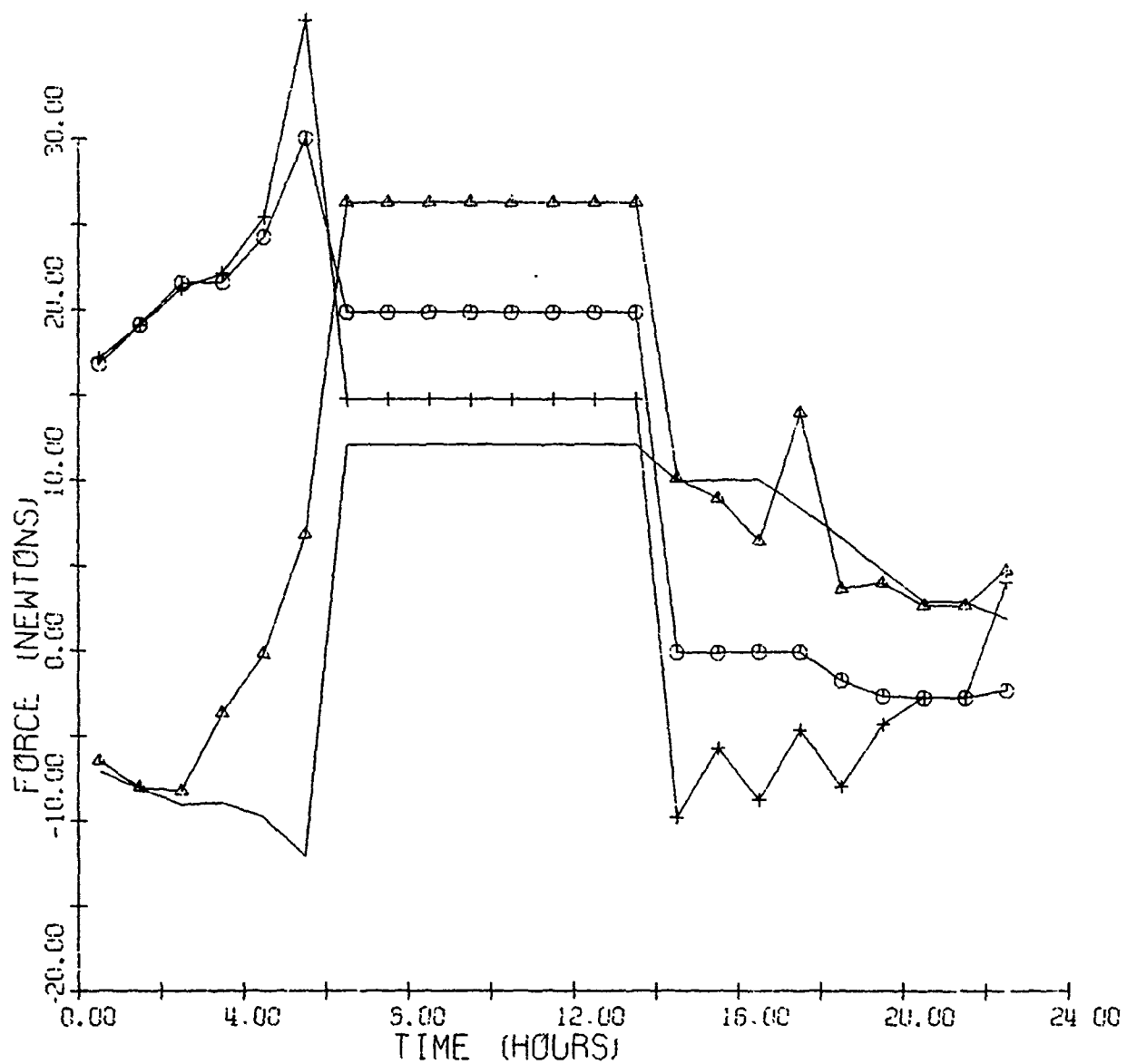


Figure 28. Estimated history of error-inducing forces on buoy-1 (Nova Buoy) after iterating on drag coefficients in order to make estimated current trajectory agree with that of buoy-2.

Legend

- W-W Component of Drogue Slippage (+ East)
- N-S Component of Drogue Slippage (+ North)

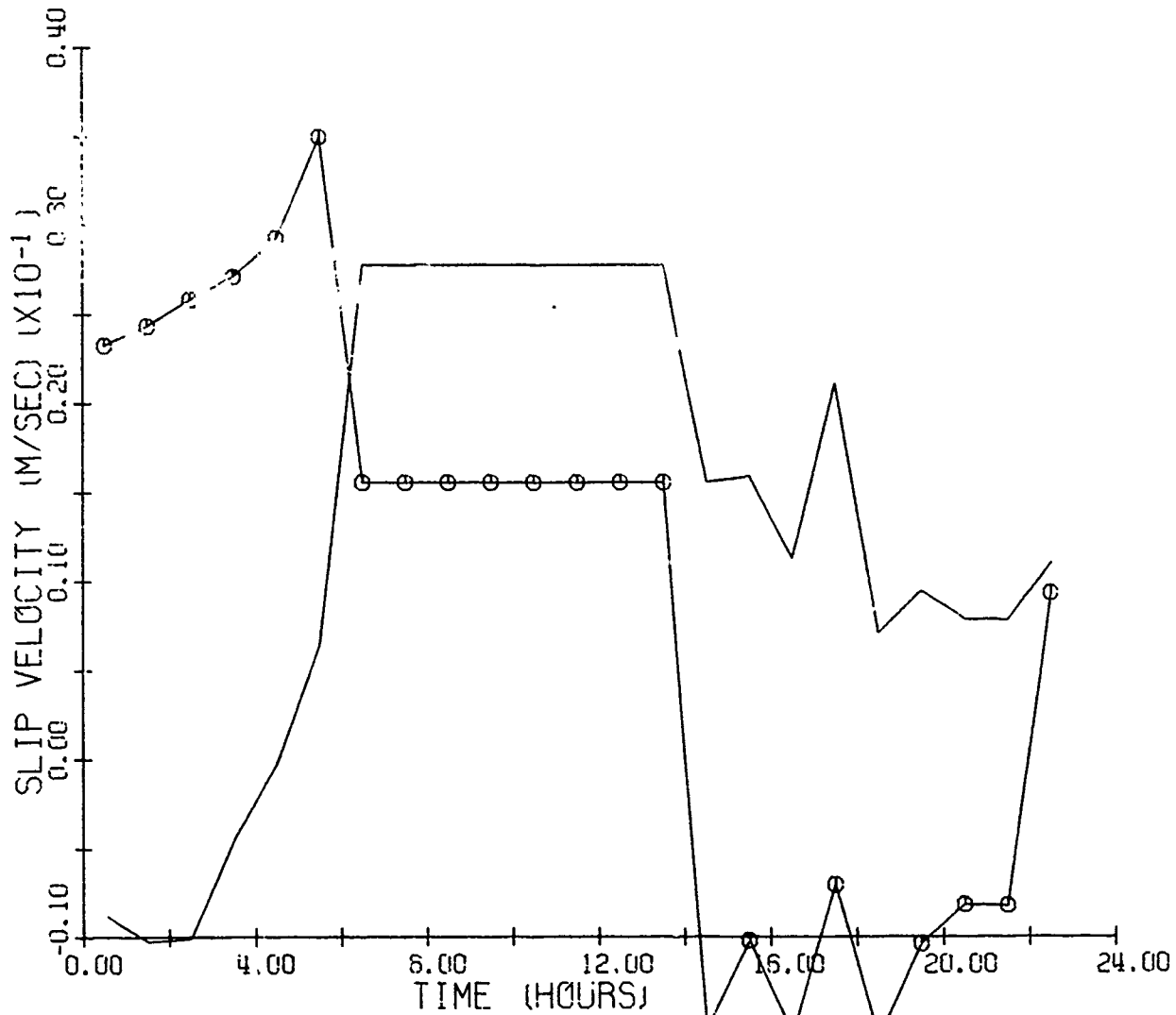


Figure 29. Estimated components of buoy-1 (Nova Buoy) drogue slip velocity after iterating on buoy-1 drag coefficients in order to make estimated current trajectory agree with that of buoy-2.

to explore the amount by which "standard" estimates of wind and surface current effects might have to be altered in order to account for such additional influences as wave excitation and buoy force rectification. The term "standard" refers to the fact that drag coefficients measured under steady flow conditions are employed. During the iterative scheme, the following assumptions were made in order to simplify the analysis.

Analytical Assumptions

(1) During any given iteration the drogue drag coefficient was assumed to be constant. The nominal drag coefficient for both drogues was assumed to be 2.6. It was, however, varied to either side of the nominal in different runs in order to explore the sensitivity of the solution to $(C_D)_{\text{drogue}}$. As will be shown later, measurements of the true drogue angle by the attached Force Vector Recorder indicate that the drogue may not have been weathervaning perpendicular to the net relative velocity vector all of the time. In such a situation the assumption of a constant $(C_D)_{\text{drogue}}$ near or at the nominal value tends to overly minimize the slippage correction.

(2) The corrected or "true" trajectory of the drogued float (buoy-2) was assumed as the correct path which the Nova buoy should be seeking for its corrected path. This assumption is tantamount to assuming that the float drag areas above and below water are more precisely known and therefore the corrected buoy trajectory is precise. This assumption, again, may be in error due to wave-induced effects, as will be discussed later, but it presents one point of departure for estimating our ability to properly account for the wind, wave and surface current influences. By reference to Table 10, it can be seen that the drag areas of the drogued float are initially estimated to be of the order of one-third of those for the Nova buoy. Therefore it is felt that any unquantifiable influence inhibiting the ability to properly correct for drogue errors (e.g., wave effects) is less by a similar factor on the drogued float. In addition, Table 11 indicates that the drogued float contains a larger drogue than that suspended beneath the Nova buoy. It is felt that the drogue beneath the float,

if properly weathervaning, will exhibit a drag coefficient in the presence of wave dynamics, that is different (and possibly higher) than that beneath the Nova buoy. In any event, it is felt that the coefficient will be closer to the value that was measured in the steady flow quarry tests and employed in slippage corrections. This feeling prevails because the drogued float is not a surface-following buoy as in the case of the Nova buoy. It will submerge with the passing of waves and should therefore not propagate a high level of vertical dynamics down to the drogue which may alter the flow pattern around the drogue or cause it to skip along with each rise and fall of the buoy. Therefore, for estimation purposes the drogued float corrected trajectory is assumed to be the "ground truth" estimate.

By comparing Figures 27 and 29 it can be seen that the peak drogue slippage has increased from approximately 2.8 cm/s to 3.6 cm/s during the most energetic time. During all other times too the slippage has been raised due to a requirement for increased windage and wetted drag area in order to make the trajectory of the Nova buoy match that of the drogued float. The amount by which the drag areas of each buoy had to be raised is shown in Table 23. Here the data for three different buoy trajectory correction analyses are shown for drogue drag coefficients of 2.3, 2.6, and 2.9. The nominal case of $(C_D)_{\text{drogue}} = 2.6$ will be used for discussion purposes. It can be seen in Table 23 (2nd row, last 2 columns) that the values of the Nova buoy drag constants which appear in equation (37), K_1 (windage constant) and K_2 (surface current constant), must be raised by 54 and 140 percent respectively in order to get the terminal points of the trajectories to coincide within 9.8 meters. Table 23 also summarizes the total displacement of the buoys from their initial launch point, as shown in Figure 24, as well as the initial displacement error before iterations (but after "standard" slippage corrections), and the final displacement error after iterations.

A few points can be inferred from the analysis described. First, because the windage coefficient, K_1 , requires on a 54% increase (i.e. for the nominal case of $(C_D)_{\text{drogue}} = 2.6$) in order to correct for drift errors in its direction, it is felt that in general the wind drag forces can be better modelled analytically than the surface current forces although the magnitude of wind-induced error is greater in this test. Secondly, because the wind forces are the predominant slippage error sources in this test, as shown by comparing Tables 16 and 19, it seems that a first order slippage error correction based

only on wind effects would not be too far wrong. It is additionally possible to assume only a knowledge of the wind and estimate that the surface current is colinear with and wholly induced by the wind at a speed equal to 3.5 percent of the wind velocity. If such an assumption is made, which has historical precedence (See Wu, 1975), the associated surface current velocities will be in excess of those values estimated in Table 17 by factors of between 1.5 and 6 and non-aligned with the estimates in Table 17. This calculation was not done, but it is felt it would not significantly enhance a slippage correction based wholly on wind forces and it may reduce the accuracy. In addition, if the drogue drag coefficient is reduced, the rationale for which seems reasonable and will be explained later, the augmentation to the required windage and surface current coefficients is less. This effect is shown by comparing rows 1 and 2 in Table 23.

An examination of Tables 16-22 can be made simpler and more concise if a tabulation is given of the more important parameters averaged over the experiment. In addition, it is illustrative to list the hourly averages of these same parameters during the most energetic time, 1500 to 1600 hours on March 6, when the wind was blowing the strongest. Table 24 lists the magnitude 23-hour average vector velocity (by component averaging), or the wind inferred surface current (using equation (39) and a measure of \bar{V}_w), the measured velocities of the three buoys, as well as the estimated "true" current and slip current after trajectory iterations. Table 25 lists the ratios of the average values of slip velocity to wind, surface current, and "true" deep current as measured by each drogued buoy. The ratio of the average value of surface to deep current is also shown.

It is somewhat misleading to look only at the velocity ratios shown in Table 25 in gaining an appreciation of the net effect that took place during the experiment. For example, if the surface current, V_s , and the deep current, V_c , were cyclic in nature, as might be found for tidally-dominated flow, it might be realistic to expect that a body of water would return to the same point approximately every 1 1/2 hours. Average currents over integral multiples of the tidal period would be essentially zero. In such cases, the ratio of the drogue slip velocity to a tidally-dominated

Average Values Over 23 Hours	Values at 1530 Hours
$ \bar{v}_w = 4.53 \text{ m/s @ } 59^\circ$	10.3 m/s @ 112° (max.)
$ \bar{v}_s = 0.039 \text{ m/s @ } 30^\circ$	0.145 m/s @ 53°
$ \bar{v}_1 = 0.048 \text{ m/s @ } 111^\circ$	0.079 m/s @ 119° (max.)
$ \bar{v}_2 = 0.049 \text{ m/s @ } 121^\circ$.059 m/s @ 122° (max.)
$ \bar{v}_3 = 0.102 \text{ m/s @ } 50^\circ$.247 m/s @ 82° (max.)
$ \bar{v}_c _1 = \bar{v}_c _2 = .047 \text{ m/s @ } 130^\circ$	0.058 m/s @ 123° (max.)
Estimated Slip Velocities	
Average	Maximum
$ \bar{v}_1 - \bar{v}_c = 0.0086 \text{ m/s @ } 21.4^\circ$	0.028 m/s @ 91°
$ \bar{v}_2 - \bar{v}_c = 0.0076 \text{ m/s @ } 42^\circ$	0.016 m/s @ 97°

Table 24. List of measured and inferred average and maximum velocities.

Velocity Ratios	
Buoy-1	Buoy-2
$\frac{ \bar{v}_1 - \bar{v}_c }{ \bar{v}_s } = \frac{ \bar{v}_{slip} }{ \bar{v}_s } = 0.22$	0.19
$\frac{ \bar{v}_1 - \bar{v}_c }{ \bar{v}_c } = \frac{ \bar{v}_{slip} }{ \bar{v}_c } = 0.18$	0.16
$\frac{ \bar{v}_1 - \bar{v}_c }{ \bar{v}_w } = \frac{ \bar{v}_{slip} }{ \bar{v}_w } = 0.0019$.0017
$\frac{ \bar{v}_s }{ \bar{v}_c } = 0.83$	$\frac{ \bar{v}_w }{ \bar{v}_s } = 116$

Table 25. List of inferred velocity ratios from measurements made during drogued ocean test (23-hour averages).

surface or deep current velocity would be infinite when averaged over an integer multiple of the semi-diurnal period. In order to appreciate the data more fully it is therefore necessary to ratio the total slip velocity error to the total average velocity of the surface and deep currents by averaging velocities over the total distance travelled by the buoys. This manner of looking at the data is analogous to the way in which the data would be examined in an open ocean test, wherein the surface and deep currents would be expected to go in much straighter paths. Therefore, it is necessary to integrate, over the time of the experiment, the hourly averages of the magnitude of the surface and deep currents as well as the estimates of the slip velocity and divide by the total time of the experiment (i.e., $t_{tot} = 23$ hours) in order to get average total velocities. These values are listed in Table 26 for each buoy and are also given in the bottom row of Tables 17, 21 and 22.

Buoy	Parameter	Average Velocity	
		Knots	m/s
3	$\overline{v_s} = \frac{\int v_s dt}{t_{tot}}$	0.17	.086
1	$\overline{(v_c)_1} = \frac{\int v_c dt}{t_{tot}}$ (for standard correction)	0.142	.073
2	$\overline{(v_c)_2} = \frac{\int v_c dt}{t_{tot}}$	0.14	.072
1	$\overline{(v_{slip})_1} = \frac{\int v_1 - v_2 dt}{t_{tot}}$	0.039	.02
2	$\overline{(v_{slip})_2} = \frac{\int v_2 - v_c dt}{t_{tot}}$	0.021	.011
Wind	$\overline{(v_w)} = \frac{\int v_w dt}{t_{tot}}$	13.84	7.1

Table 26. Summary of surface and deep current as well as slip velocity derived by hourly averages over buoy trajectories during 23-hour ocean test.

Table 27 also lists the ratios of these values for buoys 1 and 2. It can be seen that the picture changes somewhat. First, the drogue slip velocity is now 23% and 13% of the estimated surface current for buoys 1 and 2 respectively where formerly it was 22% and 19% respectively (see Table 25). Secondly, the drogue slippage for the Nova buoy is increased from 18% to 27% of the total estimated deep current motion while for buoy 2 the ratio holds about constant at 15%. It is felt that the slip would be a considerably smaller percentage if the average buoy velocities integrated over the trajectory between 1600 and 2400 hours were known. This would seem to be true because during this period a straight line assumption has been made for the buoy trajectory while all the while additive slippage errors are arising in the direction of the net force on the buoy.

It should be noted that cruder but simpler means are available to arrive at very similar numbers. Given a measurement of the trajectory of a buoy leading to a value for $|\bar{v}_1|$, an estimate of the drag constants K_1 given in section 5.2.1, and only a history of wind forces on the buoy, it is possible to nearly reproduce these ratios by neglecting surface current forces. As an example, the ratio of slip velocity to deep current velocity for the Nova buoy can be estimated from equation (37) by also neglecting the buoy velocity with respect to the wind velocity as follows:

$$K_1 \bar{v}_W |\bar{v}_W| + K_3 (\bar{v}_c - \bar{v}_1) |\bar{v}_c - \bar{v}_1| = 0$$

$$\text{or } |\bar{v}_c - \bar{v}_1| = \sqrt{\frac{K_1}{K_3}} |\bar{v}_W| \text{ (magnitudes only)}$$

Plugging in the "standard" values of K_1 and K_3 along with the scalar average wind velocity during the experiment gives:

$$\bar{v}_c - \bar{v}_1 = \sqrt{\frac{.212}{29,677}} \text{ (7.1)} = .019 \text{ m/s} = \text{ave. slip velocity.}$$

It is further possible to substitute the scalar average value for \bar{v}_1 from the bottom of Table 12 (i.e., .069 m/s) in order to arrive at a simplified estimate of the average deep current velocity:

$$\bar{v}_c = (.019 + .069) = .087 \text{ m/s}$$

Ratio	Buoy-1	Buoy-2
$\frac{\text{Slip Velocity}}{\text{Surface Current Velocity}}$	0.23*	0.13
$\frac{\text{Slip Velocity}}{\text{Deep Current Velocity}}$	0.27*	0.15
$\frac{\text{Surface Current Velocity}}{\text{Deep Current Velocity}}$	1.18*	1.19
$\frac{\text{Wind Velocity}}{\text{Surface Current Velocity}}$	82	82
$\frac{\text{Wind Velocity}}{\text{Deep Current Velocity}}$	97*	98
$\frac{\text{Wind Velocity}}{\text{Slip Velocity}}$	355*	645

*slip velocities and deep current velocities measured by buoy-1 (i.e., Nova) using only "standard" correction for slippage error.

Table 27. Ratios of total slip, water parcel, and wind velocities for both surface and deep currents by integrating velocities over complete buoy trajectory.

Both the value of slip and deep current velocity magnitudes are low but their ratio, $(\overline{V}_{\text{slip}})_1 / (\overline{V}_c)_1 = .22$, is nearly the same as that given in Table 27 (i.e., .27) but requiring less work.

Table 27 also lists the ratio of surface current to deep current which is so near unity that one is led to believe that the flow is uniform with little shear between the surface and a 24-meter depth. This, of course, is not the case as seen by comparing Figures 22 and 23. It can be seen that the average vector surface current is rotated approximately 95° clockwise from the current at 24 meters. A clear illustration of this fact is seen by a comparison of the buoy trajectories between 1600 and 2400 hours on March 6, as shown in Figures 20 and 21. It is also interesting to compare the estimated values for \overline{V}_s and \overline{V}_c during this same period in Tables 17 (for \overline{V}_s) and 22 (for \overline{V}_c). It can be seen that they are travelling in nearly opposite directions with the current at 24 meters almost twice as large as the surface current. The best explanation for this effect can be seen by studying the tidal information at the bottom of Table 22 in relation to the wind information in Tables 14 and 15. It appears that the buoys drogued at 24 meters are generally responding to the tidal influx of water to Boston to the west of the test area while at the same time the surface drogue is following the wind and surface current which is going to the northeast and then east.

6.0 Force Vector Recorder (FVR) Results During Ocean Slippage Test

Appendix C describes the various calibration values (biases and scale factors) that pertained to the FVR sensors during both the quarry towing tests and the ocean tests. Appendix D describes the manner in which the combination of the x and y-axis accelerometers and magnetometers permit an evaluation of the average Euler rotation angles θ , ϕ , and ψ over a 100-second period of data. Both the particular set of Euler angles chosen and their derivation are also given in Appendix D. The results of the quarry test and the ocean test, wherein the drogue vertical drag coefficient was measured, were both summarized in previous sections. This section will discuss the FVR results recorded during the ocean slippage test.

Figure 30 describes the manner in which the FVR is attached to the tether line and drogue top spreader bar. It should be noted that the FVR is free to pivot about an axis parallel to that of the top spreader bar while it is constrained to move in a plane dictated by the bridle and top spreader bar.

6.1 Measured Orientation of Window Shade Drogue

Table 28 lists a series of 100-second average values for the six FVR sensor outputs (in engineering units where possible) during the first 2 hours of the ocean test. After this time the data became noisy indicating that the FVR was becoming loose in its mount. The wire descending from the apex of the bridle eventually came loose and the FVR pivoted downward - supported only by the top spreader bar.

The data from Table 28 are combined as shown in Appendix D in order to arrive at estimates of the three Euler angles shown in Table 29. The simplest possible assumption of zero dynamic acceleration (i.e., $A_x = A_y = A_z = 0$) was made in order to get the Euler angles ϕ and θ . This assumption was found to be a good simplifying approximation based on a simple mathematical dynamic model of a drogued buoy with an FVR attached. The values of ϕ and θ were then computed. In all cases shown the data are 100-second average values for each sensor output.

The true average azimuth angle of the x-axis of the FVR and window shade drogue is computed by resolving the Euler angles onto a horizontal plane according to the relation:

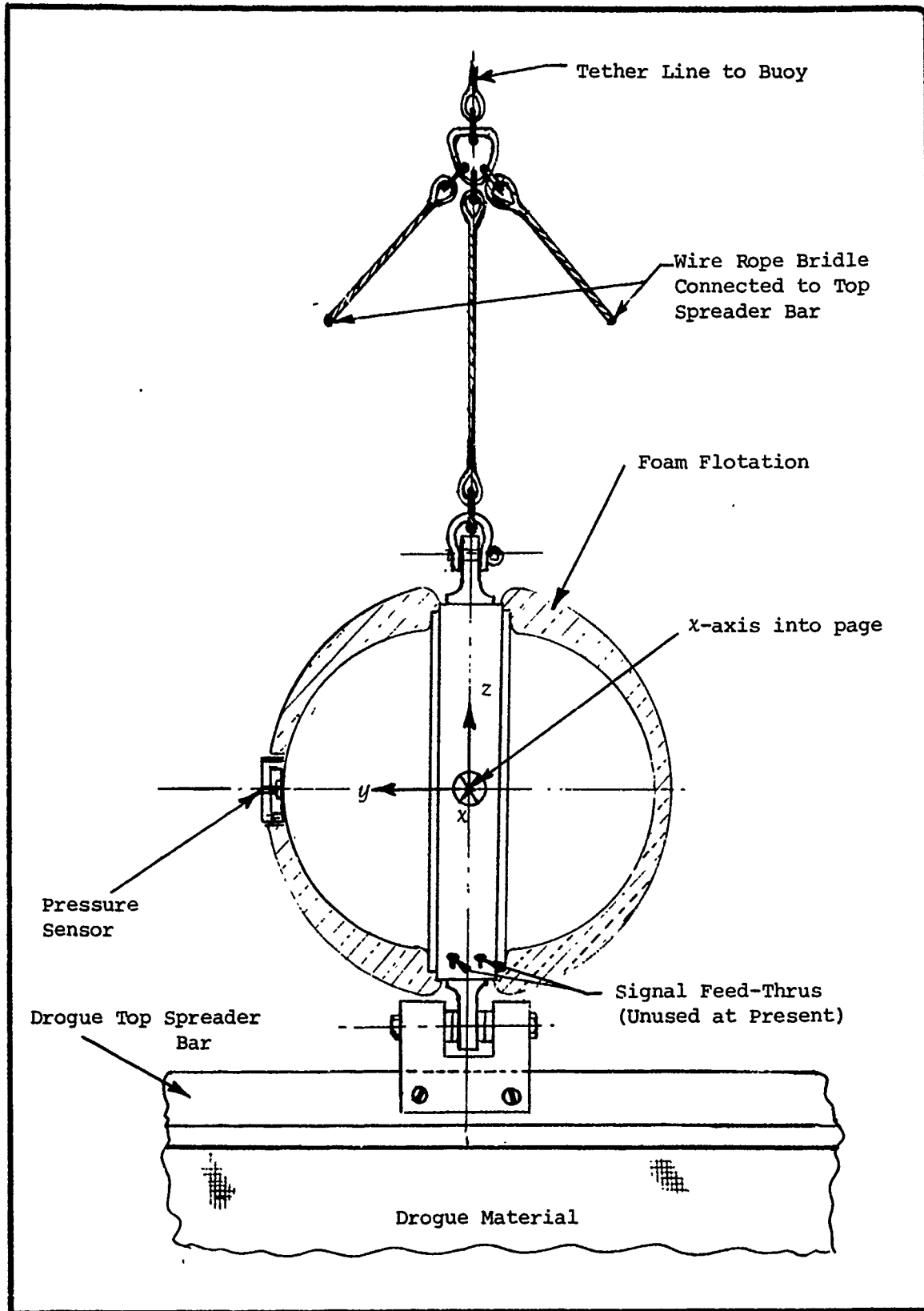


Figure 30. Force vector recorder attachment to drogue top spreader bar, illustrating co-ordinate system employed.

Parameter	Burst 1	Burst 2	Burst 3	Burst 4 (Beginning of Burst)	Burst 4 (End of Burst)
Local Time when FVR Data Acquired	1013 hours	1034 hours	1116 hours	1158 hours	1203 hours
\bar{f}_x (g's)	-.00033	-.0937	-.0622	-.099	-.0963
\bar{f}_y (g's)	.0877	.0622	.1119	.096	.0964
\bar{f}_z (g's)	.9939	.9897	1.017	.989	.9845
\bar{M}_x (counts)	408.1	559.5	537.5	564.6	565.3
\bar{M}_y (counts)	187.5	287.9	274.0	332.7	321.6
\bar{p} (meters)	18.7	18.8	18.4	18.8	18.9

Notes: (1) Local Earth Magnetic Field Dip Angle Estimated to be $\alpha = -69.5^\circ \rightarrow \tan \alpha = -2.675$
(2) Local Declination of Earth's Magnetic Field Assumed = 15° W. of N.
(3) Ratio of magnetic field strength at test site to laboratory estimated to be 1.64 (see Padhi, 1976)
(4) Depth of FVR in calm seas assumed to be 19.3 meters

Table 28. One-Hundred Second Average Values of FVR Data from First Four Bursts taken During Drogued Ocean Test

Parameter	Burst 1	Burst 2	Burst 3	Burst 4 (Beginning of Burst)	Burst 4 (End of Burst)
Local Time	1013 (6 Mar.)	1034	1116	1158	1203
Measured $\bar{\phi}$	-22°	-56.4°	-29°	-45.9°	-45°
Measured $\bar{\theta}$	4.98°	6.4°	7.3°	7.9°	7.8°
Measured $\bar{\psi}$	90°	110°	75.6°	85.6°	86.5°
Measured True Cartesian Azimuth Angle $Az = \psi + \phi \cos \theta + 105^\circ$	194.8°	159°	151.8°	145.1°	146.9°
Direction of Net Estimated Slip Velocity from Table 21	111.5°	111.5°	112.9°	112°	112°
Difference in Azimuth Angle ($Az_{meas.} - Az_{estimated}$)	83.3°	47.5°	38.9°	33.1°	34.9°

Table 29. Summary of Measured Euler and Azimuth Angles of Drogue Top Spreader Bar and Comparison with Estimated Slip Velocity Direction in Table 21

$$Az = \bar{\psi} + \bar{\phi} \cos \theta \quad (40)$$

This relation can be seen by reference to the Euler angle definitions in Figure D-2 (Appendix D). Furthermore, because the azimuth is measured with respect to the magnetic north direction ($\sim 15^\circ$ west of North in Massachusetts Bay), the measured azimuth angle must be related to the previously-calculated Cartesian value by adding 105° . These values are also listed in Table 29 along with an estimate of the azimuth angle of the normal to the drogue based on the net external force arising from wind and surface current influences given in Table 20 or the direction of the slip velocity vector given in Table 21.

It can be seen in the last row of Table 29 that the measured azimuth of the drogue does not closely coincide with the estimated value during the 5 sections of data analyzed. In addition, the measured azimuth of the drogue normal differs even more from the trajectory of the drogue itself as seen in Figure 23. These measurements indicate that the drogue is either side-slipping or not weathervaning as expected. If such were true, the effective drag coefficient of the drogue would be greatly reduced. This result gains additional support from the computer iterative study in section 5 which summarily shows in Table 23 that if the drogue drag coefficient is reduced, the amount of wind correction required for coincident trajectories of 2 different buoys is less.

One might look at the problem from the point of view that the drogue in fact weathervanes normal to the net relative velocity, and that the azimuth orientation measured by the FVR is correct. Based on these assumptions, one could ask how the wind and surface current forces might be altered in order to bring the resultant error force in line with the measured drogue azimuth. Figure 31 illustrates the velocities as well as the wind and surface current forces acting on the Nova buoy and the measured drogue azimuth during the first FVR burst. The data are derived from Tables 16 and 19. It can be seen that because the measured azimuth of the drogue (or 180° from that value) does not lie within the included angle of the wind and surface current forces, no alteration of buoy forces can result in the direction of the net error force coinciding with the measured drogue normal. This fact again points to poor drogue directional performance.

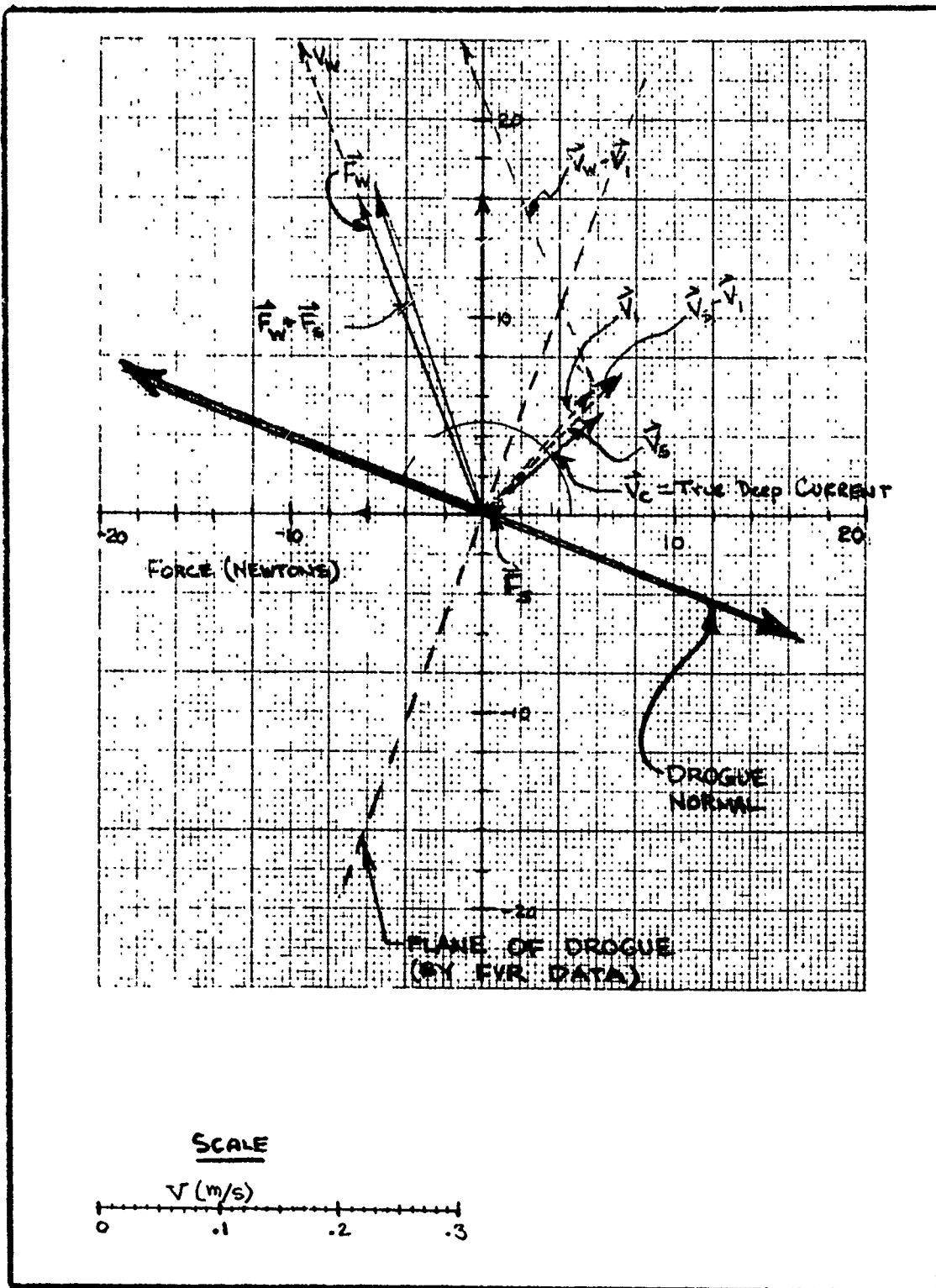


Figure 31. Estimated Forces, Velocities and Measured Drogue Azimuth for Nova Minibuoy

It should be emphasized that for approximately the first 6 hours of the test the drogued buoys stayed remarkably close to each other in the presence of this postulated directional error. For such good trajectory agreement, the drogues must have been experiencing similar errors or possibly the azimuth of the drogue is not as important to its performance as surmised. These questions can only be answered by further instrumented tests.

6.2 Drogue Dynamics

The high frequency dynamics of the top spreader bar of the window shade drogue have been computed for a 100-second block of data during the second burst. The data are plotted in Figures 32 through 36. Figure 32 is a plot of the pressure sensor output indicating that the drogue vertical excursions are approximately ± 1 foot (± 0.3 m). At approximately 40 seconds into the record the drogue is suddenly pulled upward by approximately 7 feet (2m). It does return to its equilibrium depth but only slowly and after about 20 seconds. The dynamic loads incurred on the first major excursion may have been very large but were not measured because a load cell was not present.

The next three plots of drogue Euler angles, Figures 33, 34, and 35; show the effects of the sudden upward motion. It is felt that some of the Euler angle response is due to the fact that dynamic acceleration perpendicular to the tether line is neglected. These plots are still of great value because separate computer simulations of FVR errors in such a drogue configuration indicate the errors are small for benign sea states. This error, which might be greater in heavy seas, could be greatly alleviated if a math model of the drogue were developed and the FVR simulated in the model. The output of the real FVR could then be compared with that of the simulation and a verified model developed. The model could then be used to look at Euler angles.

The following should be noted in the three Euler angle plots:

- (1) The drogue is suddenly changing its tilt angle by up to 8° as the buoy heaves upward (Figure 33).
- (2) As the drogue tilts and rises in the water, the top spreader bar rotates somewhat (Figure 34).
- (3) The drogue top spreader bar is changing its ψ azimuth angle suddenly as well (Figure 35).

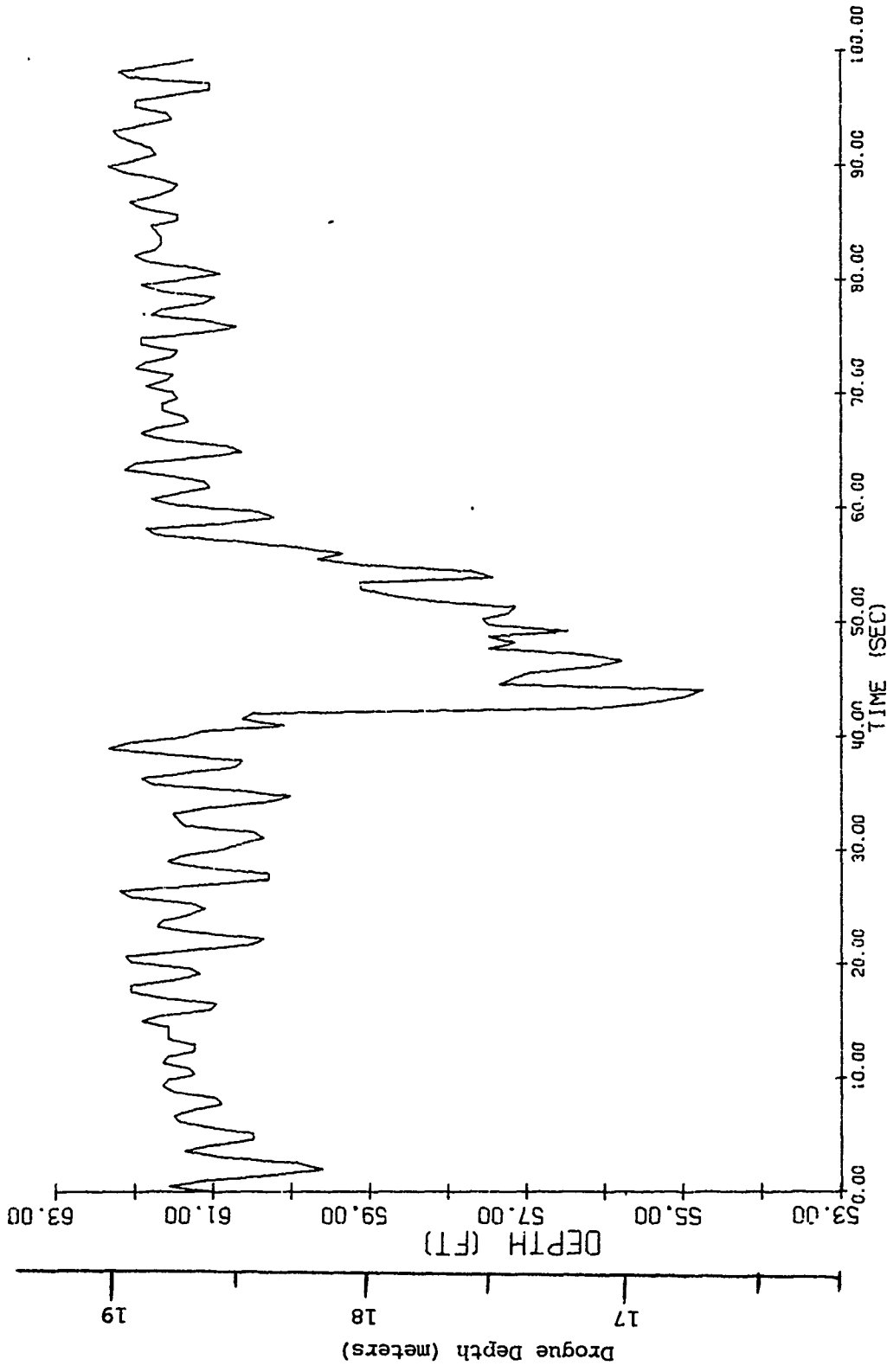


Figure 32. Droque Depth History during Portion of Second FVR Burst

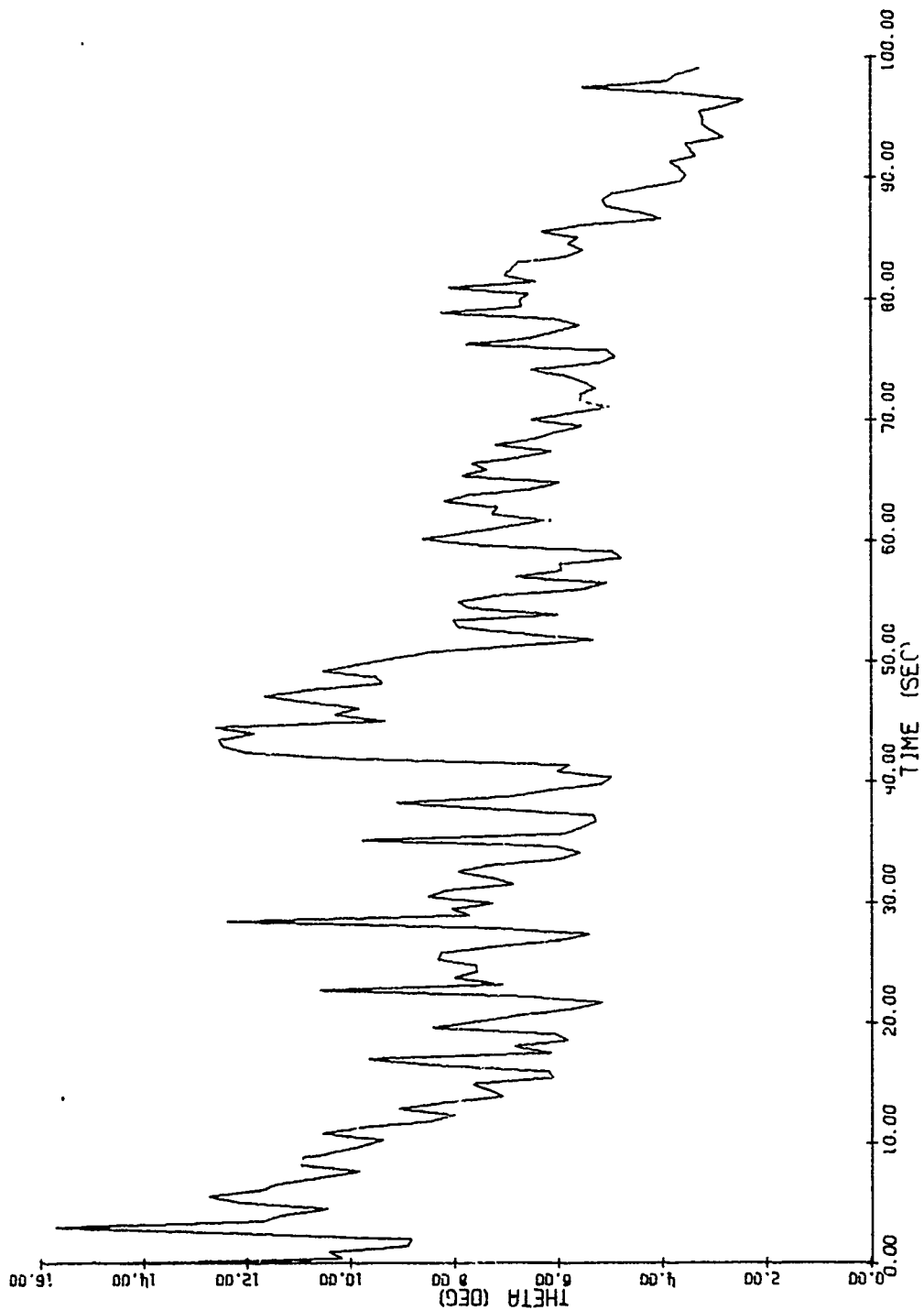


Figure 33. Drogue Tilt Angle History (θ) during Portion of Second FVR Burst

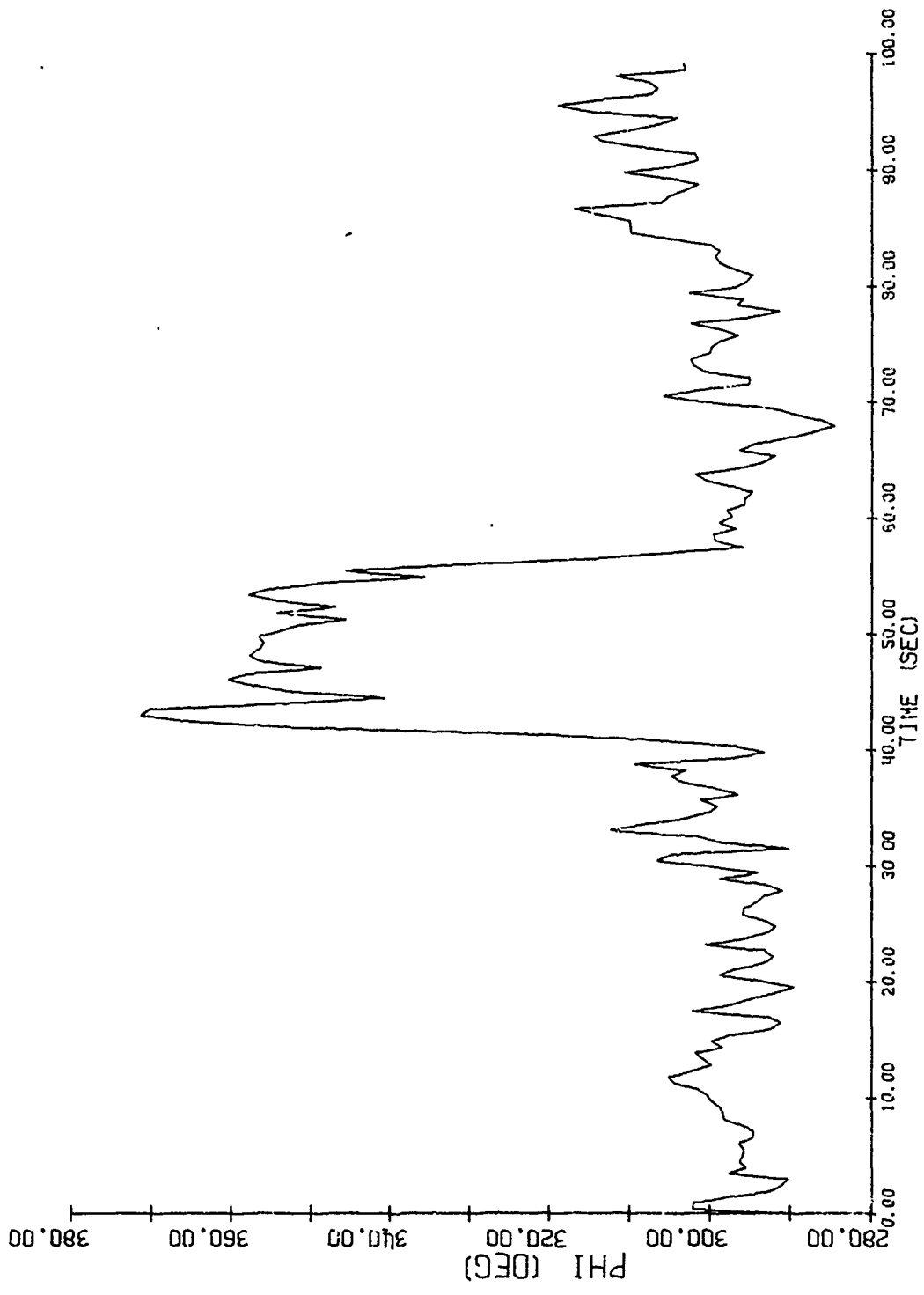


Figure 34. History of Drogue ϕ Euler Angle (Roll) during Portion of Second FVR Burst

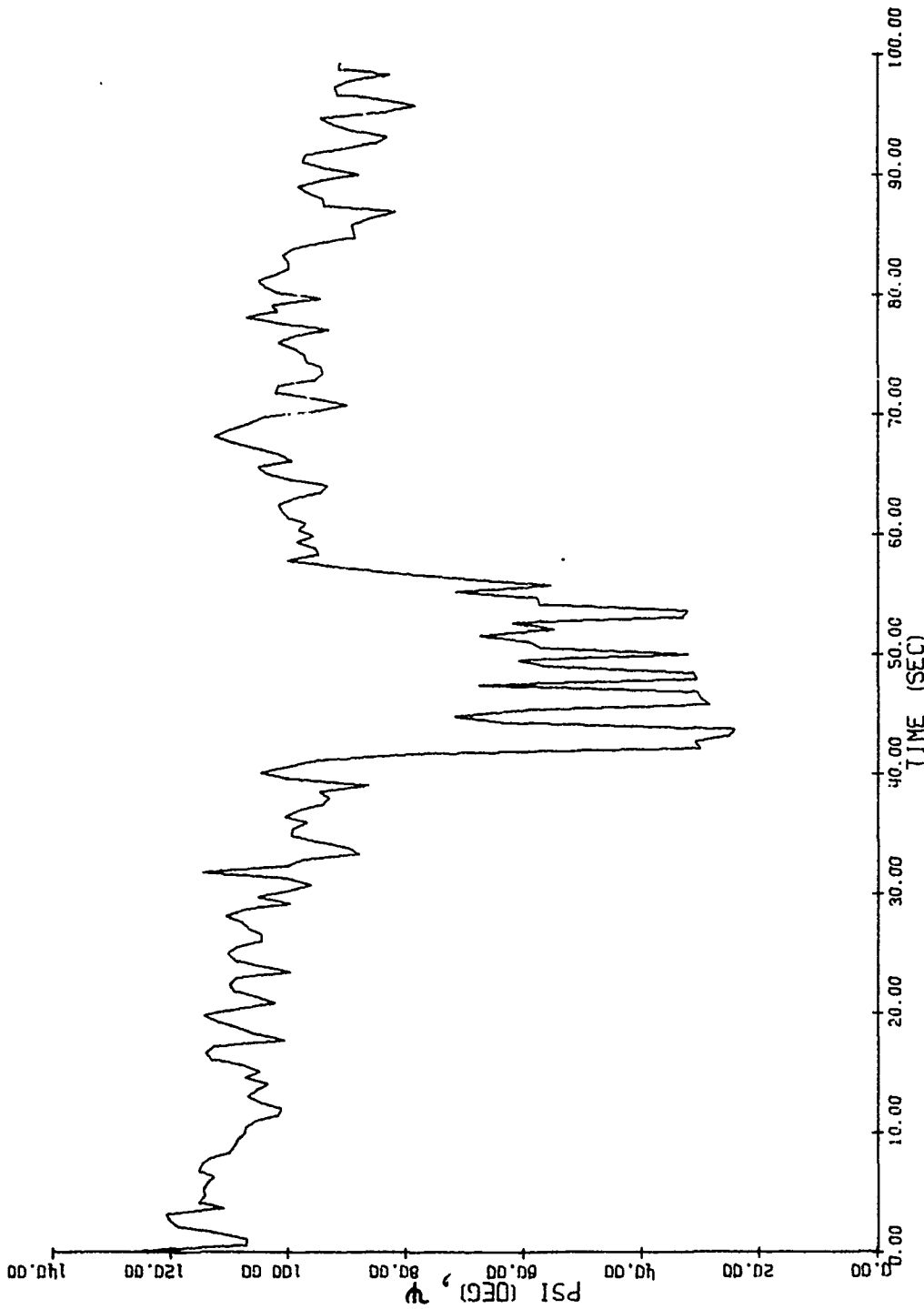


Figure 35. History of Drogue ψ Euler Angle (Yaw) during Portion of Second FVR Burst

In order to get a better idea of the measured azimuth response of the drogue, the computation of the true azimuth angle, given by equation (40), is given in Figure 36 for the same 100-second data sample as Figures 32-35. This value is referenced to magnetic north which is 105° counterclockwise from the Cartesian 0° reference along the x-axis. It should be observed that the true azimuth changes are greatly diminished from those shown in Figure 35 for ψ alone. It is felt that the sudden azimuth changes arising between 40 and 60 seconds are somewhat mathematically induced, owing to the method of data handling. The degree to which this is not true indicates that the top of the drogue is rotating as it is pulled upward. Because of its immense added mass, the whole drogue could not be rotating in azimuth, as indicated in Figure 36. Therefore, the FVR data shown in Figure 36 indicate that the top spreader bar of the drogue rotates with respect to the bottom bar during vertical motion, forming puckers along one or both side hems or a billowing sail effect in general. Both of these surmised responses indicate that in more severe seas, the drogue could be subject to severe dynamical effects which could fatigue or overstress elements of the buoy-drogue system. It is felt that a visualization of the phenomenon and/or a more instrumented test would be sufficient to describe the phenomenon better.

6.3 Estimated Drogue Horizontal Drag Force from FVR Tilt Angle

As discussed in Sections 3 and 4 and summarized in equation (18), it is possible to relate the horizontal component of drag force on the drogue to the tilt angle of the top of the drogue and the total weight of the drogue in water, W . As discussed in section 4, the quarry towing tests indicated that if W was equal to the sum of the wetted ballast weight and one-half the weight of the drogue in water, equation (18) was a fair manner by which to estimate F_D under ideal, non-dynamic conditions (i.e., good to $\pm 20\%$). The results for the first 4 bursts of the drogued ocean test are given in Table 30 and compared with the estimated value of drag force, given in Table 19, which is based solely on calculations of wind and surface current forces. The fourth column of Table 30 is a tabulation of the estimated forces based on standard drag coefficients for the dry and wetted portions of the buoy while the sixth column are similar estimates after the drag areas are revised based on the trajectory iteration described in section 5. It can be seen that the standard mathematical

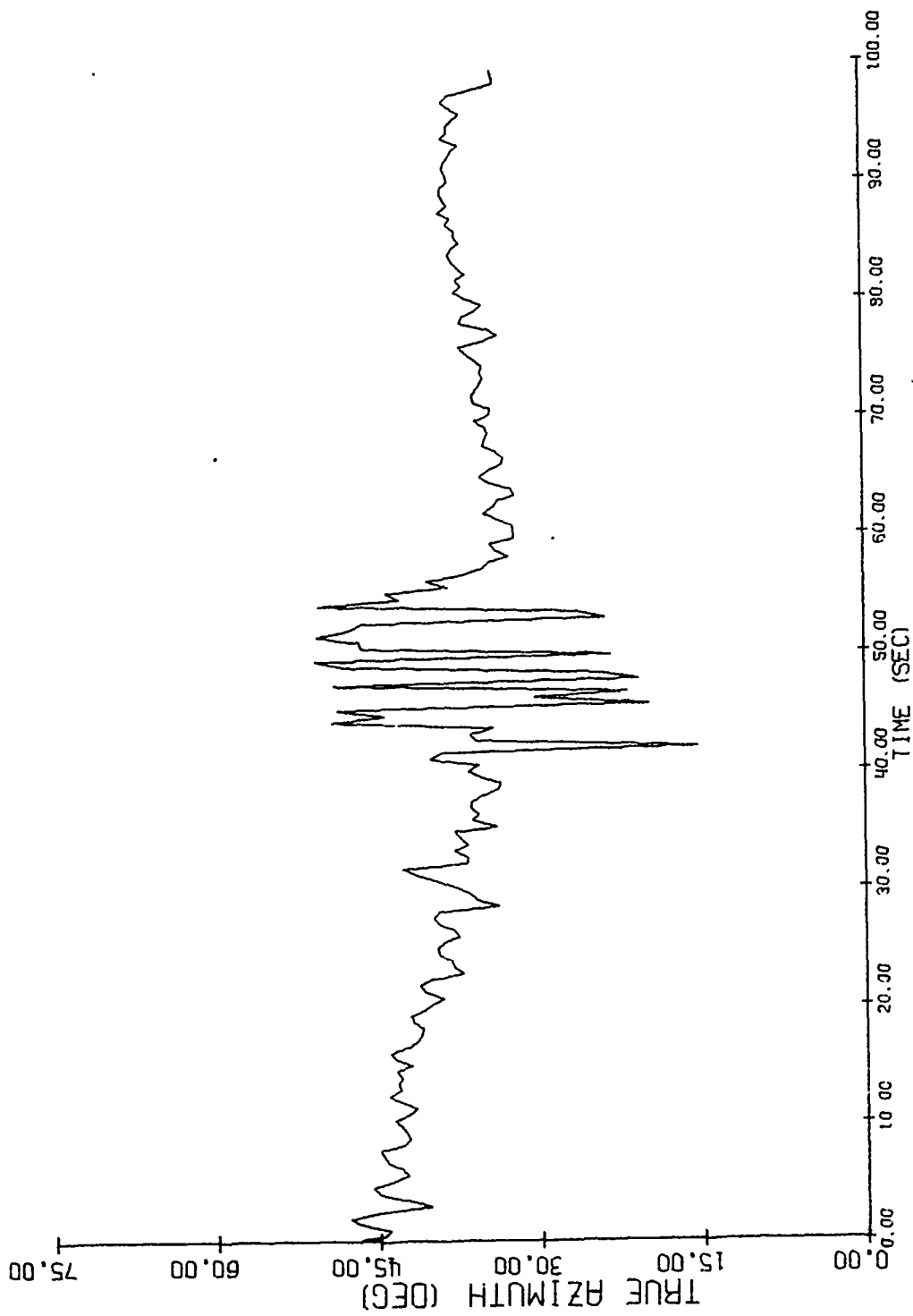


Figure 36. History of Drogue True Azimuth Angle during Portion of Second FVR Burst

Local Time (Hours)	Measured Average θ_{FVR}	Predicted Horizontal Drag on Drogue $F_D = W \sin \theta_{FVR}$ (Newtons) *	Estimated Sum of Wind & Surface Current Forces (**) F_{est-1} (Newtons)	Ratio $\frac{(F_D)}{(F_{est-1})}$	Estimated Sum of Wind & Surface Current Forces + F_{est-2} (Newtons)	Ratio $\frac{(F_D)}{(F_{est-2})}$
1013 (6 Mar '75) (Burst 1)	5.0°	24.6	12.5	1.97	19.5	1.26
1034 (Burst 2)	6.4°	31.5	12.5	2.52	19.5	1.62
1116 (Burst 3)	7.3°	35.9	14.2	2.53	22.1	1.62
1158 (Burst 4)	7.9°	38.8	~15.0	2.59	~23.4	1.66
1202 (Burst 4)	7.8°	38.3	~15.0	2.55	~23.4	1.63

*Based on an assumed weight, W, of 282.6 Newtons (63.5 pounds) for ballast and drogue.

**See Table 19 for estimated forces based on standard handbook values for drag coefficients derived under steady flow conditions.

+Force estimates based on results of section 5 trajectory iteration.

Table 30. Summary of One-Minute Average Values of FVR Euler Angles and a Comparison of the Horizontal Drag Forces Inferred from FVR Data and those from Wind and Surface Current Effects

estimate of the sum of wind and surface current forces does not measure up to the type of force that the average tilt angle of the FVR would indicate (i.e., column 3). The fifth column of Table 30 indicates that a nearby constant force ratio of approximately 2.5 exists between the 2 estimated values. After trajectory iteration, however, the estimate of the total error-inducing force is considerably larger, but still is not as large as the value estimated from the measured tilt angle at the top of the drogue. For this case, though, the FVR tilt angle overestimates the total force by approximately 60%, as seen by the last column of Table 30. Such a factor might possibly be used in future tests as a means of obtaining a first order estimate of the total slippage force in lieu of a better analytical understanding of how this force arises from wind and water action.

It is felt that the validity of equation (18) in a dynamic environment is more questionable than the estimates of wind and surface current forces. Such may be true if the drogue drag coefficient is much less than expected or if the tilt angle of the top of the drogue is biased upwards by the influence of buoy dynamics.

7.0 Conclusions and Recommendations from Ocean Slippage and FVR Tests

The following general statements can be made regarding the data derived from and the overall utility of the comparative drogue slippage test:

- (1) Drogues of similar design suspended from buoys of dissimilar design will diverge in the presence of dynamic exciting forces. The buoy exhibiting the most drag area to wind and water forces will be found more in the direction of this net force.
- (2) First order mathematical techniques for correcting the slippage errors of a Nova minibuoy, based on best estimates drag coefficients derived under steady flow conditions, will only correct a maximum of 75% of the total slippage error.
- (3) Wind forces on the Nova minibuoy are estimated to be the largest slippage error force by a considerable margin for the seas encountered in the test described. This estimate may change somewhat when the effects of waves and surface currents can be better quantified analytically and more severe seas are encountered.
- (4) Considerable testing and analytical modelling work should be undertaken in order to allow for mathematical slippage estimation in severe seas. In benign sea states (0-1m), as encountered during the described test, slippage estimation and "correction" based on wind forces alone appears to be a good technique to first order.
- (5) Computerized analytical techniques for trajectory correction provide a simple means for testing the sensitivity of a trajectory correction to various drag coefficient assumptions.

- (6) The conduct of drogued buoy slippage or monitoring tests through the use of ship LORAN C for buoy positioning is a viable test technique (see Appendix B) if 2 properly-located LORAN C station pairs are available. Higher frequency trajectory variations may, however, require more smoothing than the Decca Trisponder data employed in the described test, but the convenience, cost and simplicity of LORAN C far outweigh this consideration.

The following general conclusions can be drawn regarding the data and the use of a Force Vector Recorder for measuring drogue dynamics.

- (1) The FVR is an extremely valuable tool for measuring drogue dynamics (including both accelerations, depth, Euler angles, and even tension).
- (2) The FVR showed that vertical excursions of the drogue, as measured by the pressure sensor, agreed in general with the motion that would be predicted by a double integration of the vertical acceleration sensed by the FVR. This fact indicated that the time-varying pressure field due to wave action did not significantly penetrate to the drogue depth. Secondly, the magnitude of the vertical displacement was approximately equal to the height of the waves and swells, indicating that the drogue followed the buoy motion.
- (3) The present crude models for relating the average drogue tilt angle to the net horizontal force acting on the drogue are inadequate. More sophisticated mathematical models must be developed and verified.
- (4) The FVR appears to be able to reliably measure average Euler angles with the simple math outlined in Appendix D. This claim is reinforced by past instrument simulations and can also be inferred by comparing the Euler angles and true

azimuth angles shown in the last 2 columns of Table
the data for which were both measured during Burst 4.

- (5) The window shade drogue does not seem to align itself normal to what one would estimate as the net slip velocity vector computed by summing wind and surface current forces. This finding, if generally true, has serious implications on the future widespread use of a window shade drogue. As a minimum, it has shown that our mathematical understanding of drogue behavior is grossly inadequate. It is hoped that this type of test could be repeated without the FVR coming loose from its mount or the ship losing its rudder at the most critically-important time. Furthermore, it is hoped that future tests will measure the same drogue parameters in heavier seas (6-10 foot wave height) and look for conditions of zero tether line tension and shock loading (described in Appendix E) which can cause failures of the buoy, drogue, tether line, or fittings.

The above conclusions illustrate that a measurement technique has been used which looks promising. It also has highlighted a potentially serious problem surrounding the weathervaning of the window shade drogue. It is recommended that further full scale instrumented drifting buoy tests be conducted with the following goals:

- (1) Measure both buoy and drogue dynamics as a source of data for the creation of representative mathematical models of a given system. Such measurements would be most useful in conjunction with a measurement of the sea input and the value of surface current. If a measure of the current profile from the surface to below the drogue were available, it would be of immeasurable value in predicting slippage performance.

- (2) Examine the problem of window shade drogue weathervaning. It is possible that such a drogue may not be employed in near-surface applications where wave activity may alter its performance.
- (3) Attempt to measure drogue slippage directly by properly designing and instrumenting a representative drifting buoy configuration. Attempt to get closure on the force balance equations (wind, surface current, drogue force), after achieving a successful slippage measurement, as a means of achieving a generally useful scheme for estimating slippage on the part of oceanographer users.
- (4) Consider the use of alternative drogues if the weathervaning problem persists.
- (5) Consider the use of non-surface-following buoys, distributed buoyancy buoys, or energy absorbers as a means of minimizing dynamic loads in the system and decoupling the drogue from surface wave activity.

REFERENCES

- Hoerner, S.F., 1965, "Fluid-Dynamic Drag, Theoretical, Experimental, and Statistical Information," published by the Author, Midland Park, N.J.
- Kirwan, A.D., and G. McNally, 1975, "A Note on Observations of Long-Term Trajectories of the North Pacific Current." Jour. Phys. Ocean, 5, 1, pp. 188-191.
- Knacke, T. and A. Hegele, 1949, Model Parachutes, Comparison Tests of Various Types, Report MCREXE-672012B, Wright-Patterson AFB, Dayton, Ohio.
- McCullough, James R., 1974, "In Search of Moored Current Sensors," Proceedings of MTS Conference 1974, pp. 31-54.
- Pierson, W.J., Jr. and L. Moskowitz, 1964, "A Proposed Spectral Form for Fully Developed Wind Seas Based on the Similarity Theory of S. A. Kitaigorodski," Jour. Geophys. Res., Vol. 69, No. 24, pp. 5181-5190.
- Pritchard, D.W., and W.V. Burt, 1951, "An Inexpensive and Rapid Technique for Obtaining Current Profiles in Estuarine Waters," Jour. Marine Research, Vol. 10, No. 2, pp. 180-189.
- Roshko, 1953 & 1954, "Analytical and Experimental Studies on Drag and Flow of 2-Dimensional Bodies," NACA Tech. Notes No. 9213 and 3169.
- Terhune, L.D.B., 1968, "Free Floating Current Followers," Fisheries Research Board of Canada, Technical Report No. 85.
- Vachon, J.A., 1973, Scale Model Testing of Drogues for Free Drifting Buoys, C. S. Draper Laboratory Report R-769.
- Woodward, R.B., 1973, "Differential LORAN-C Time Stability Study," Report No. DOT-CG-31146-A, Dept. of Transportation, U.S. Coast Guard.
- Wu, Jin, 1975, "Sea Surface Drift Currents," Proceedings of Offshore Technology Conference, Paper No. OTC 2294, pp. 477-484.

Appendix A

Ocean Test Data Derived During Drogue Slippage Test - Including Computer-Derived Velocity Vectors

Tables A-1 through A-3 list the times and the buoy position fixes during the sea test. The buoys' positions were determined by two means, employing the ship as a positioning vehicle. A Decca trisponder system giving two radial lines of position was the prime navigation system. This system, working in the "range-range" mode gives a fix accuracy to better than ± 3 meters, according to Decca Survey Systems, Inc. Columns 2 and 3 reflect true estimates of buoy position after position estimates relative to the ship are taken into account. In general, the ship was within 10-15 meters of the buoys when the fixes were taken. Thus, the overall accuracy of each radial position is assumed to be within $\pm 10-15$ meters. The LORAN C lines of position determined from columns 4 and 5 are those of the ship only with no correction for the buoy position relative to the ship.

The "range-range" mode of operation for the Trisponder system gave radii R_1 and R_2 as shown in Figure 18. The base-leg for the radar system, between the two lighthouses, was 8.8 nautical miles long. Eastern Point, Gloucester lies at a true geographic angle of approximately 60 degrees from the lighthouse at Marblehead Neck, the more westerly station. From these data and that shown in Tables A-1 through A-3 considerable engineering as well as oceanographic information can potentially be derived.

The "range-range" data from Tables A-1 through A-3 were computerized in order to derive vector velocities in a cartesian co-ordinate frame. The program listing is shown in Figure A-1. The program simply employs the law of cosines to obtuse or scalene triangles composed of three sides of known length (i.e., base-leg, R_1 and R_2) -the orientation of one side being also known relative to true north. The positions so determined are taken as a function of time in order to derive vector velocities for the three buoys.

The buoy velocities derived as above were then examined for obviously "bad" points in which the value is unrealistic due to poor data logging or that the buoy was manually towed adjacent to another buoy between fixes. For uniformity of data portrayal the velocities were then converted to 1-hour average values. These values are listed in Tables 11 and 12 for the 23-hour test.

Time (Hours)	Radius to Marblehead Lite R ₁ (Meters)	Radius to Eastern Pt., Gl. R ₂ (Meters)	LORAN C Fix on Cape Race, Newfoundland (μsecs)	LORAN C Fix on Nantucket, Mass. (μsecs)	Comments
10:12	10,784	13,930	37,541.20	49,279.69	
10:34	10,816	13,793	37,540.10	49,279.16	Wind: 17 knots from 135°.
11:22	10,987	13,370	37,535.90	49,279.02	
11:41	11,060	13,251	37,535.93	49,277.56	
12:05	11,126	13,036	37,534.61	49,277.22	Wind: 17 knots from 150°
12:26	11,172	12,860	37,533.20	49,276.70	
12:44	11,185	12,730	37,532.62	49,276.80	
13:20	11,237	12,480	37,530.90	49,276.33	
13:49	11,204	12,315	37,530.26	49,276.30	
14:45	11,140	12,030	37,528.90	49,276.22	
15:10	11,079	11,930	37,528.42	49,276.30	
16:05	10,891	11,759	-	-	
23:10	9,589	11,698	37,532.24	49,281.27	
01:08	9,560	11,265	37,530.14	49,281.20	
01:55	9,500	11,111	37,529.40	49,281.37	
02:32	9,420	11,025	37,529.44	49,281.53	

Table A-1. Drogued NOVA buoy (buoy-1) position data during sea test of 6-7 March 1975.

Time (Hours)	Radius to Marblehead Lite R ₁ (Meters)	Radius to Eastern Pt., Gl. R ₂ (Meters)	LORAN C Fix O'1 Cape Race, Newfoundland (µsecs)	LORAN C Fix on Nantucket, Mass. (µsecs)	Comments
3:09	9,345	10,967	37,529.21	49,281.80	
03:47	9,228	10,905	37,529.25	49,282.25	
04:48	8,992	10,900	-	-	
05:19	8,850	10,932	37,530.42	49,283.57	Wind: 7 knots from 285°
06:00	8,669	11,023	37,531.43	49,284.07	
06:10	8,622	11,060	37,531.65	49,284.10	
06:31	8,565	11,102	37,532.07	49,284.40	
06:42	8,525	11,123	37,532.50	49,284.85	
07:15	8,438	11,217	37,533.02	49,284.80	
07:35	8,392	11,249	37,533.40	49,285.02	Wind: 9 knots from 315°
08:29	8,326	11,251	37,533.41	49,285.10	Wind: 11 knots from 325°
09:00	8,306	11,209	37,533.23	49,285.20	Retrieve buoy-1.
Notes: (1)	High Tides (Boston Harbor), 18:36	(3/6/75) & 06:57	(3/7/75)		
(2)	Low Tides (Boston Harbor), 12:21	(3/6/75) & 00:35	(3/7/75)		
(3)	Nova Buoy drogued area: 22.1m ² (wt = 282.5 newtons); FVR turned off at 09:30 hrs. (3/7/75).				=28.2m ² (wt.=214Newts.)

Table A-1 (cont.). Drogued NOVA buoy (buoy-1) position data during sea test of 6-7 March 1975.

Time (Hours)	Radius to Marblehead Lite R ₁ (Meters)	Radius to Eastern Pt., Gl. R ₂ (Meters)	LORAN C Fix on Cape Race, Newfoundland (μsecs)	LORAN C Fix on Nantucket, Mass. (μsecs)	Comments
10:28	10,821	13,850	37,540.43	49,279.30	Deploy buoy-2.
10:35	10,762	13,680	37,539.68	49,279.22	#1, 12m. N. of #2
11:34	11,014	13,241	37,536.30	49,277.71	
12:34	11,155	12,790	37,533.00	49,277.13	
12:55	11,200	12,435	37,530.92	49,276.33	
13:20	11,217	12,390	-	-	
13:57	11,167	12,164	37,529.51	49,276.35	
14:43	11,125	11,923	37,528.42	49,276.71	
15:09	11,083	11,830	37,528.02	49,276.23	
16:07	10,922	11,708	-	-	
23:03	9,560	11,857	37,533.22	49,281.33	
01:05	9,381	11,501	37,531.80	49,281.69	Radar range between buoys 1&2 ≈ 300 meters
01:25	9,328	11,460	37,531.72	49,281.99	
01:52	9,224	11,413	37,531.98	49,282.37	
02:02	9,188	11,406	37,531.80	49,282.59	
02:27	9,074	11,384	37,532.05	49,282.97	

Table A-2. Drogued float (buoy-2) position data during sea test of 6-7 March 1975.

Time (Hours)	Radius to Marblehead Lite R ₁ (Meters)	Radius to Eastern Pt., Gl. R ₂ (Meters)	LORAN C Fix on Cape Race, Newfoundland (μsecs)	LORAN C Fix on Nantucket, Mass. (μsecs)	Comments
02:42	9,019	11,370	37,522.19	49,288.10	Question this data pt.
03:16	8,835	11,356	37,532.40	49,283.50	
04:04	8,591	11,298	37,533.02	49,284.41	
05:03	8,301	11,369	37,534.20	49,285.27	
05:45	8,119	11,488	37,535.12	49,285.79	
05:57	8,547	11,123	37,532.25	49,284.50	
06:12	8,490	11,183	37,532.40	49,284.56	
06:29	8,459	11,236	37,533.00	49,284.88	
06:40	8,418	11,266	37,533.10	49,284.87	
06:47	8,391	11,284	37,533.40	49,285.05	
07:20	8,316	11,350	37,533.98	49,285.47	
07:34	8,282	11,372	37,534.14	49,285.54	
07:57	8,241	11,385	37,534.52	49,285.70	
08:31	8,198	11,385	37,534.40	49,285.51	
8:42	8,179	11,380	37,534.56	49,285.67	

Tow and redeploy adjacent to buoy-1 at following position

Table A-2 (cont.). Drogued float (buoy-2) position data during sea test of 6-7 March 1975.

Time (Hours)	Radius to Marblehead Lite R ₁ (Meters)	Radius to Eastern Pt., Gl. R ₂ (Meters)	LORAN C Fix on Cape Race, Newfoundland (μsecs)	LORAN C Fix on Nantucket, Mass. (μsecs)	Comments
10:20	10,751	13,850	37,540.76	49,279.33	Deploy buoy-3.
11:00	10,701	13,324	37,537.87	49,279.00	
11:01	10,695	13,275	37,537.39	49,279.89	
11:07	Retrieve 10,945	buoy-3 and redeploy 13,574	adjacent to buoy-1 37,538.19	at following 49,239.46	position.
11:24	10,889	13,253	37,535.60	49,279.13	
11:44	10,878	12,402	37,534.70	49,277.77	
11:55	Retrieve 11,090	buoy-3 and redeploy 13,151	adjacent to buoy-1 37,534.40	at following 49,277.68	position.
12:22	11,076	12,701	37,532.85	49,277.20	
13:10	10,017	12,091	37,529.74	49,276.90	Question this data point
13:40	11,009	11,682	37,527.30	49,276.50	
13:49	Retrieve 11,204	buoy-3 and redeploy 12,315	adjacent to buoy-1 37,530.26	at following 49,276.30	position.
14:41	11,139	11,660	37,526.80	49,276.11	
15:17	11,128	11,194	37,524.60	49,276.16	

Table A-3. Surface drogued float (buoy-3) position data during sea test of 6-7 March 1975.

Time (Hours)	Radius to Marblehead Lite R ₁ (Meters)	Radius to Eastern Pt., Gl. R ₂ (Meters)	LORAN C Fix on Cape Race, Newfoundland (μsecs)	LORAN C Fix on Nantucket, Mass. (μsecs)	Comments
15:27	11,090	10,986	37,529.10	49,276.78	
16:15	10,913	Ship rudder disabled 11,631	at following time 37,527.67	and position. 49,276.80	Wind: 18 knots from 185°
00:20	14,347	8,493	37,597.73	49,265.40	
01:00	9,182	11,828	near buoy-1 at following position. 37,534.20	49,282.80	Wind: 5 knots from 315°
01:45	9,433	11,798	37,533.10	49,282.01	
01:48	9,428	11,778	37,533.20	49,282.03	
02:08	9,500	11,778	37,532.88	49,281.64	
02:21	9,535	11,782	37,532.90	49,281.30	
02:30	9,362	Retrieve buoy-3 and redeploy 11,064	near buoy-1 at following position. 37,529.50	49,281.80	
02:48	8,974	11,351	37,532.30	49,283.13	
03:32	9,469	11,141	37,529.50	49,281.50	
04:25	9,474	11,147	37,529.67	49,281.50	

Table A-3 (cont.). Surface drogued float (buoy-3) position data during sea test of 6-7 March 1975.

Time (Hours)	Radius to Marblehead Lite R ₁ (Meters)	Radius to Eastern Pt., Gl. R ₂ (Meters)	LORAN C Fix on Cape Race, Newfoundland (μsecs)	LORAN C Fix on Nantucket, Mass. (μsecs)	Comments
04:36	9,457	11,166	37,529.86	49,281.57	
04:52	8,900	10,873	37,530.00	49,283.07	
05:26	8,847	11,005	37,530.77	49,283.25	Wind: 7 knots from 285°
06:02	8,777	11,157	37,531.58	49,283.70	
06:17	8,747	11,212	37,532.30	49,284.08	
06:34	8,713	11,292	37,532.49	49,283.81	
06:53	8,695	11,336	37,532.98	49,283.93	
07:25	8,676	11,420	37,533.42	49,284.10	Wind: 9 knots from 315°
07:49	8,680	11,464	37,533.63	49,284.10	
08:25	8,682	11,444	37,533.73	49,284.20	
08:35	8,703	11,400	37,533.40	49,284.19	Retrieve buoy-3.

Table A-3 (cont.). Surface drogued float (buoy-3) position data during sea test of 6-7 March 1975.

```

PROGRAM SLD1
C ANALYSIS OF DATA FROM 23-HOUR DROGUE SLIPPAGE TEST
C IN MASS BAY
COMMON R1B(3, 36), R2B(3, 36), TB(3, 36), VB(3, 36), XB(3, 36), YB(3, 36),
1ANGVB(3, 36), VBX(3, 36), VBY(3, 36)
LUIN=5
LP=20
ALPHA=0.532
B=.18254
WRITE(LP, 14)
14 FORMAT(/"ENTER DATA"/)
DO 20 I=1, 3
READ(LUIN, *) (R1B(I, J), J=1, 36)
READ(LUIN, *) (R2B(I, J), J=1, 36)
READ(LUIN, *) (TB(I, J), J=1, 36)
20 CONTINUE
DO 370 I=1, 3
WRITE(LP, 22) (R1B(I, J), J=1, 36)
WRITE(LP, 22) (R2B(I, J), J=1, 36)
22 FORMAT(6(2X, F8. 2))
WRITE(LP, 24) (TB(I, J), J=1, 36)
24 FORMAT(9(3X, I4))
DO 360 J=1, 36
CO=((B**2+R1B(I, J)**2-R2B(I, J)**2)/(2*B*R1B(I, J)))
WRITE(LP, 26) CO
26 FORMAT(5X, "COSINE THETA=", F7. 3)
WRITE(LP, 29) THETA
29 FORMAT(5X, "ANGLE THETA(RADIANS)=", F8. 4)
SI=SQRT(1-CO**2)
THETA=ATAN2(SI, CO)
50 BETA=ALPHA-THETA
70 YB(I, J)=R1B(I, J)*SIN(BETA)
80 XB(I, J)=R1B(I, J)*COS(BETA)
IF(J-1)86, 82, 86
82 WRITE(LP, 310)
WRITE(LP, 84) I, XB(I, J), YB(I, J)
84 FORMAT(2X, "BUOY NO=", I2, 3X, "X0 POSN=", F10. 3, 3X, "Y0 POSN=", F10. 3)
GO TO 360
86 VBX(I, J)=(XB(I, J)-XB(I, J-1))/(TB(I, J)-TB(I, J-1))
VBY(I, J)=(YB(I, J)-YB(I, J-1))/(TB(I, J)-TB(I, J-1))
C CONVERT FROM METERS/MIN TO METERS/SEC
VBX(I, J)=VBX(I, J)/60
VBY(I, J)=VBY(I, J)/60
VB(I, J)=SQRT(VBX(I, J)**2+VBY(I, J)**2)
90 ANGVB(I, J)=ATAN2(VBY(I, J), VBX(I, J))
C CONVERT RADIANS TO DEGREES
ANGVB(I, J)=ANGVB(I, J)*57. 3
310 FORMAT(/"SUMMARY OF COMPUTED DATA"/)
WRITE(LP, 315) TB(I, J), I, J
315 FORMAT("TIME=", F9. 2, 3X, "BUOY NO=", I2, 3X, "POINT NO=", I2)
WRITE(LP, 320)
320 FORMAT(5X, "X-POSN", 4X, "Y-POSN", 10X, "X-VELOC", 6X, "Y-VELOC(M/S)")
328 WRITE(LP, 330) XB(I, J), YB(I, J), VBX(I, J), VBY(I, J)
330 FORMAT(2(2X, F10. 3), 2X, F10. 6, 7X, F10. 6)
WRITE(LP, 340)
340 FORMAT(5X, "BUOY VELOC(M/S)", 5X, "DIRECTION(DEGREES)")
WRITE(LP, 350) VB(I, J), ANGVB(I, J)
350 FORMAT(8X, F7. 3, 16X, F7. 3, /)
360 CONTINUE
370 CONTINUE
END

```

THIS PAGE IS UNCLASSIFIED
 EXCEPT WHERE SHOWN OTHERWISE

FIGURE A-1

Appendix B

Trajectories of Drogued Buoys Employing Differential Ship LORAN C for Position-Fixing

The LORAN C data, appearing in columns 4 and 5 of Tables A-1 through A-3, reflect the hyperbolic LORAN C lines-of-position of the ship at the time it was alongside a particular buoy. The data shown were hand-recorded from the output of a Simrad/Internav LORAN C navigator. A similar Epsco system was also employed while coupled to a separate antenna. The Epsco unit gave essentially the same third cycle crossing information as the Internav unit although the Internav displayed an additional digit to the right of the decimal point for averaging purposes.

The Cape Race, Newfoundland and Nantucket, Mass. stations were employed because at the time of the test there were suspected difficulties with the Dana, Indiana station. Nantucket was less desirable than Dana because it placed the test location on a baseline extension region between Cape Race and the master station at Carolina Beach, North Carolina. Such a situation leads to undesirable line-of-position crossing angles much less than 90 degrees which lead to what is commonly called geometric dilution of position (GDOP) which degrades positional accuracy.

The raw LORAN C position data shown in Tables A-1 through A-3 contains all the errors inherent in a LORAN C measurement. It is, however, possible to account for a good deal of the errors arising from time-varying signal propagation or from sky-wave interference. Most often these types of errors are greatest at sunrise and sunset when the ionosphere or earth moisture content may be changing. By installing a nearby fixed LORAN C recording station that monitors the same station, some of the buoy position errors can be corrected by differential techniques. This technique described by Woodward (1973) was employed during the drogued ocean test. The fixed station was at the International Navigation Co. (Internav) in Bedford, Mass., approximately 20 miles from the coast and 40 miles from the test site. Any differences between the two locations were neglected.

At Internav the time differences from the station pairs were

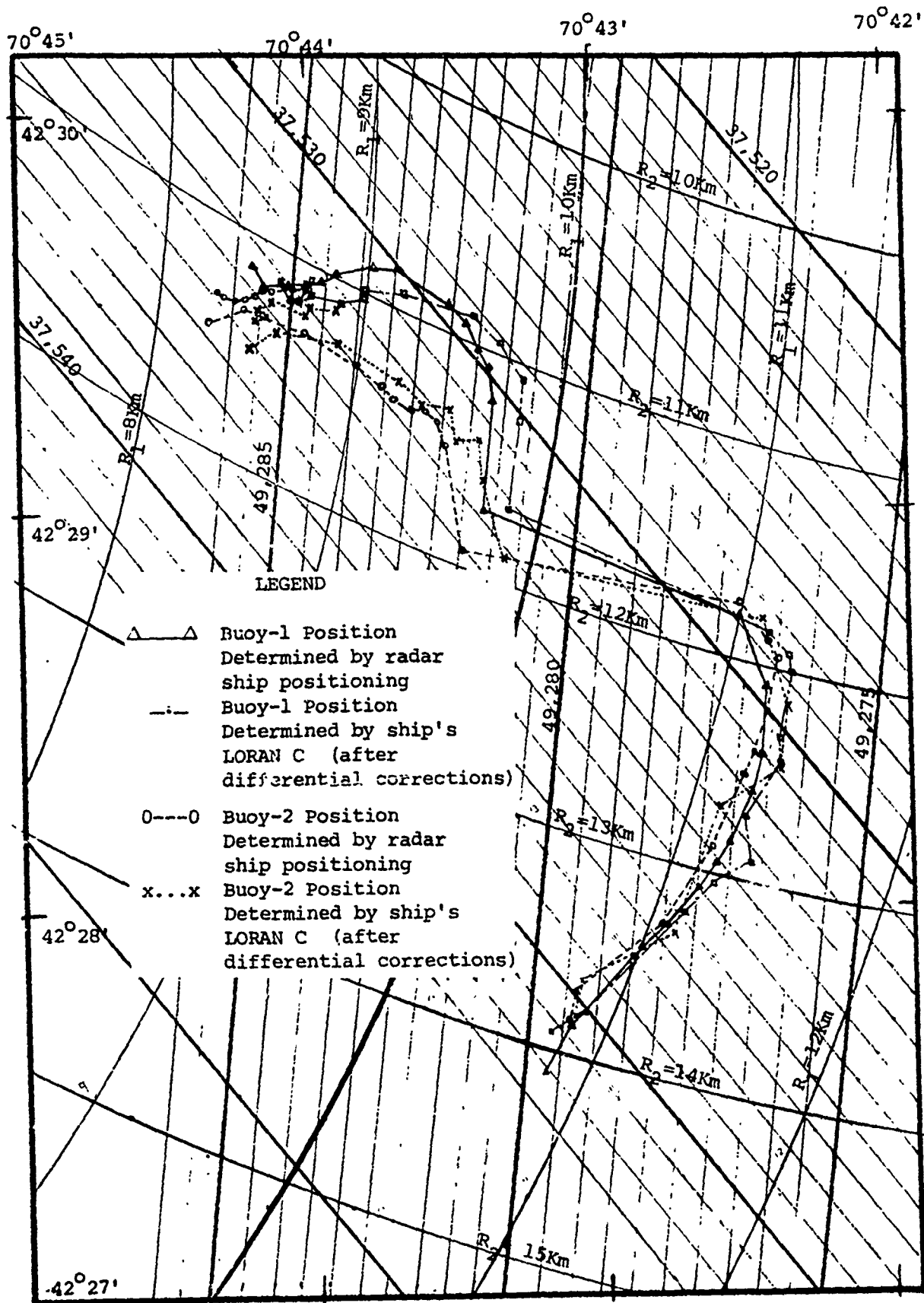


Figure B-1 Buoy Trajectories Determined by DECCA Radar Positioning and Differential LORAN C

averaged and recorded every 100 seconds. It was found that differential techniques produced a maximum time difference variation as received from the Cape Race station of +0.17 to -0.12 microseconds (i.e., +25 to -18 meters position variation) with respect to the value at the start of the experiment. The Nantucket station produced maximum values of +0.14 and -0.02 microseconds (i.e., +34 to -5 meters) over the same time frame. These values agree in general with those reported by Woodward (1973).

Figure B-1 illustrates the paths of Buoys 1 and 2 during the ocean test derived by both means. All obviously "bad" points due to improper data logging have been omitted. The legend enables one to compare the trajectories derived by the primary positioning mode, radar, and by ship LORAN C after differential corrections have been applied. The LORAN C data without differential corrections appear essentially the same. It can be seen that the buoy positions derived by LORAN C data places the buoys to varying degrees at a more easterly and in some cases southeasterly position from those positions derived by the radar system. It is felt that this disparity can be accounted for by slight errors in the calibration of the 2 Decca Trisponder radar units. For example the position error is a maximum of approximately .2 Km at the end of the drift test at a radius of approximately 8 Km. to the nearest radar transponder (Marblehead Neck). The assumed absolute position error in this case would then be on the order of .2 Km. out of 8 Km. or 2.5% - a large but not unreasonable error.

Other sources of error could be the proper scaling and placement of radar range lines on the same grid pattern as the LORAN C lines in Figure B-1. Only careful rechecks could highlight this source. In addition it is suspected that the revised 1207 chart, with new LORAN C lines, that was used in creating Figure B-1 may have also been in slight error.

It should be noted, also, that at various times there appears to be an unreasonable amount of "bumpiness" to the buoy trajectories. Because the data employed differential techniques most of the effects of the ionospheric variations, which are more pronounced at sunrise and sunset, should have been eliminated. Only differences between the monitor station and the

ship would contaminate the data. It is felt that much of the "bumpiness" results from large distances between the buoy and ship at the time of data recording. When such phenomena at high frequencies (1-2 cycles/hr) would be seen on future LORAN C data portraying drifting buoy trajectories, a least squares curve fit to the data points would in general be calculated.

The main purpose of presenting the LORAN C data and the comparative trajectories in Figure B-1 is not to illustrate a great absolute position accuracy for LORAN C. It is, rather, to show, first, that for all practical purposes differential techniques do not significantly improve the drift data derived by LORAN C buoy positioning. Secondly, the drogued buoy trajectories, which are indicative of water mass motion, are well reproduced over the given time frame by using only ship LORAN C. The possible errors in the absolute position of the buoys are of very little significance in evaluating both oceanographic and engineering data from such a drift test. Should the test be shortened in time to such an extent that LORAN C position errors would become a large part of the total buoy travel in that time frame a different and more accurate positioning system should be sought. As a result of this comparative test, it is felt that in the future similar drift tests in regions of good LORAN C coverage could be adequately carried out using a similar LORAN C system. The savings in time and money, by not having to use a costly radar set (rental fee) would be greatly appreciated. In addition, it appears very feasible that a drifting buoy could be automatically positioned by an on-board LORAN C retransmitter relaying time difference information from a remote ocean station to a laboratory or shore-based recording station. The benefits of such a system are obvious. High frequency data (a few samples per hour) of good positional accuracy could be automatically obtained on a multi-buoyed array out to distances of the order of 1000 Km from east and west coast shores. The main limitation to such a system would seem to be the power, cost, size, and complexity of the retransmitter section in order to get adequate signal back on shore.

APPENDIX C

Force Vector Recorder Timing and Calibration Data

Timing

During the quarry test, the FVR was operating in the continuous record mode, recording a data frame of 6 channels of information every 2.56 seconds. In this mode the instrument will fill its data tape, of 2.2×10^6 bit capacity, in approximately 15.6 hours. A data frame consists of 100 bits of data.

During the two ocean tests the instrument was wired to record in a burst mode in which it recorded a 6-channel data frame every .52 seconds (i.e., 100 bits of data) in the timing sequence shown in Figure C-1. The first burst length and off-time is different from all of the rest-initiated with the removal of the ON-OFF magnet.

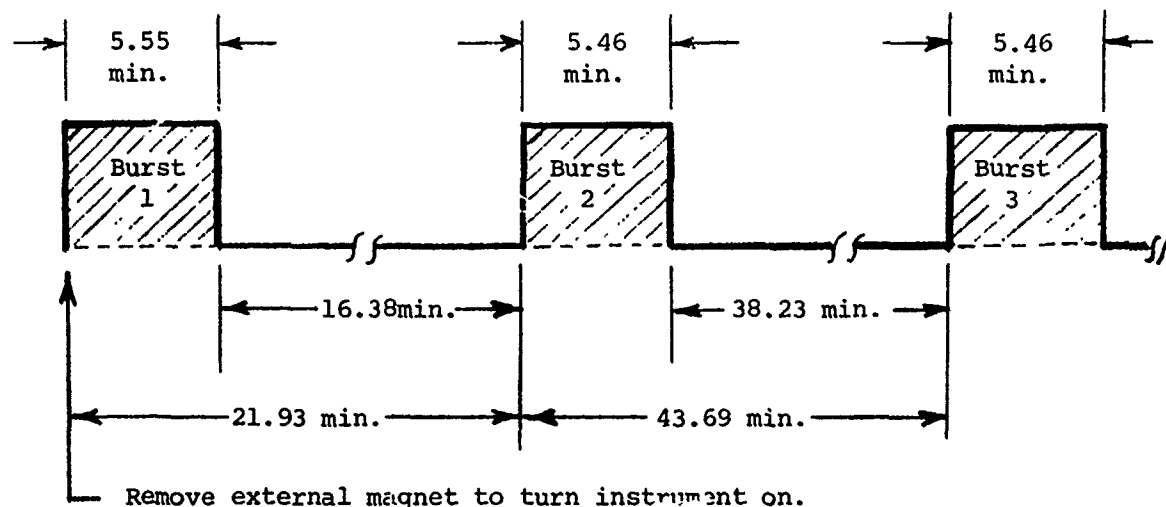


Figure C-1. Force Vector Recorder burst mode timing sequence during ocean tests.

By using the burst record mode shown, a higher frequency response was achieved on the recorded data (i.e., Nyquist frequency \approx 1Hz) and yet the useful life of the instrument was stretched to approximately 25 hours before the data tape was filled. The burst mode that was selected fulfilled the needs of the given ocean test that was planned to last approximately 24 hours. Other modes of variable burst length and off-time are available but the Nyquist frequency cannot be increased beyond 1Hz due to speed limitations on the present tape recorder.

The precise FVR time profile versus frame count for the Massachusetts Bay test is shown in Figure C-2. After the fourth record burst the data indicate that the instrument mounting loosened to such an extent that the data are nearly impossible to interpret. The data recorded during the first four bursts are, however, among the most energetic due to the existing sea conditions and therefore felt to be most useful.

Time	Data Block	Frame Count	Total Frames	Comments
10:09 AM	1	1	1	Start FVR.
10:14:33	5	128	640	End 1st burst.
10:30:55	6	1	641	Start 2nd burst.
10:36:22	10	118	1270	End 2nd burst.
11:14:36	10	119	1271	Start 3rd burst.
11:20:03	15	109	1900	End 3rd burst.
11:58:17	15	110	1901	Start 4th burst.
12:03:44	20	100	2530	End 4th burst.

Figure C-2. FVR time profile for initial portion of drogued ocean test in Massachusetts Bay.

Calibration

Calibrations were performed on the Force Vector Recorder (FVR) prior to the quarry test of 18 and 19 November 1974 and again prior to the ocean

tests in February and March 1975. The calibration of the magnetometers is sensitive to the local dip angle and the magnitude of the local magnetic vector. These values were derived from tests at the quarry site approximately 10 miles north of the site of the ocean test. Because the pressure sensor on the FVR is sensitive to absolute pressure, it is important that the barometric pressure on the day of the test be compared to the value measured the day on which the unit was calibrated. This fact is reflected in the pressure sensor calibration. The relations to follow describe the sensor outputs during the two test periods for which the following parameter designations hold:

f_x, f_y, f_z = measured accelerations (specific force), [g's]

A_x, A_y, A_z = accelerometer outputs [counts]

p_{atm} = atmospheric pressure, [in. Hg]

p = measured pressure (psig)

P = pressure sensor output [counts]

m_x, m_y = magnetometer outputs [counts]

B_x, B_y = magnetometer bias values (counts)

m_{xh}, m_{yh} = magnetometer outputs when horizontal and pointing towards magnetic north (counts)

G_x, G_y = scale factors of magnetometers (counts/gauss)

θ = instrument tilt angle

ψ = instrument azimuth orientation angle counterclockwise from magnetic north

ϕ = instrument rotation angle about body Z-axis

The equations that describe the manner in which accelerometer data are used as input data to the magnetometers equations are as follows (see Appendix D):

$$f_x = g \sin\theta \sin\phi \quad (C-1)$$

$$f_y = g \sin\theta \cos\phi \quad (C-2)$$

or

$$\sin\theta = \frac{1}{g} (f_x^2 + f_y^2)^{1/2} \quad (C-3)$$

where θ is the inclination angle of the mooring line and ϕ is the rotation of the FVR about the mooring line. The value of θ derived by equation (B-3) is then plugged back into equation (C-1) or (C-2) to solve for ϕ . The values of θ and ϕ are then plugged into either of the following equations in order to solve for ψ , the azimuth angle of the instrument.

$$\sin\psi = -\frac{m_x - B_x}{m_{xh} - B_x} \sin\phi - \frac{m_y - B_y}{m_{yh} - B_y} \cos\phi \quad (C-4)$$

or:

$$\cos\psi = \frac{m_x - B_x}{m_{xh} - B_x} \frac{\cos\phi}{\cos\theta} - \frac{m_y - B_y}{m_{yh} - B_y} \frac{\sin\phi}{\cos\theta} - \tan\alpha \tan\theta \quad (C-5)$$

Ambiguities in ψ can be resolved by the use of both equations (C-4) and (C-5). The derivation of these equations is given in Appendix D.

The following is a list of FVR sensor output functions (biases and scale factors) for both the quarry and ocean tests conducted during the past year:

Quarry Test

Accelerometer outputs:

$$f_x = \frac{489 - A_x}{510} \text{ g's}$$

$$f_y = \frac{484 - A_y}{710} \text{ g's}$$

$$f_z = \frac{1015 - A_z}{515} \text{ g's}$$

Pressure sensor output:

$$p = \frac{P - 20 - (p_{atm} - 30.14)(16.207)}{32.63} \text{ psi} \quad (P_{atm} = 29.95 \text{ in. Hg})$$

Magnetometer outputs:

(p(units) = psig)

$$B_x = 500.83 \text{ counts}$$

$$\chi_{G_x} = -138.68 \text{ "}$$

$$m_{xh} = 362.15 \text{ "}$$

B_y, G_y, m_{yh} : not available

α = measured dip angle of local earth's magnetic field = 75°

Ocean Tests

Accelerometer outputs:

$$f_x = \frac{488 - A_x}{775} \text{ g's}$$

$$f_y = \frac{487 - A_y}{510} \text{ g's}$$

$$f_z = \frac{-1259 + A_z}{780} \text{ g's}$$

Pressure sensor output:

$$p = \frac{P - 13.5 - (p_{\text{atm}} - 29.77)(16.207)}{32.63} \text{ psi}$$

where: $p_{\text{atm}} = 30.19 \text{ in. Hg}$

Magnetometer outputs:

$$B_x = 406.75$$

$$B_y = 495.5$$

$$G_x = -138.68$$

$$G_y = -167.79$$

$$m_{xh} = 268.05$$

$$m_{yh} = 327.68$$

$$\alpha = \text{dip angle} = 70^\circ$$

APPENDIX D

Force Vector Recorder (FVR) Euler Angle Determination

Figure D-1 Describes the axis system to be employed in the derivation of the FVR Euler angles. It is the same but a more complete definition than shown in Figure 23. It should be observed that the X, Y, Z co-ordinate system is assumed fixed with respect to inertial space while the x, y, z system is fixed to and moves with the instrument. Figure D-2 defines the three Euler angles to be employed in defining the FVR attitude. The following definitions are also employed in deriving the angles:

- \vec{a} = acceleration of FVR w.r.t. inertial space (acceleration LT^{-2})
- \vec{f} = specific force on FVR (acceleration LT^{-2})
- \vec{g} = gravitational field of earth (acceleration LT^{-2})
- $\vec{\gamma}$ = earth's magnetic field (Mag. flux density $MT^{-1}Q^{-1}$)
- $\gamma_h = \gamma_X$ = horizontal component of the earth's magnetic field
- $\gamma_v = -\gamma_Z$ = vertical component of the earth's magnetic field

The basic equation relating accelerations is given by:

$$\vec{f} + \vec{g} = \vec{a} \quad (D-1)$$

In order to convert any vector \vec{l} (i.e., $\vec{l} = l_X \vec{i}_X + l_Y \vec{i}_Y + l_Z \vec{i}_Z = l_x \vec{i}_x + l_y \vec{i}_y + l_z \vec{i}_z$) from inertial to body-fixed axes, it is necessary to derive a transformation matrix. By reference to Figure D-2, the first rotation (ψ), about the Z-axis, is described by the following transformation for which positive rotations are for x rotated towards y.

$$\begin{Bmatrix} x_1 \\ y_1 \\ z_1 \end{Bmatrix} = A \begin{Bmatrix} X \\ Y \\ Z \end{Bmatrix} = \begin{bmatrix} \cos\psi & \sin\psi & 0 \\ -\sin\psi & \cos\psi & 0 \\ 0 & 0 & 1 \end{bmatrix} \begin{Bmatrix} X \\ Y \\ Z \end{Bmatrix} \quad (D-2)$$

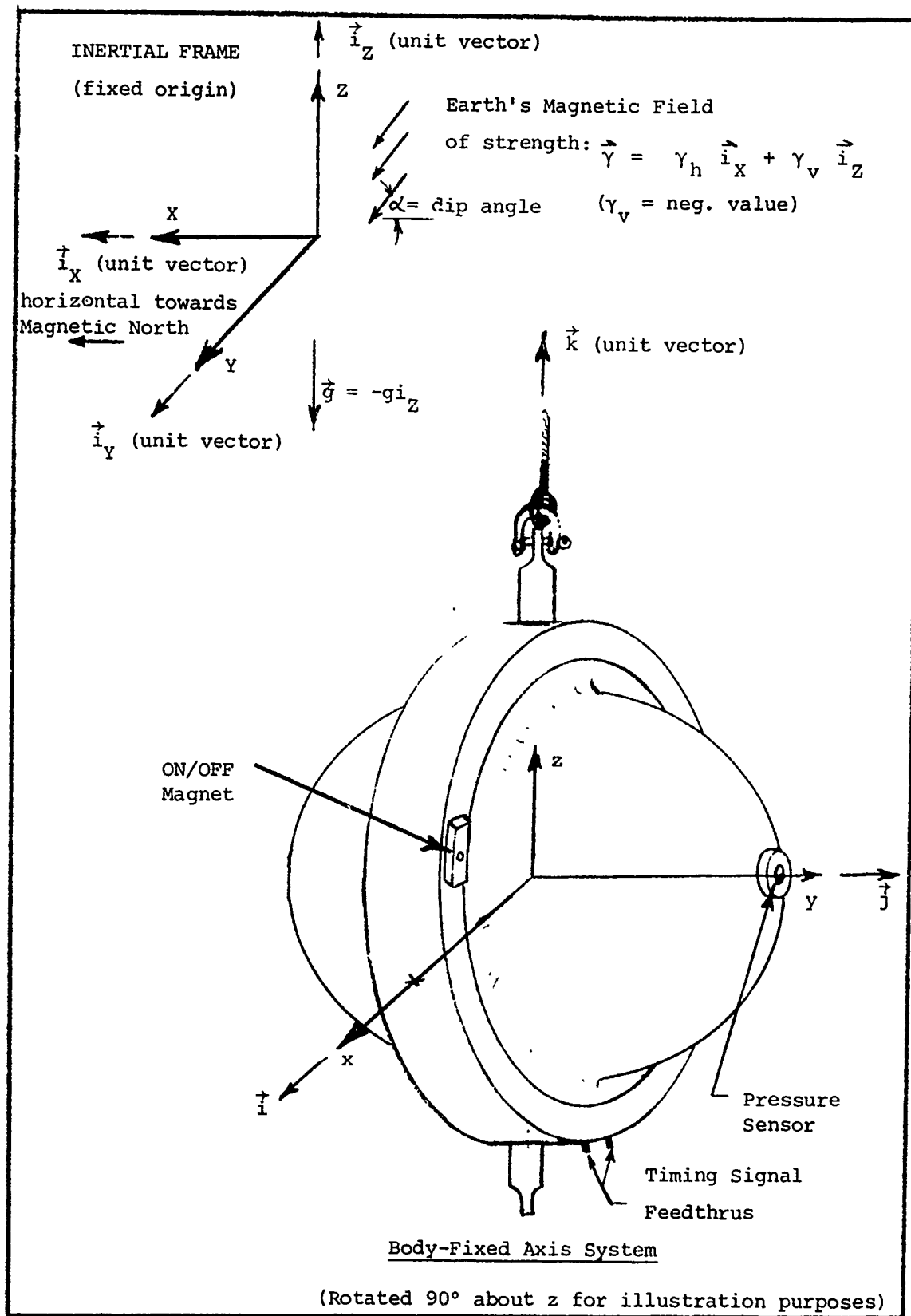
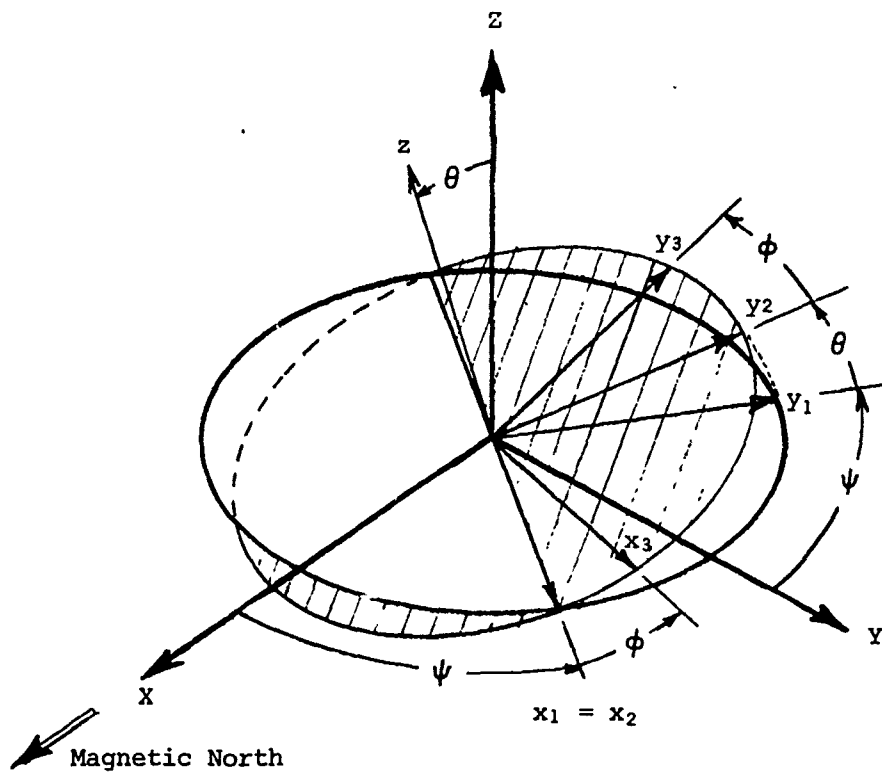


Figure D-1. Force Vector Recorder axis definitions.



Summary Definition of Rotations

- (1) ψ = Rotation about z-axis (aligned with Z-axis).
(pos. for x rotated into y)
- (2) θ = Rotation about displaced x-axis. (positive for y
into z)
- (3) ϕ = Rotation about tilted z-axis. (positive for x into y)

Figure D-2. FVR Euler Angle Definitions

or:

$$\{\vec{l}_1\} = A \{\vec{l}_0\} \quad (D-3)$$

The second rotation (θ) is about the displaced x-axis (i.e., x_1 axis) and is described by the following transformation in which positive angles are for y into z.

$$\begin{Bmatrix} x_2 \\ y_2 \\ z_2 \end{Bmatrix} = B \begin{Bmatrix} x_1 \\ y_1 \\ z_1 \end{Bmatrix} = \begin{bmatrix} 1 & 0 & 0 \\ 0 & \cos\theta & \sin\theta \\ 0 & -\sin\theta & \cos\theta \end{bmatrix} \begin{Bmatrix} x_1 \\ y_1 \\ z_1 \end{Bmatrix} \quad (D-4)$$

or:

$$\{\vec{l}_2\} = B \{\vec{l}_1\} \quad (D-5)$$

The third and last rotation (ϕ) is about the displaced z-axis (i.e., z_2) and given by the following transformation for which x is rotated into y.

$$\begin{Bmatrix} x_3 \\ y_3 \\ z_3 \end{Bmatrix} = \begin{bmatrix} \cos\phi & \sin\phi & 0 \\ -\sin\phi & \cos\phi & 0 \\ 0 & 0 & 1 \end{bmatrix} \begin{Bmatrix} x_2 \\ y_2 \\ z_2 \end{Bmatrix} \quad (D-6)$$

or:

$$\{\vec{l}_3\} = C\{\vec{l}_2\} \quad (D-7)$$

The complete transformation matrix is given by the relation:

$$\{\vec{l}_3\} = \begin{Bmatrix} x_3 \\ y_3 \\ z_3 \end{Bmatrix} = [CBA] \begin{Bmatrix} X \\ Y \\ Z \end{Bmatrix} \quad (D-8)$$

where:

$$[CBA] = \begin{bmatrix} \cos\psi \cos\phi & \sin\psi \cos\phi & \sin\phi \sin\theta \\ \sin\psi \cos\phi & +\cos\psi \sin\phi \cos\theta & \\ -\cos\psi \sin\phi & -\sin\phi \sin\psi & \cos\phi \sin\theta \\ -\sin\psi \cos\phi \cos\theta & +\cos\psi \cos\psi \cos\theta & \\ \sin\psi \sin\theta & -\cos\psi \sin\theta & \cos\theta \end{bmatrix} \quad (D-9)$$

A useful property of the transformation matrix (D-9) is that its inverse $(CBA)^{-1}$ is equal to its transpose $(CBA)^T$.

For the static case (i.e., $\vec{a} = 0$) the values of θ and ϕ are determined from equation (D-1) at each data point. If the time average for \vec{a} is assumed to be zero over many wave periods the same equations hold but the average values of θ, ϕ , and ψ can only be evaluated at lower frequencies. For both cases the accelerometer outputs are given as follows (where $\vec{g} = -g\hat{k}$):

$$\hat{f}_x = -\hat{g}_x = g(\sin\hat{\theta}\hat{\sin}\phi) \quad (D-10)$$

$$\hat{f}_y = -\hat{g}_y = g(\sin\hat{\theta}\hat{\cos}\phi) \quad (D-11)$$

The $\hat{}$ symbol denotes the average value over a time interval. The static assumption appropriate to equations (D-10) and (D-11) assumes that $\hat{a}_x = \hat{a}_y = 0$. This assumption may also be a fair approximation in some buoy dynamic situations. It is further assumed that $(\sin\hat{\theta}\hat{\cos}\phi)$ and $(\sin\hat{\theta}\hat{\sin}\phi)$ are equal to $\hat{\sin}\theta \hat{\cos}\phi$ and $\hat{\sin}\theta \hat{\sin}\phi$ respectively. This is true for the static case and probably a fair approximation in some buoy dynamic situations. Therefore, the following equations result (see equations (11) and (12)):

$$f_x = g \hat{\sin}\theta \hat{\sin}\phi \quad (D-12)$$

$$f_y = g \hat{\sin}\theta \hat{\cos}\phi \quad (D-13)$$

Equations (D-12) and (D-13) may be solved for $\hat{\sin}\theta$, $\hat{\theta}$, and $\hat{\phi}$ under the assumptions that $\hat{\sin}\theta = \sin\hat{\theta}$, $\hat{\sin}\phi = \sin\hat{\phi}$, and $\hat{\cos}\phi = \cos\hat{\phi}$. The value of $\hat{\theta}$ is found from the relation:

$$\sin\hat{\theta} = \pm \frac{1}{g} (f_x^2 + f_y^2)^{1/2} \quad (D-14)$$

This value is plugged back into (D-12) and (D-13) in order to get $\hat{\phi}$. It is not possible to ascertain the sign of the angle θ because it is lost in the squaring process. This is not important in this test because the

drogue can pivot two ways about the top spreader bar, both values of which are valuable. This fact leads to 180° ambiguities in ϕ and ψ also. For simplicity, assume θ is always positive and for best accuracy the following is suggested:

- (a) If $|\sin \phi| > |\cos \phi|$, find ϕ from (D-12) and use equation (D-13) to resolve the ambiguity.
- (b) If $|\sin \phi| < |\cos \phi|$, find ϕ from (D-13) and use equation (D-12) to resolve the ambiguity.

In order to employ the magnetometers as a sensor for the remaining Euler angle, ψ , it is necessary to have information on the local magnetic field and also the bias values for the two magnetometers (x and y-axes). If the bias values of the magnetometer outputs are given by B_x and B_y , and the output sensitivities are given by G_x and G_y the output of the magnetometers are given by the relations:

$$\begin{aligned} m_x &= B_x + G_x \gamma_x \quad (\text{counts}) \\ m_y &= B_y + G_y \gamma_y \quad (\text{counts}) \end{aligned} \tag{D-15}$$

Because the magnetometers are used as angle sensors it is desirable to calibrate the magnetometers without having to know the local magnetic field strength. In the test procedure it is necessary to know the outputs of the magnetometers when their input axis are pointed toward magnetic north (i.e., m_{xh} and m_{yh}) and vertically down (i.e., m_{xv} and m_{yv}) in the same field area where the FVR is to be used:

$$\begin{aligned} m_{xh} &= B_x + G_x \gamma_h & m_{yh} &= B_y + G_y \gamma_h \\ m_{xv} &= B_x - G_x \gamma_v & m_{yv} &= B_y - G_y \gamma_v \end{aligned} \tag{D-16}$$

Hence m_{xh} ; m_{yh} ; m_{xv} and/or m_{yv} are measured constants for the local axes.

In order to eliminate the instrument sensitivity, G , from the calibration, equations (D-15) and (D-16) are employed to get:

$$\frac{\gamma_x}{\gamma_h} = \frac{m_x - B_x}{m_{xh} - B_x} \quad (D-17)$$

$$\frac{\gamma_y}{\gamma_h} = \frac{m_y - B_y}{m_{yh} - B_y}$$

and:

$$\frac{\gamma_v}{\gamma_h} = \frac{m_{xv} - B_x}{m_{xh} - B_x} \quad \text{or} \quad \frac{\gamma_v}{\gamma_h} = \frac{m_{yv} - B_y}{m_{yh} - B_y} \quad (D-18)$$

In equations (D-18) $\gamma_v/\gamma_h = \tan \alpha$ where α is the value of the dip angle of the local magnetic field.

For the static case the components of the magnetic field sensed by the FVR are given by the following equations in body co-ordinates:

$$\gamma_x = \gamma_h (\cos\phi \cos\psi - \sin\phi \sin\psi \cos\theta) + (\sin\phi \sin\theta) \gamma_v$$

$$\gamma_y = \gamma_h (-\cos\psi \sin\phi - \sin\psi \cos\phi \cos\theta) + (\cos\phi \sin\theta) \gamma_v \quad (D-19)$$

where $\cos\hat{\theta} = \cos\hat{\theta}$, etc. Equations (D-19) can be multiplied by $\sin\phi$ and $\cos\phi$ respectively and added in order to solve for ψ in terms of θ , ϕ , γ_x , γ_y , γ_v , and γ_h as follows:

$$\sin\psi = \frac{\gamma_v}{\gamma_h} \tan\theta - \frac{\gamma_x \sin\phi}{\gamma_h \cos\theta} - \frac{\gamma_y \cos\phi}{\gamma_h \cos\theta} \quad (D-20)$$

In a similar way equations (D-19) can be multiplied by $\cos\phi$ and $\sin\phi$ respectively and added to give the following:

$$\cos\psi = \frac{\gamma_x}{\gamma_h} \cos\phi - \frac{\gamma_y}{\gamma_h} \sin\phi \quad (D-21)$$

The values of $\frac{\gamma_v}{\gamma_h}$, $\frac{\gamma_x}{\gamma_h}$, and $\frac{\gamma_y}{\gamma_h}$ as shown in equations (D-17) and (D-18) are substituted into equations (D-20) and (D-21) in order to arrive at the following equations in terms of measurable quantities:

(where again γ_v/γ_h should have a negative sign and equals $\tan \alpha = \tan$ (dip angle))

$$\sin\psi = \frac{m_{xv}^{-B}}{m_{xh}^{-B}} \tan\theta - \frac{m_x^{-B}}{m_{xh}^{-B}} \frac{\sin\phi}{\cos\theta} - \frac{m_y^{-B}}{m_{yh}^{-B}} \frac{\cos\phi}{\cos\theta} \quad (D-22)$$

$$\cos\psi = \frac{m_x^{-B}}{m_{xh}^{-B}} \cos\phi - \frac{m_y^{-B}}{m_{yh}^{-B}} \sin\phi \quad (D-23)$$

Other useful relationships could also be derived by which ψ can be derived. The most accurate procedure is to use the most sensitive equation. If, for example, the x magnetometer input axis were pointing near North, a small error in m_x would result in a large error in ψ if we were to use Equation (D-23) because small errors in $\cos\psi$ result in large errors in ψ for values of the argument near zero. Based on this thinking it is recommended that the following be applied.

If $|\sin\psi| < |\cos\psi|$ use (D-22) to calculate ψ and use (D-23) to resolve ambiguity.

If $|\sin\psi| > |\cos\psi|$ use (D-23) to calculate ψ and use (D-22) to resolve ambiguity.

In summary, with the suggested calibration scheme, the magnetometers require a knowledge of the local value of the dip angle of the magnetic field (derived from the charts), the instrument biases (measured in the lab), plus the values of the horizontal and vertical components of the local magnetic field in instrument counts (not Webers per square meter). These values are combined with the θ and ϕ values derived from the FVR accelerometers in order to get ψ , the azimuth angle of the FVR with respect to magnetic north. The frequency range over which the values of Euler angle, derived by the above method, are valid is determined by the nature of the particular response being measured and also the period over which the dynamic component of acceleration, \vec{a} , is assumed to average to zero. In most cases, the longer this period is assumed to be the more correct the assumption for moorings whose shape and orientation does not change greatly during the averaging period.

APPENDIX E

Estimated Window Shade Drogue

Dynamic Loads Induced by an Inelastic Tether Line to a Surface-Following Buoy

It is possible to employ the measured value of the vertical drag coefficient of a window shade drogue (from section 5.1) to derive analytical estimates of the dynamic loads imparted to a tether line connecting the drogue to a buoy. The following analysis will be exactly like that found in Vachon (1973) except that updated (lower) values of $(C_D)_{//}$, the vertical drag coefficient, will be used.

In order to carry out the analysis, the following simplifying assumptions are necessary:

- (1) Perfect surface-following buoy, unaffected by dynamic loads imparted from the drogue tether line.
- (2) Drogue hangs straight beneath the buoy, with no catenary shape that could attenuate buoy motion seen by the drogue.
- (3) Inelastic tether line.
- (4) Seas impart pure sinusoidal motion of varying amplitude, frequency and wave height according to Pierson-Moskowitz sea spectra for fully developed, wind-driven seas (Pierson and Moskowitz, 1964).
- (5) Added mass of tether line, drogue, and ballast weight equals inertial mass.

Two cases of dynamic loading on the buoy/drogue combination will be analyzed:

- (1) The maximum downward drag force imparted on a surface-following buoy by a window shade drogue as the buoy rises on the leading edge of a wave.
- (2) The wave height that can potentially cause shock loads in a drogue tether line as a function of drogue area and ballast weight.

For the first analysis the assumption is made that the vertical forces on the buoy are primarily composed of three elements as follows:

$$T_v = \frac{1}{2} \rho (C_D)_{//} A_{\perp} \dot{y} |\dot{y}| + (m_o + m_a) \ddot{y} + m_o g \quad (E-1)$$

where y is assumed positive upwards and

- T_v = Vertical component of tether line tension.
- $(C_D)_{//}$ = Drag coefficient of drogue parallel to area, A .
- y = Vertical position of drogue.
- m_o = Mass of cable, drogue, and ballast weight.
- m_a = Added mass of cable, drogue, and ballast weight for vertical motion.

The dots over the y terms in equation (E-1) signify derivatives with respect to time; a single dot signifying a single derivative, etc.

The assumed sinusoidal motion permits the substitution of the following:

$$y = y_m \sin(\omega t) \quad (E-2)$$

where y_m is half the peak-to-trough height (i.e., wave amplitude) of the waves and ω is the wave frequency ($\omega = 2\pi f$). The substitution of (E-2) in (E-1) produces the following:

$$T_v = \frac{1}{2} \rho (C_D)_{//} A_{\perp} (y_m \omega \cos \omega t) |y_m \omega \cos \omega t| - (m_o + m_a) y_m \omega^2 \sin \omega t + m_o g \quad (E-3)$$

An independent evaluation of the first two terms in equation (E-3) is plotted in Figure E-1 assuming that $(C_D)_{//} = 0.03$ (i.e., plastic material). The height of the seas listed are assumed to be the peak-to-trough height or equal to $2y_m$. The combined mass of the cable, drogue, and ballast weight in kilograms-mass is arbitrarily assumed to be equal to 42% of the drogue area in square meters. This ratio is chosen because it results in a ballast weight which is assumed to be heavy enough for

minimizing drift errors and shock loading in the majority of sea states (to be explained later in this Appendix) and yet not submerging most surface buoys. It is also the approximate characteristics of the two drogues tested in section 5.1.

Wherever possible the ballast weight should be as large as possible limited only by two design constraints:

- (1) the reserve buoyancy of the buoy and,
- (2) the inertia loading on the tether line and buoy.

The second design constraint will only become important when the ballast weight is much larger compared to the drogue area than the case shown in Figure E-1.

It can be seen that the friction forces for plastic or canvas window shade drogues are dominant. The minus sign on the inertia term in equation (E-3) indicates that the maximum friction force occurs 90 degrees in phase after the maximum inertia force. If the ratio of ballast weight to drogue area is increased, the curve for inertia loading will shift vertically upward in direct proportion to the ballast weight. In order to find the maximum value of the sum of the drag and inertia loading at a given wave height and frequency a derivative is taken of equation (E-3) with respect to time and set equal to zero. The value of ωt for maximum total loading is given by the relation:

$$\omega t = \sin^{-1} - \left\{ \frac{m_o + m_a}{\rho (C_D)_{//} A_d y_m} \right\} \quad (E-4)$$

This value for the argument is then substituted into equation (E-3) for which the maximum value of tether line tension is calculated. It should be remembered, however, that the drag loading curves are potentially higher (i.e., more conservative) than in reality due to the manner in which the value of $(C_D)_{//}$ was derived. That is, the value of $(C_D)_{//}$ was derived for a condition of very little tension in the drogue. It is felt that such a situation will lead to a measured value of $(C_D)_{//}$ higher than if the drogue was under tension as in this case.

because of the relatively high vertical drag coefficient of a

window shade drogue in the presence of turbulent slip motion, a problem of shock loading can also arise when a buoy is descending to the trough of a wave. At this time the slip drag force of the drogue is opposing the ballast weight according to equation (E-1), where y is positive upwards. The inertia term in equation (E-1) can be neglected because it is generally small compared to other terms. This assumption is good for drogue areas, in square meters, which is greater than 5% of the combined weight of the drogue and ballast in Newtons. It can be visualized that if the vertical velocity is sufficiently large the vertical drag will offset the weight force ($m_0 g$) and the tether line will go slack. At this time it can be theorized that the drogue will be descending at its terminal velocity with zero tension in the tether line. Such a condition may exist until an upward motion of the buoy takes up the slack in the tether line. At this time the tether line should feel a shock load as it rapidly accelerates the drogue upward again.

The condition of zero tension in a drogue tether line should be avoided in order to prolong the life of the whole buoy. A series of nominal design curves are presented in Figure E-2 in order to adequately size the ballast weight for a given drogue area and expected sea state. It can be seen that the larger the drogue area the larger is the ballast weight which must be employed in order to avoid shock loads in a given sea condition. This analysis points out that an overly large window shade drogue cannot be freely employed with impunity unless the surface buoy has sufficient reserve buoyancy to accommodate the required ballast weight.

Solutions to the dynamic problems outlined here should be explored if window shade drogues are to be employed for long duration, unattended ocean deployments. Simple solutions to the problem can be explored through one or more of the following routes:

- (1) Use a non-surface-following buoy (i.e., a spar).
- (2) Employ distributed surface buoyancy to attenuate dynamic wave motion at the buoy.
- (3) Install an elastic element in the vertical tether line.
- (4) Make every element as gutty and strong as possible.

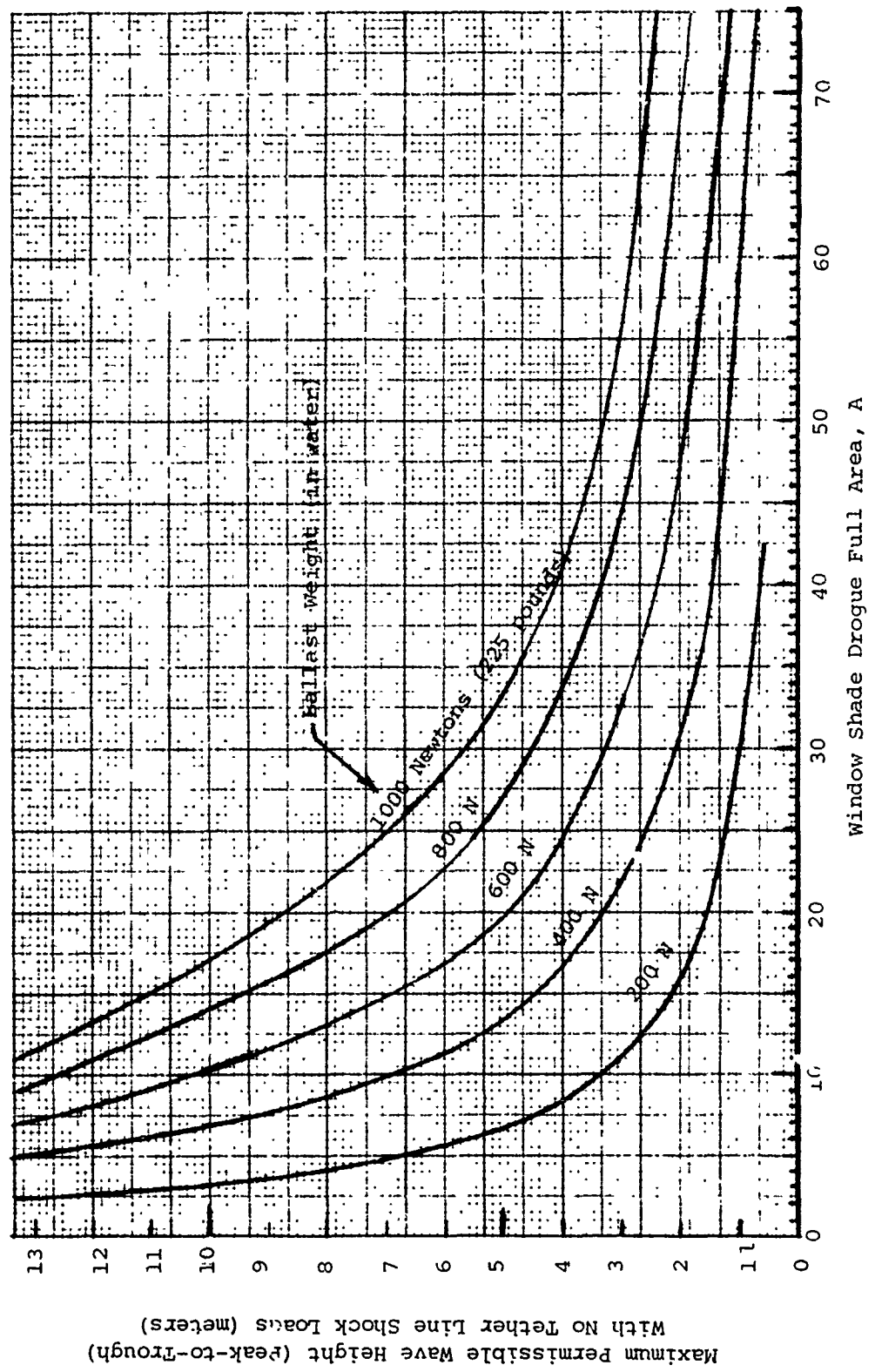


Figure E-2. Estimated window shade drogue dynamic shock load conditions based on full scale measurements of the drogue vertical drag coefficient, $(C_D)_{//}$.

These suggested approaches have their own set of potential problems in terms of size, cost, line fouling, fishbite, and handling. To really understand the trade-offs a more comprehensive math model of the drogue-buoy system should be developed and, if possible, validated by ocean tests.

APPENDIX F

Listing of Computer Program Employed to Correct Drogued Buoy Trajectories Based on Wind and Surface Current Forces (Containing Section which Iterates on Nova Buoy Drag Areas in Order to Produce a Corrected Trajectory Coincident with that of a Drogued Float)

```
C      CALCULATION OF MINIBUOY DROGUE SLIPPAGE BASED ON WIND
C      AND SURFACE CURRENT FORCES ON BUOYS. MINIBUOY DRAG AREAS
C      BOTH ABOVE AND BELOW WATER ARE OPTIMIZED IN ORDER TO
C      PRODUCE THE SAME VIRTUAL DISPLACEMENT AS THE DROGUED
C      FLOAT.
COMMON VBX(3,23),VBY(3,23),VWX(23),VWY(23),VSURX(23),VSURY(23),
1VSUR(23),ANVSU(23),VC1X(23),VC1Y(23),VC1(23),ANVC1(23),
2VC2X(23),VC2Y(23),VC2(23),ANVC2(23),DVC1X(23),DVC1Y(23),
3DVC2X(23),DVC2Y(23),DVS3X(23),DVS3Y(23),VSRT3(23),VSR3X(23),
4VSP3Y(23),AVC1D(23)
C      DEFINE WIND AND SURF CONVERGENCE COEFFICIENTS
CW=1.09
CS=1.06
LWIN=5
LWOUT=6
CDITW=0.0
CCITS=0.0
FW2XT=0.0
FW2YT=0.0
FS2XT=0.0
FS2YT=0.0
FW1XT=0.0
FW1YT=0.0
FS1XT=0.0
FS1YT=0.0
FNW2X=0.0
FNW2Y=0.0
FNS2X=0.0
FNS2Y=0.0
FWS2X=0.0
FWS2Y=0.0
SVC2X=0.0
SVC2Y=0.0
SVC1X=0.0
SVC1Y=0.0
SVS3X=0.0
SVS3Y=0.0
TOT3X=0.0
TOT3Y=0.0
TOT2X=0.0
TOT2Y=0.0
TOT1X=0.0
TOT1Y=0.0
W1=305
W2=253
300 WRITE(LWOUT,390)
   FORMAT(' ENTER DATA: /')
391 READ(LWIN,391) C1,C2,C3,C4,C5,C6,C7
   FORMAT(7F10.3)
   WRITE(LWOUT,392) C1,C2,C3,C4
```

THIS FILE IS UNCLASSIFIED
DATE 05-14-2014 BY 60322/UC/LPQ


```

        WRITE(LUOUT,393) C5,C6,C7
392  FORMAT(' C1(KG/M)=',F9.3,' C2=',F9.3,2X,' C3=',F9.3,2X,' C4=',F9.3)
393  FORMAT(' C5=',F9.3,3X,' C6=',F9.3,3X,' C7=',F9.3)
        READ(LUIN,394) (VWX(J),J=1,23)
        WRITE(LUOUT,394)(VWX(J),J=1,23)
        READ(LUIN,394) (VWY(J),J=1,23)
        WRITE(LUOUT,394)(VWY(J),J=1,23)
        DO 400 I=1,3
        READ(LUIN,394) (VBX(I,J),J=1,23)
        WRITE(LUOUT,394)(VBX(I,J),J=1,23)
        READ(LUIN,394) (VBY(I,J),J=1,23)
        WRITE(LUOUT,394)(VBY(I,J),J=1,23)
394  FORMAT(6(F8.4))
400  CCNTINUE

C
C
C
C
        CALCULATE CORRECTED VALUE OF SURFACE CURRENT

        WRITE(LUOUT,410)
410  FORMAT(' ESTIMATE SURF CURRT USING V(WIND) & V(B3) DATA',//)
        DO 440 J=1,23
C
C
        CALCULATE DRAG FORCE ON BUOY 3 DUE TO WIND
        I SIGNIFIES BUOY NUMBER, J SIGNIFIES HOUR WHERE J=1=10 AM TO 11 AM
        I=3
        VB3=SQRT(VBX(I,J)**2 + VBY(I,J)**2)
        AVB3R=ATAN2(VBY(I,J),VBX(I,J))
        AVB3D=57.3*AVB3R
        WRITE(LUOUT,414) VB3,AVB3D
414  FORMAT('/ BUOY 3 VFL(M/S)=',F7.4,2X,' ANGLE(DEG)=',F7.1)
C
        COMPUTE TOTAL DIST ANCE MOVED BY BUCY-3 IF UNRETRIVED
        XVB3X= VBX(I,J)*3600
        TOT3X= TOT3X +XVB3X
        YVB3Y= VBY(I,J)*3600
        TOT3Y= TOT3Y + YVB3Y
        WRITE(LUOUT,416) TOT3X,TOT3Y
416  FORMAT(' TOT X-DIST MOVED BY BUOY-3(M)=',F9.3,2X,' Y DIST=',F9.3)
        VWR3X=VWX(J)-VBX(I,J)
        VWR3Y=VWY(J)-VBY(I,J)
        WRITE(LUOUT,422) J,VWR3X,VWR3Y
422  FORMAT('/ HOUR=',I2,2X,' VX(WIND)-V(B3)=',F6.2,2X,' VWY-VB3=',F6.2)
        VWR3=SQRT(VWR3X**2+VWR3Y**2)
        ANVW3=ATAN2(VWR3Y,VWR3X)
        ADVW3= 57.3*ANVW3
        FW3=C4*(VWR3**2)
        WRITE(LUOUT,429) FW3,ADVW3
        FW3X=COS(ANVW3)*FW3
        FW3Y=SIN(ANVW3)*FW3
        WRITE(LUOUT,425) FW3X,FW3Y
425  FORMAT(' WIND X-FORCE(N)=',F6.2,2X,' WIND Y-FORCE=',F6.2)

```

THIS PAGE IS BEST QUALITY PRACTICABLE
FROM COPY FURNISHED TO EDC

```

C      CALCULATE SURFACE CURRENT VELOCITY REL. TO BUOY-3
      VSRT3(J)=SQRT(FW3/C7)
      WRITE(LUCUT,428) VSRT3(J),J
      VSR3X(J)=VSRT3(J)*COS(ANVW3)
      VSR3Y(J)=VSRT3(J)*SIN(ANVW3)
      WRITE(LUCUT,427) VSR3X(J),VSR3Y(J)
      VSURX(J)=VRX(I,J)-VSR3X(J)
      VSURY(J)=VRY(I,J)-VSR3Y(J)
C      CONVERT FROM METERS /SEC TO METERS /HOUR
      DVS3X(J)=VSURX(J)*3600
C      COMPUTE TOTAL X-DISTANCE TRAVELLED BY SURFACE CURRENT
      SVS3X=SVS3X+DVS3X(J)
C      COMPUTE TOTAL Y-DISTANCE TRAVELLED BY SURF. CURRENT
      SVS3Y=SVS3Y + DVS3Y(J)
      WRITE(LUCUT,426) J,VSURX(J),VSURY(J)
426  FORMAT(' HOUR=' ,I2,3X,'VSURX(M/S)' ,F7.4,3X,'VSURY(M/S)' ,F7.4)
427  FORMAT(' X-COMPON OF R3 SLIP=' ,F7.3,2X,'Y-COMP=' ,F7.3)
428  FORMAT(' SLIP VEL OF BUOY-3=' ,F7.3,2X,'FOR HOUR=' ,I2)
429  FORMAT(' WIND FORCE ON BUOY-3(N)' ,F7.3,2X,'ANG(DFG)' ,F7.2)
      VSUR(J)=SQRT(VSURX(J)**2+VSURY(J)**2)
      ANVSU(J)=ATAN2(VSURY(J),VSURX(J))
C      CONVERT FROM RADAINS TO DEGREES
      ANVSU(J)=ANVSU(J)*57.3
      WRITE(LUCUT,430) J,VSUR(J),ANVSU(J)
430  FORMAT(' HR=' ,I2,3X,'SURF VEL (M/S)' ,F7.4,3X,'ANG(DFG)' ,F7.1,/)
      WRITE(LUCUT,434) SVS3X,SVS3Y
434  FORMAT(' X-DISPL OF VSURF=' ,F9.2,2X,'Y-DISP(METERS)' ,F9.2,/)
440  CONTINUE
C
C      CALCULATE CORRECTED TRAJECTORY OF BUOY-2 AND "TRUE" DEEP
C      CURRENT MEASURED BY BUOY-2
C
442  FORMAT(// ' BEGIN CALCULATIONS ON BUOY-2',//)
C
      WRITE(LUCUT,442)
C      CALCULATE WIND FORCES ON BUOY-2
      I=2
      DO 445 J=1,23
      XVR2X=VRX(I,J)*3600
      TOT2X=TOT2X + XVR2X
      YVR2Y= VRY(I,J)*3600
      TOT2Y= TOT2Y + YVR2Y
      WRITE(LUCUT,444) TOT2X,TOT2Y
448  FORMAT(' TOT X-DIST MOVED BY BUOY-2(M)' ,F9.3,2X,'Y-DIST=' ,F9.3)
      VWR2X=VWX(J)-VRX(I,J)
      VWR2Y=VWY(J)-VRY(I,J)
      WRITE(LUCUT,450) J,VWR2X,VWR2Y
450  FORMAT(' HR=' ,I2,2X,'VW-V(R2)' ,F6.1,2X,'VWY-V(R2)(M/S)' ,F6.1)

```

THIS PAGE IS A QUALITY PRODUCTION
 AND WILL BE REPRODUCED TO THE
 BEST OF OUR ABILITY

```

VWR2=SQRT(VWR2X**2+VWR2Y**2)
ANVW2=ATAN2(VWR2Y,VWR2X)
AVW2D=57.3*ANVW2
FW2=C4*(VWR2**2)
C COMPUTE COMPONENTS OF WIND EFFECT ON BUOY-2
FW2X=COS(ANVW2)*FW2
FW2Y=SIN(ANVW2)*FW2
C COMPUTE COMPONENTS OF TOTAL WIND EFFECT ON BUOY-2
FW2XT=FW2XT + FW2X
FW2YT=FW2YT + FW2Y
452 WRITE(LUOUT,452) FW2,AVW2D
FORMAT(' WIND FORCE(N) ON B2=',F7.3,2X,'ANGLE(DEG)=' ,F7.1)
WRITE(LUOUT,425) FW2X,FW2Y
C CALCULATE SURFACE CURRENT FORCES ON BUOY 2
VSR2X=VSURX(J)-VBX(I,J)
VSR2Y=VSURY(J)-VBY(I,J)
450 WRITE(LUOUT,460) J,VSR2X,VSR2Y
FORMAT(' VR=',I2,2X,'VSX-V(B2)X=' ,F6.3,2X,'VSX-V(B2)Y=' ,F6.3)
C CALCULATE VALUE OF SURFACE VELOCITY RELATIVE TO BUOY-2
VSR2=SQRT(VSR2X**2+VSR2Y**2)
ANVS2=ATAN2(VSR2Y,VSR2X)
AVS2D=57.3*ANVS2
C COMPUTE SURF CURRENT FORCE ON BUOY-2
FS2=C5*(VSR2**2)
FS2X=COS(ANVS2)*FS2
FS2Y=SIN(ANVS2)*FS2
FS2XT= FS2XT + FS2X
FS2YT = FS2YT + FS2Y
464 WRITE(LUOUT,464) FS2X,FS2Y
FORMAT(' VSURF/B2,X-FORCE(N)=' ,F6.2,2X,'Y-FORCE=' ,F6.2)
WRITE(LUOUT,465) FS2,AVS2D
465 FORMAT(' VSURF FORCE ON2(N)=' ,F6.3,2X,'ANGLE(DEG)=' ,F7.1)
C SUM COMPONENTS OF WIND AND SURF CURRENT FORCES ON BUOY-2
F2X=FW2X+FS2X
F2Y=FW2Y+FS2Y
C CALCULATE TOTAL VECTOR FORCE ON BUOY-2 & ANGLE
F2=SQRT(F2X**2+ F2Y**2)
AER2R=ATAN2(F2Y,F2X)
C DIRECTION OF ERROR FORCE IN DEGREES
ANER2=57.3*ATAN2(F2Y,F2X)
WRITE(LUOUT,466) F2,ANER2
466 FORMAT(' TOT B2 ERROR FORCE(N)=' ,F7.2,2X,'ANGLE(DEG)=' ,F7.1)
C CALCULATE SLIP VELOCITY V(2)-V(C) & ANGLE OF SLIP
V2SL=SQRT((1.0/C6)*F2)
WRITE(LUCUT,470) V2SL,ANER2
470 FORMAT(' BUOY-2 SLIP VLL(M/S)=' ,F6.4,2X,'ANGLE(DEG)=' ,F7.1)
C CALCULATE COMPONENTS OF SLIP RELATIVE VELOCITY
V2SLX= V2SL*COS(AER2R)
V2SLY=V2SL*SIN(AER2R)
WRITE(LUCUT,472) V2SLX,V2SLY

```

THIS PART IS OF QUALITY PRACTICABLE
FROM COPY


```

SVC1Y=0.0
TOT1X=0.0
TOT1Y=0.0
FW1XT=0.0
FW1YT=0.0
FS1XT=0.0
FS1YT=0.0
WRITE(LUCOUT,511) C2
C
C BEGIN '00' LOOP FOR 23-HOUR, HOURLY COMPUTATIONS FOR BUOY-1
C
508 DO 550 J=1,23
C CALCULATE WIND VELOCITY RELATIVE TO BUOY-1
509 VWR1X=VWX(J)-VRX(I,J)
VWR1Y = VWY(J)-VBY(I,J)
VWR1=SQRT(VWR1X**2+VWR1Y**2)
ANWR1=ATAN2(VWR1Y,VWR1X)
AWR1D=57.3*ANWR1
C CALCULATE WIND FORCE ON BUOY-1
FW1=C1*(VWR1**2)
FW1X=COS(ANWR1)*FW1
C COMPUTE 23-HOUR TOTAL FORCE ON P1 DUE TO V(WIND)-V(B1)
FW1XT = FW1XT + FW1X
FW1Y=SIN(ANWR1)*FW1
FW1YT=FW1YT + FW1Y
XVB1X=VRX(I,J)*3600
TOT1X= TOT1X + XVB1X
YVB1Y= VBY(I,J)*3600
TOT1Y= TOT1Y + YVB1Y
WRITE(LUCOUT,515) TOT1X,TOT1Y
WRITE(LUCOUT,512) VWR1,AWR1D
WRITE(LUCOUT,510) J,VWR1X,VWR1Y
WRITE(LUCOUT,498) FW1XT, FW1YT
WRITE(LUCOUT,514) FW1X,FW1Y
WRITE(LUCOUT,513) FW1,AWR1D
510 FORMAT(' HR=' ,I2,2X,'VX(WIND)-V(P1)=' ,F6.2,2X,'VY(WIND)-VY(B1)=' ,F
15.2)
511 FORMAT(' CURRENT VALUE OF DRAG CONST C2(KG/M)=' ,F8.3,/)
512 FORMAT(' WIND VEL REL TO B1(M/S)=' ,F6.3,2X,'ANGLE(DEG)=' ,F7.1)
513 FORMAT(' WIND FORCE(N) ON 1=' ,F7.3,2X,'ANGLE(DEG)=' ,F7.1)
514 FORMAT(' WIND/B1 X-FORCE(N)=' ,F6.2,2X,'Y-FORCE=' ,F6.2)
515 FORMAT(' TOT X-DIST MOVD BY BUOY-1(M)=' ,F9.3,2X,'Y-DIST=' ,F9.3)
AWR1X=ABS(VWR1X)
AWR1Y=ABS(VWR1Y)
C CALCULATE VALUE OF SURF CURRENT RELATIVE TO BUOY-1
VSR1X=VSURX(J)-VRX(I,J)
VSR1Y=VSURY(J)-VRY(I,J)
WRITE(LUCOUT,520)J,VSR1X,VSR1Y
520 FORMAT(' HR=' ,I2,3X,'VX(SUR)-V(P1)X=' ,F6.4,2X,'VY(SUR)-V(B1)=' ,F6.
14)

```

THIS PART TO BE AS MUCH AS PRACTICABLE
~~FROM THE ORIGINAL DOCUMENT TO THE~~

```

VSR1=SQRT(VSR1X**2 + VSR1Y**2)
ANVS1=ATAN2(VSR1Y,VSR1X)
AVS1D=57.3*ANVS1
WRITE(LUCUT,521) VSR1,AVS1D
521 FORMAT(' VSURF VEL TO R1=',F7.3,2X,' ANGLE( DEG)=' ,F7.1)
C CALCULATE SURFACE CURRENT FORCE TERM ON BUDY-1
FS1=C2*(VSR1**2)
FS1X=FS1*COS(ANVS1)
C COMPUTE 23-HOUR TOTAL FORCE ON B1 DUE TO V(SURF)-V(R1)
FS1XT=FS1XT + FS1X
FS1YT=FS1YT + FS1Y
FS1Y=FS1*SIN(ANVS1)
FS1YT=FS1YT + FS1Y
WRITE(LUCUT,522) FS1,AVS1D
522 FORMAT(' VSURF FORCE (N) ON 1=',F6.3,2X,' ANGLE (DEG)=' ,F7.1)
WRITE(LUCUT,524) FS1X,FS1Y
524 FORMAT(' VSURF/R1, X-FORCE(N)=' ,F6.2,2X,' Y-FORCE=' ,F6.2)
WRITE(LUCUT,499) FS1XT,FS1YT
C SUM WIND & SURF CURRENT COMPONENTS
F1X=FW1X + FS1X
F1Y=FW1Y + FS1Y
WRITE(LUCUT,525) F1X,F1Y
525 FORMAT(' NET X-FORCE ON BUDY-1(N)=' ,F7.2,2X,' Y-FORCE=' ,F7.2)
F1=SQRT(F1X**2 + F1Y**2)
ANFR1=ATAN2(F1Y,F1X)
ANFR1= 57.3*ANFR1
WRITE(LUCUT,526) F1,ANFR1
526 FORMAT(' TOT B1 FPP FORCE(N)=' ,F7.2,2X,' ANGLE( DEG)=' ,F7.1)
C CALCULATE SLIP VELOCITY V(1)-V(C)
VISL=SQRT((1.0/C3)*F1)
WRITE(LUCUT,528) VISL,ANFR1
528 FORMAT(' BUDY-1 SLIP VEL(M/S)=' ,F6.4,2X,' ANGLE( DEG)=' ,F7.1)
C CALCULATE COMPONENTS OF SLIP RELATIVE VELOCITY
VISLX=VISL*COS(ANFR1)
VISLY=VISL*SIN(ANFR1)
VC1X(J)=VBX(I,J)-VISLX
VC1Y(J)=VBY(I,J)-VISLY
WRITE(LUCUT,530) VC1X(J),VC1Y(J)
530 FORMAT(' V(C)1X=' ,F7.4,4X,' V(C)1Y(M/S)=' ,F7.4)
C SUM COMPONENTS OF DEEP CURRENT MEASURED BY MINIRUDY-1(B-1)
DVC1X(J)=VC1X(J)*3600.
SVC1X=SVC1X+DVC1X(J)
DVC1Y(J)=VC1Y(J)*3600.
SVC1Y=SVC1Y+DVC1Y(J)
C COMPUTE MAGNITUDE & DIRECTION OF "DEEP" CURRENT
VC1(J)=SQRT((VC1X(J))**2+(VC1Y(J))**2)
ANVC1(J)=ATAN2(VC1Y(J),VC1X(J))
AVC1D(J)=ANVC1(J)*57.3
WRITE(LUCUT,540) J,VC1(J),AVC1D(J)
540 FORMAT(' HR=' ,I2,3X,' DEEP VEL(M/S)=' ,F6.4,3X,' ANGLE=' ,F7.1)
WRITE(LUCUT,544) SVC1X,SVC1Y

```

THIS PAGE IS BEST QUALITY AVAILABLE
 FROM GPO. 1-25-64. O-311-150-10-000

```

544 FORMAT(' X-DISP OF VC1X(M)=' ,F9.2,2X,'Y-DISPLACEMENT=' ,F9.2,/)
550 CONTINUE
C
C END 'DO' LOOP. CHECK FOR FINAL POSITION OF BUOY-1 REL TO BUOY-2
C
C COMPUTE ANGLE OF NET SURFACE CURRENT FORCE ON BUOY-1
FW1T=SQRT(FW1XT**2 + FW1YT**2)
AFW1R= ATAN2(FW1YT,FW1XT)
AFW1D= 57.3*AFW1R
WRITE(LUCUT,498) FW1XT,FW1YT
WRITE(LUCUT,548) FW1T,AFW1D
548 FORMAT(' TOTAL WIND FORCE ON R1=' ,F8.2,2X,'ANGLE=' ,F7.1)
FS1T=SQRT(FS1XT**2+FS1YT**2)
AFS1R=ATAN2(FS1YT,FS1XT)
AFS1D=57.3*AFS1R
WRITE(LUCUT,556) FS1T,AFS1D
556 FORMAT(' TOT SURF FORCE ON1=' ,F8.2,2X,'ANGLE=' ,F7.1)
WRITE(LUCUT,554) SVC1X,SVC1Y
IF(COITS=1) 551,640,640
C
C BEGIN BUOY-1 WIND ITERATIONS
C
C CALCULATE COMPONENT DIFFERENCES IN BUOY VIRTUAL DISPLACEMENT
551 DSVCX=SVC2X-SVC1X
DSVCY=SVC2Y-SVC1Y
WRITE(LUCUT,555) DSVCX,DSVCY
C CALCULATE TOTL VIRTUAL DISPLACEMENT ERROR
DSVCT=SQRT(DSVCX**2+DSVCY**2)
WRITE(LUCUT,553) COITW,DSVCT
C MINIMIZE B2-B1 POSITION DIFF (AT END) TO < 50 METERS
IF(DSVCT-50) 552,558,559
C CLOSING PRINTOUT FOR WIND ITERATIONS
552 WRITE(LUCUT,553)COITW,DSVCT
553 FORMAT(' NO WIND ITER=' ,F4.1,2X,'DISPLACEMENT ERROR=' ,F6.1,///)
554 FORMAT(' TOT X-DISP OFVC1(M)=' ,F9.2,2X,'TOT Y-DISP=' ,F9.2,/)
555 FORMAT(' TOT WIND VCX ERR(B2-B1)=' ,F8.2,2X,'TOT Y-ERR=' ,F8.2)
C LOGIC FOR DETFR CONVERGENCE SIGN AND DIRECTION OF WIND EFFECTS
C CALC. WHETHER TO INCREASE OR DECREASE DISPLACEMENT OF BUOY-1
C CHECK TO SEE IF DOING WIND OR SURFACE CURRENT ITERATION
IF(COITW=11) 558,640,640
C COMPUTE ANGLE OF FINAL VIRTUAL DISPLACEMENT VECTOR
558 ADVCT=ATAN2(DSVCY,DSVCX)
ADVCD=57.3*ADVCT
C CHECK FOR LINEUP OF DISPL ERROR AND SURF CURR'T FORCE
IF(ABS(ADVCT-AFS1R)-0.3) 559,559,560
559 WRITE(LUCUT,570) C1,ADVCD,COITW
570 FORMAT(' C1=' ,F9.3,2X,'ANG(B2-B1)=' ,F8.3,2X,'NO.WIND ITER=' ,F4.1)
GO TO 675

```

THIS PROGRAM IS BEST QUALITY. ACCURACY
FROM COMPUTER PRINTED OUTPUT

```

C      CHECK FOR 180 DEGREE ORIENTATION ERROR BETWEEN POSNS & VSURF EFF
560  IF(ABS((ADVCT-3.14159)-AFS1R)-0.3)562,562,572
562  WRITE(LUOUT,570) C1,ADVCT,CCITW
      GO TO 570
572  WRITE(LUOUT,574) ADVCT,AFS1R
574  FORMAT(' WIND EFF IMPROPER, ERR ANG=',F8.3,2X,' VSURF ANG=',F8.3)
C      BEGIN FIRST STEP OF WIND ITERATION
C      DETERMINE WHETHER TO INCREASE OR DECREASE BUOY-1 WIND COEF AFTER
C      FIRST CHECKING ON VIRTUAL POSITION OF BUOYS REL TO WIND EFFECT
      IF(FW1XT*DSVCX) 590,590,600
C      CORRECT FOR DIFFERENCES BY CHNGE OF DRAG COEF ABOVE WATER
590  C1=C1*CW
      GO TO 620
600  C1=C1/CW
      GO TO 620
620  CCITW=CCITW + 1
      WRITE(LUOUT,622) C1
622  FORMAT(' CURRENT VALUE OF WIND DRAG COEF OF BUOY-1,C1=',F8.3)
640  CONTINUE
C
C      BEGIN SURF CURRENT ITERATIONS
C
C      CALCULATE COMPONENT DIFFERENCES IN BUOY VIRTUAL DISPLACEMENT
660  DSVCX=SVC2X-SVC1X
      DSVCY=SVC2Y-SVC1Y
564  FORMAT(' TOT VCX ERR(SURF ITER),R2-R1=',F8.2,2X,' Y- R=',F8.2)
      WRITE(LUOUT,511) C2
      DSVCT=SQRT(DSVCX**2+DSVCY**2)
      WRITE(LUOUT,752) CCITS,DSVCT
C      MINIMIZE BUOY-2- BUOY-1 POSN ERROR TO < 50 METERS
      IF(DSVCT-DSVCF) 668,668,666
666  CCITS=0.0
      CCITW=0.0
      WRITE(LUOUT,667)
667  FORMAT(' BEGIN BUOY-1 WIND ITERATIONS AGAIN',//)
      GO TO 507
668  IF(DSVCT-30) 750,670,670
670  C2=C2*CS
      DSVCF=DSVCT
      GO TO 680
676  C2=C2/CS
      DSVCF=DSVCT
680  CCITS=CCITS + 1
      IF(CCITS-20) 607,750,750
750  WRITE(LUOUT,752)CCITS,DSVCT
752  FORMAT(' NO SURF CURF ITER=',F4.1,3X,' DISPL ERROR=',F6.1,///)
      END

```

THIS PAGE IS BEST QUALITY PRACTICABLE
 23 JUN 1964 11:00 AM 10 LDC

MANDATORY DISTRIBUTION LIST

FOR UNCLASSIFIED TECHNICAL REPORTS, REPRINTS, & FINAL REPORTS
PUBLISHED BY OCEANOGRAPHIC CONTRACTORS
OF THE OCEAN SCIENCE AND TECHNOLOGY DIVISION
OF THE OFFICE OF NAVAL RESEARCH
(REVISED JAN 1975)

1	Director of Defense Research and Engineering Office of the Secretary of Defense Washington, D. C. 20301 ATTN: Office, Assistant Director (Research)	12**	Defense Documentation Center Cameron Station Alexandria, Virginia 22314
	Office of Naval Research Arlington, Virginia 22217		Commander Naval Oceanographic Office Washington, D. C. 20390
3	ATTN: (Code 480)*	1	ATTN: Code 1640
1	ATTN: (Code 460)	1	ATTN: Code 70
1	ATTN: (Code 102-OS)		
6	ATTN: (Code 102IP)		
1	ATTN: Code 200		
1	ONR ResRep (if any)	1	NODC/NOAA Rockville, MD 20882
	Director Naval Research Laboratory Washington, D. C. 20375		
6	ATTN: Library, Code 2620		

TOTAL REQUIRED - 35 copies

* Add one separate copy of
Form DD-1473

** Send with these 12 copies
two completed forms DDC-50,
one self addressed back to
contractor, the other ad-
dressed to ONR, Code 480

DISTRIBUTION

CHARLES STARK DRAPER LABORATORY, INC.

10	Library	1	Morey, Ronald I.
1	Araujo, Richard	1	Reid, Robert
1	Bowditch, Philip N.	1	Shillingford, John T.
1	Chhabra, Narender	1	Soikkeli, Matti
1	Coccoli, Joseph D.	1	Suomala, John S.
1	Dahlen, John M.	1	Toth, William E.
1	Grossman, Arthur	70	Vachon, William

M.I.T. DEPARTMENT OF EARTH & PLANETARY PHYSICS

1	Press, Prof. Frank	1	Wunsch, Prof. Carl I.
---	--------------------	---	-----------------------

M.I.T. DEPARTMENT OF METEOROLOGY

1	Stommel, Prof. Henry M.	1	Mollo-Christensen, Prof. Erik
1	Heinmiller, Robert		

M.I.T. DEPT. OF NAVAL ARCHITECTURE & MARINE ENGINEERING

1	Newman, Prof. John N.	1	Milgram, Prof. Jerome H.
1	Devanney, Prof. John W. III	1	Abkowitz, Prof. Martin A.

M.I.T. DEPT. OF CIVIL ENGINEERING

1	Pearce, Dr. Bryan R.		
---	----------------------	--	--

DISTRIBUTION

RESEARCH LABORATORIES

- 1 Garrett, Dr. John
Environment Canada, Pacific Region
Marine Sciences Directorate
Patricia Bay
Victoria B.C.
CANADA
- 1 Gerard, R. D.
1 Gordon, Dr. ARnold
Lamont-Doherty Geological Observatory
Palisades, NY 10964
- 1 Monohan, Dr. Edward C.
Sea Education Association
UNOLS Office
Woods Hole Oceanographic Institute
Woods Hole, Mass. 02543
- 1 Kirwan Dr. A. D.
1 Nowlin, Dr. Worth
Texas A&M University
College of Geosciences
College Station, TX 77843
- 1 Masterson, John E.
National Center for Atmospheric Research
P. O. Box 1470
Boulder, CO 80302
- 1 Damon, Henry
1 Moore, Dr. Dennis
NOVA University
Dania, FL 33002
- 1 Knaus, Dr. John A.
2 Possby, Dr. Thomas
Narragansett Marine Laboratory
University of Rhode Island
Kingston, RI 02881
- 1 Martin, Pat
Project AIDJEX
4059 Roosevelt Way, N.E.
Seattle, WA 98105

DISTRIBUTION (Cont'd)

Research Laboratories

1 Barnett Dr. T.
1 Davis, Dr. Russ
1 McNally, Gerald
1 Niiler, Dr. Peter
1 Sessions, Meredith
1 Snodgrass, Frank
 Scripps Institution of Oceanography
 La Jolla, CA 92037

1 Catlow, James
1 Whitaker, Walter
 U.S.N. Underwater Sound Laboratory
 New London, CT 06321

1 Curtis, H. Gray
1 Ling, Shun
1 Silva, Eugene, Dr.
 Ocean Engineering & Construction Project Office
 Navy Facilities Engineering Command
 Chesapeake Division
 FPO 1P, Bldg. 200
 Washington Navy Yard
 Washington, DC 20374

1 Mesecar, Dr. Roderick
1 Nath, Dr. John
1 Pillsbury, Dr. Dale
 Department of Oceanography
 Oregon State University
 Corvallis, OR 97331

1 Director
1 Welch, Dr. Christopher
1 Lobecker, Robert
1 Ruzicki, Evan
 Virginia Institute of Marine Science
 Gloucester Point, VA 23062

1 Cox, John W.
1 McFall, John
1 Usry, J. W.
1 Wallace, John W.
 MS 214
 NASA/Langley Research Center
 Langley Station
 Hampton, VA 23362

DISTRIBUTION (Cont'd)

Research Laboratories

- 1 Charnel, Dr. Robert
- 1 Hansen, Dr. Donald
- 1 Leetma, Dr. Ants
- 1 Molinari, Dr. Robert
- 1 Mofjeld, Dr. Harold
 - Atlantic Oceanographic & Meteorological Laboratory
 - 15 Pickenbacker Causeway
 - Virginia Key
 - Miami, FL 33149

- 1 Bowman, Dr. Malcolm J.
 - Marine Sciences Research Center
 - Surge J, South Campus
 - State University of New York
 - Stony Brook, NY 11790

- 1 Clark, Dan
 - Scientific Marine, Inc.
 - Millfield Street
 - Woods Hole, MA 02543

- 1 Brown, Dr. Wendell
- 1 Savage, Dr. Godfrey H.
 - Director, Engineering Design and Development Lab
 - University of New Hampshire
 - Durham, NH 03824

- 1 Christenson, Lt. Tom
- 1 Gregory, John B.
 - NORDA, Code 450
 - National Space Technology Laboratories
 - Bay St. Louis, Miss. 39520

- 1 Lange, Dr. Edward
- 1 Wilson, Dr. Stanley
 - NORDA, Code 410
 - National Space Technology Laboratories
 - Bay St. Louis, Miss. 39520

- 1 Baker, Dr. D. James
- 1 Taft, Dr. Bruce
 - Dept. of Oceanography
 - University of Washington
 - Seattle, WA 98195

- 1 Beardsley, Dr. Robert
- 1 Berteaux, Henri
- 1 Bumpus, Dean
- 1 Fofonoff, Dr. Nicolas P.
- 1 Mason, David
- 1 Mavor, James
- 1 McCullough, James

DISTRIBUTION (Cont'd)

Research Laboratories

1 Metcalf, Gary
1 Moller, Donald
1 Parker, Charles E.
1 Porter, Dr. Robert
1 Regier, Lloyd
1 Richardson, Philip
1 Saunders, Peter
1 Spindel, Dr. Robert
1 Stalcup, M. D.
1 Volkman, Gordon
1 Voorhis, Arthur
1 Walden, Robert
1 Warren, Dr. Bruce
1 Webb, Douglas
1 Webster, Ferris
 Woods Hole Oceanographic Institute
 Woods Hole, MA 02543

1 Bierly, Dr. Gene
1 Collins, Dr. Curt
1 Greenfield, Dr. Richard
1 Jennings, Dr. Feenan D.
1 Lambert, Dr. Richard
1 Merrill, Dr. William
 National Science Foundation
 1800 G. Street, N.W.
 Washington, DC 20550

1 Wolfe, Robert
 Interstate Electronics Corporation
 P. O. Box 3117
 707 E. Vermont Avenue
 Anaheim, CA 92803

25 Director
1 Canada, Raymond
1 DeBok, Lt. Donald
1 Kerut, Edmund
1 Livingston, Iane
1 Michelina, Dr. Edward
1 Niederman, Cmdr. Charles
 NOAA Data Buoy Office
 Code C-623
 Mississippi Test Facility
 Bay St. Louis, MS 39520

1 Geunther, Gary
1 Ringenbach, Maurice
 NOAA/NOS
 Engineering Development Laboratory
 6015 Executive Blvd.
 Rockville, MD 20853

DISTRIBUTION (Cont'd)

Research Laboratories

- 1 Kearse, Charles D.
NOAA/NOS
Engineering Development Laboratory
1600 Port Blvd.
Miami, FL

- 1 Dr. David A. Booth
Dr. J. R. Hunter
Dept. of Physical Oceanography
Marine Sciences Laboratory
Manai Bridge
North Wales LL59 5EY
United Kingdom

- 1 Mr. Angelo Denegri
Consiglio Nazionale delle Ricerche
Via Bagnara
2 - 19036 S. Terenzo
Italy

- 1 Dr. J. M. Coudeville
Centre Oceanologique de Bretagne
Boite Postale 337
29.273 Brest CEDEX
France

- 1 Mr. David Mountain
Coast Guard Oceanographic Unit
Bldg. 159-E
Navy Yard Annex
Washington, DC 20590

- 1 Dr. Michel R. Froidevaux
Aerospatiale
Subdivision Systemes, SYX/E
78130, Les Mureaux
France

- 1 Mr. John Lazier
Atlantic Oceanographic Laboratory
Bedford Institute of Oceanography
P. O. Box 1006
Dartmouth, Nova Scotia
B2Y 4A2